Spring 2019

Plenum-to-plenum heat transfer characteristics under natural circulation in a scaled-down prismatic modular reactor

Salman Mohammed Alshehri

Department: Nuclear Engineering and Radiation Science

PLENUM-TO-PLENUM HEAT TRANSFER CHARACTERISTICS UNDER NATURAL CIRCULATION IN A SCALED-DOWN PRISMATIC MODULAR REACTOR

by

SALMAN MOHAMMED ALSHEHRI

A DISSERTATION

Presented to the Faculty of Graduate School of the

MISSOURI UNIVERSITY OF SCIENCE AND TECHNOLOGY

In Partial Fulfillment of the Requirements for the Degree

DOCTOR OF PHILOSOPHY

in

NUCLEAR ENGINEERING

2019

Approved by

Shoaib Usman, Advisor
Carlos Castano
Ayodeji Babatunde Alajo
Lana Alagha
Ibrahim Abdallah

ABSTRACT

Gas-cooled reactor (GCR) is being developed under the Next Generation Nuclear Plant Program (NGNP) in nuclear engineering studies. As the world searches for an energy source with high energy density, clean, abundant, and storable nature to avoid global warming issues, GCR seems to be a promising solution, particularly the possibility of producing hydrogen. Studying and developing the safety analysis and GCR technologies are required for the optimum design and safety of GCR system. Multiphase Reactors Engineering and Applications Laboratory (mReal) at Missouri University of Science and Technology (S&T) has developed a natural convection heat transfer test facility with one riser and one downcomer between two plena to investigate loss of flow accident scenario (LOFA) for a prismatic very high temperature reactor (VHTR). Using advanced heat transfer coefficient probe and T-thermocouples. The facility represents a scaled down prismatic modular reactor with a reference to High-Temperature Test Facility at Oregon State University (OSU-HTTF). The natural circulation heat transfer in terms of temperature fields and heat transfer coefficients across the core of current facility (i.e., channels) has been investigated at different conditions to understand the passive safety features of prismatic modular reactors (PMR). This dissertation advance knowledge and understanding of the intra core natural circulation phenomenon in the PMRs. Moreover, fill the gaps in the open literature and understanding of the natural circulation heat transfer and gaseous dynamics in the prismatic VHTR and provide experimental benchmark data, which is much needed and is missing in the literature for verification and validation.

ACKNOWLEDGMENTS

First and foremost, my praises and thanks are to ALLAH for his kindness and so many blessings in my life.

As an appreciation, I would like to dedicate my Ph.D. degree to my parents whom are the reasons of the success in my life by their support and encouragement throughout the years. I express gratitude from the depth of my heart to my advisor, Dr. Shoaib Usman, who gave me an opportunity to conduct my research under his supervision. Dr. Usman is my teacher, inspirational, and big brother since I began my research with him. I thanks Dr. Usman for his supervision, advice, knowledge and support, which have made this work possible and successful. I would also like to acknowledge Professor Muthanna Al-Dahhan to support me and allow me to use Multiphase Reactors Engineering and Applications Laboratory (mREAL) in Missouri S&T and I ran my experiments. I appreciatively would also like to thank my advisory committee members, Dr. Carlos Castano, Dr. Ayodeji Alajo, Dr. Lana Alagha, and Dr. Ibrahim Abdallah for taking an interest in my work and examining my dissertation. I express a deep sense of appreciation to my wife and daughters, who stood by my side during I faced the difficulties, for believing in me and supporting my dreams and ambitions. I would also like to acknowledge my brothers and sisters for their support and encouragement throughout the years. Words are far from adequate to thank them, and what I can do is to keep a deep feeling in my heart forever. I would also like to acknowledge King Abdulaziz City for Science and Technology in Riyadh (KACST), Saudi Arabia for sponsoring my Ph.D. studies, and Saudi Arabian Cultural Mission (SACM) in Washington, D.C. USA for their support.

TABLE OF CONTENTS

Page

LIST OF ILLUSTRATIONS

Page

LIST OF TABLES

Page

NOMENCLATURE

Symbol	Description
h_i	Local instantaneous heat-transfer coefficient (W/m^2 K)
h_{avg}	Time-averaged local heat-transfer coefficients (W/m^2 K)
k	Thermal conductivity of helium (W/m K)
L	Length of the riser channel (m)
N	Number of data points
q_i	Local instantaneous heat flux (W/m^2)
Z/L	Dimensionless axial position
T_S	Channel inner surface temperature
T_b	Coolant bulk temperature
$\bar{h}_L$	Average values of the heat transfer coefficient (W/m^2 K)
$\overline{Nu}_L$	Average Nusselt number.
l	Characteristic length (m)
$\overline{T}_S$	Axial average value of inner surface temperature
$\overline{T}_b$	Axial average value of air bulk temperature
$\overline{T}_f$	Average film temperature

1. INTRODUCTION

1.1. OVERVIEW

A gas-cooled nuclear reactor (GCR) is the one, which typically uses graphite moderator and carbon dioxide or helium gas as the coolant. Helium is preferable than CO_2 as is it more efficient and highly resistant to corrosion although CO_2 is much cheaper. On the other hand, helium need purification prior to entering the reactor as any impurity may cause direct corrosion at high temperatures especially in Very High Temperature Reactors (VHTR) [1]. The GCR is a fundamental configuration of nuclear reactors, which appeared in generation I of nuclear systems. The Magnox reactors in the United Kingdom and the Uranium Naturel Graphite Gaz (UUNG) reactor developed by France were two main types of generation I with gas cooling. Both reactors used CO_2 as the coolant fluid. In the UK, the Magnox was replaced by the advanced gas-cooled reactors (AGR), which is an improved generation II gas-cooled reactors. In France, the UUNG was replaced by the Pressurized water reactor (PWR) [2]. There are many nuclear reactors classified as GCR such as; Heavy Water Gas Cooled Reactor (HWGCR), Gas-cooled Fast Reactors (GFS), Gas Turbine Modular Helium Reactor (GT-MHR), High Temperature Gas Cooled Reactors (HTGR), and Very High Temperature Reactors (VHTR). It is noteworthy to mention that, the VHTR term refers to 1000 ℃ or above outlet coolant temperature. This term is typically used to refer to the next stage in the development of HTGRs [1].

The history of GCR begins with the graphite moderated and air-cooled X-10 reactor, which was developed at Oak Ridge, Tennessee and went critical in 1943 [1]. This

reactor was capable of generating 3.5 MW. The first HTGR was the Dragon reactor. The commissioning work of this reactor started in 1959 in the UK [1]. This reactor reached its full-power in 1966, and operated until 1974. It produced 20 MW of heat and did not have an electricity generator circuit. In Germany, the Arbeitsgemeinschaft Versuchsreaktor (AVR) plant construction, which was based on pebble bed concept, was also started in 1959. It was a 15 MW power plant and operated for 12 years until cancellation. The first prototype in USA, was based on the design with prismatic fuel, was Peach Bottom Unit 1. It was commissioned in 1967 and operated until 1974 generating 40 MW of electricity [1]. The USA was the first country to generate electricity using an HTGR power plant. Following the successful prototype HTGR plants, larger plants were constructed to further study the commercial viability of the HTGR concept. In the USA, the Fort St. Vrain (FSV) began to produce electricity in 1976 and was not declared commercial until 1979. In Germany, the successor nuclear plant, which is Thorium High Temperature Reactor (THTR-300), was ordered in 1970. It was based on the pebble bed concept. In 1985 it was connected to the electrical grid producing 300 MW of electricity and operated until 1989 as it was subsidized by the government because of the safety regulator and other technical problems encountered during plant operation although all repairs were completed in February 1989 [1]. Afterwards, Japan Atomic Energy Research Institute (JAERI) began construction of the High Temperature Engineering Test Reactor (HTTR) in Japan in 1991. In 2000, the construction of High Temperature Gas-Cooled Reactor Test Module (HTR-10), which was developed by the Institute of Nuclear Energy Technology (INET), was completed in China. Both reactors are considered the state of art in the HTGR design, with the HTTR using prismatic block fuel and the HTR-10 using

pebble fuel concept. The most recent attempt to develop a commercial VHTR based on pebble fuel concept started in South Africa in 1998 but in 2010 the final closure of the program was declared after the expenditure of a large amount of South Africa public money on the project. On the other hand, the US (General Atomics) and Russian Federation program cooperated to develop the prismatic fuel based GT-MHR and brought it into operation by 2010. The HTGR coolant temperatures for previously mentioned different reactors are shown in Figure 1.1 [1,2].

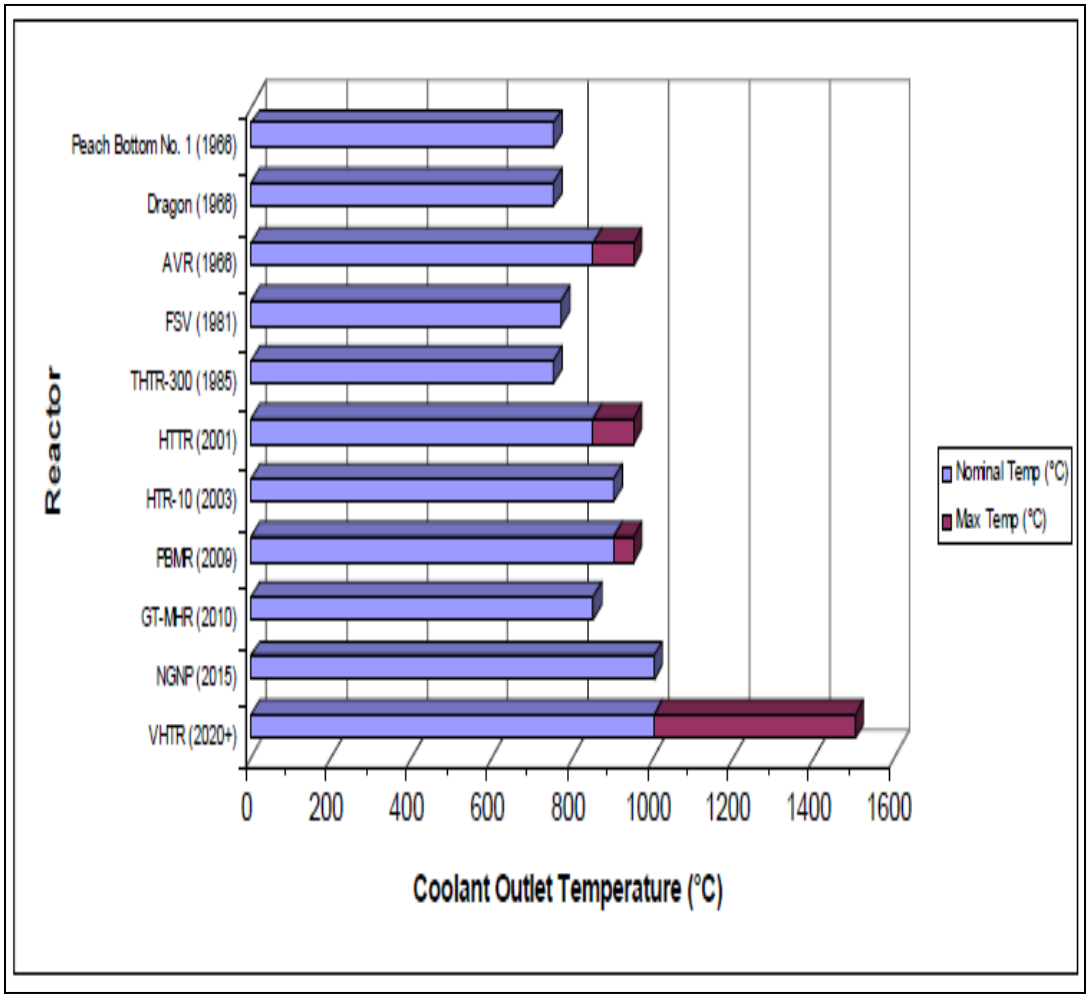

Figure 1.1. HTGR coolant outlet temperature [1]

Interest in GCR has been renewed, and a number of HTGR designs have been developed for near-term deployment (i.e., generation III+ reactors). These include the Pebble Bed Modular Reactor (PBMR) project, led by Eskom, and the Gas Turbine Modular Helium Reactor (GT-MHT), which composed of a prismatic core. The renewal interest is attributed to the successful commercial scale deployment of carbon dioxide cooled reactor developed in UK. The success of these reactors motivates subsidy of the VHTR, which is the evolution design of previous GCR. The VHTR is characterized by the ability to produce very high coolant temperature, which exceeds 1000 ℃ and is planned to reach 1500 ℃ in the long term as shown above in Figure 1.1. It is one of the six reactors released by the Generation IV International Forum (GIF) and it is expected to be the final design of this generation of nuclear systems [1].

Generation IV reactors (Gen IV) are a set of theoretical nuclear reactor designs currently being researched. Most of these designs not expected to be available for commercial constructions before 2030. Generation IV International Forum (GIF) was set up in the early 2000s, at the initiative of the US Department of Energy. The role of GIF is to advance research and development on the design of nuclear energy systems for future applications. These systems include fast neutron reactors cooled by sodium (SFR), lead (LFR) or helium gas (GFR); very-high-temperature gas-cooled reactors (VHTR); supercritical-water-cooled reactors (SCWR) and molten salt reactors (MSR). One of the more immediate benefits of this international collaboration is the sharing of research outcomes among the signatories of each system agreement as well as a more general exchange of information; but the conceptual designs under development also benefit from the discussions taking place among scientists and engineers from different backgrounds

and experience. The current status and different project arrangements for Gen IV different systems are shown in Figure 1.2 [3]. Gen IV reactors are supposed to be more safe, secure, sustainable, competitive, and versatile than previous generation reactors. Enhanced safety is one of the major design criteria for Generation IV reactors, made all the more important by the recent accident at Fukushima Daiichi nuclear power plant. It is for this reason that GIF has set up a special task force to develop “safety design criteria” – in essence, design-independent safety requirements or options proposed by technology developers. The focus for Gen IV systems is on the usage of inherent safety features and designs. Sustainability means that Gen IV has the ability to meet the present and future energy needs for next generations. Economic goals focus on reducing operating and capital costs through increased efficiency, design simplification, and advances in fabrication and construction techniques. The high outlet temperature of the Gen IV systems (i.e, especially VHTR) affords high efficiency (i.e., >50%) electrical generation and the use of nuclear power for potential process heat applications, especially carbon-free hydrogen production using nuclear heat. Hydrogen production is a major potential use for Gen IV systems as it is the key element for the future US energy policy for reduced carbon emissions and increased energy independence. The long term vision of the GIF is to allow a 600 MWe VHTR dedicated to hydrogen production to produce 2 million cubic meters of hydrogen per day. This amount of energy is equivalent to 160,000 gallons of gasoline per day. The production of hydrogen may be carried out by using one of the following methods; steam reformation methane, electrolysis, or thermochemical cycles. Utilizing the high temperature effluents from VHTR as industrial process heat is one of the targeted applications in GIF. Nuclear Process Heat (NPH) range from

desalination and district heating on the low-end of the temperature scale to iron and glass manufacture on the high-end as shown in Figure 1.3 [1, 4].

System	Status	Signatories
GFR Conceptual Design and Safety	Effective since December 2009	Euratom, France, Switzerland
SCWR Thermal-hydraulics and Safety	Effective since October 2009	Canada, Euratom, Japan
SCWR Materials and Chemistry	Effective since December 2010	Canada, Euratom, Japan
SFR Advanced Fuel	Effective since March 2007	Euratom, France, Japan, Korea, United States
SFR Global Actinide Cycle International Demonstration	Effective since September 2007	France, Japan, United State
SFR Component Design and BOP	Effective since October 2007	France, Japan, Korea, United State
SFR Safety and Operation	Effective since June 2009. New PA signed in November 2012 with 3 new partners: CIAE (China),JRC (Euratom) and Rosatom (Russia)	China, Euratom, France, Japan, Korea, Russia, United States
SFR System Integration and Assessment	Signature process ongoing	China, Euratom, France, Japan, Korea, Russia, United State
VHTR Materials	Effective since April 2010	Euratom, France, Japan, Korea, Switzerland, United State
VHTR Fuel and Fuel Cycle	Effective since January 2008	Euratom, France, Japan, Korea, United States
VHTR Hydrogen Production	Effective since March 2008	Canada, Euratom, France, Japan, Korea, United States

Figure 1.2. Gen IV projects [3]

1.2. GAS COOLED REACTOR

The concept of the gas cooled reactors in the UK began with two air cooled graphite moderated reactors commissioned at Harwell in 1947 and 1948 by the United Kingdom Atomic Energy Authority. Then UK used Carbon dioxide as a coolant in the 11 commercial 'Magnox' power plants and the 7 commercial advanced GCRs [2]. Helium was used in the Dragon reactor, which was completed in 1964 and operated until 1974.

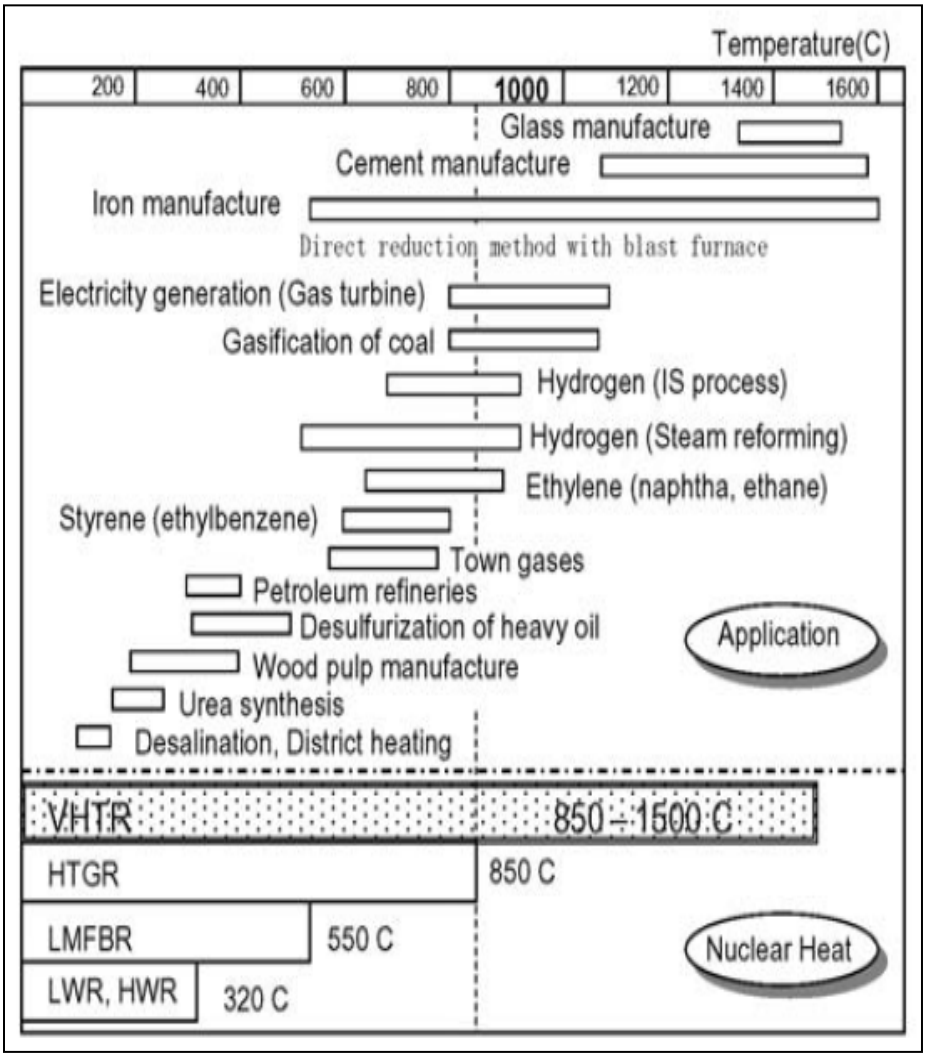

Figure 1.3. Nuclear process heat applications and required temperatures [1]

This reactor produced 20 MW of heat and did not have an electricity generation circuit [2, 5, 6]. Germany has a long history with HTGR that based on pebble bed concept. The Arbeitsgemeinschaft Versuchsreaktor (AVR) in Julich was sponsored by 16 municipal utilities in 1959. Construction began in 1961 and the reactor went into operation in 1966. This reactor is considered the first helium-cooled high temperature plant which used pebble-shaped fuel elements. This feature of fuel design enables continuous change and feed of new fuel material during ongoing operation with no need to shut down the plant. This reactor arrangement includes the arrangement of the steam generator above the core. The AVR consists of a pebble bed with 100,000 fuel elements. It is cylindrical and surrounded on all sides by a graphite reflector. The steam generator is situated above the reactor core and is shielded by the upper graphite reflector. Cold helium is transported through the reactor by blowers and is fed into the steam generator in a heated state. The helium returned to the lower reactor system, where the blowers are situated, in a cooled state [7, 8]. Some of the results and investigations on the AVR reactor is found in [9]. Then the German government subside the THTR-300 (300 MWe) pebble bed reactor. This reactor is a stream cycle plant for the generation of electric power. The heat generated in the reactor core of the helium-cooled, graphite-moderated, high-temperature reactor is transported via the helium gas coolant circuit to the steam generators where the heat is taken over by the steam/feedwater circuit and transferred to the turboset. The commissioning program with its results and operational experience are shown in [10].

Fort St. Vrain (FSV) is the first nuclear system in the USA to use a prestressed concrete reactor vessel (PCRV). This reactor, which was completed in 1967, was

designed and constructed by the General atomic company. This reactor uses U-235 as the fissile material, Th-232 as the fertile material, graphite as the moderated, cladding structures, and reflector and helium as the primary coolant. The graphite structure is a hexagonal prism. The helium coolant flows down through the reactor core and emerges to flow directly to the steam generators to convert water into superheated steam which then fed to main turbine generator to generate electricity [11]. More details about the performance of the FSV reactor could be found in [11-15].

The Japan Atomic Energy Research Institute (JAERI) designed and constructed the high temperature engineering test reactor (HTTR) in order to establish and upgrade the technology basis for the HTGR and develop the technology for high temperature heat applications. The reactor construction started in 1991. The HTTR is a helium-cooled and graphite-moderated HTGR with a thermal power of 30 MW and a maximum reactor outlet coolant temperature of 950 ℃ [16]. This reactor is considered the basis for the design of GTHTR300. The GTHTR300 is a high temperature gas cooled reactor with a gas turbine electric generation system. Its design and commission was started also by JAERI in 2001. More details about GTHTR300 design phases and application is found in [17, 18]. The reactor core of HTTR consists of hexagonal fuel blocks, control rod guide blocks and replaceable reflector blocks as shown in Figure 1.4. The design features of this reactor is shown in great detail in [16, 19]. Also, the development of the high temperature gas-cooled reactor (HTGR) fuel in Japan is mentioned in [20].

The Modular High Temperature Gas-cooled Reactor concept which was proposed originally as the ‘HTR-Module’ by Siemens German in 1979, shown in Figure 1.4, was applied to the HTR-10. These preliminary design features involve; the use of spherical

pebbles which are capable of retaining all radiologically relevant fission products up to fuel element temperatures of 1600 ℃.

Generally, graphite moderator is used in the core of the reactor to moderate the fast neutrons so as to the nuclear fission reaction criticality is maintained. The core of the HTR-10 is formed as a pebble bed with 27,000 spherical fuel elements. The pebble bed reactor is considered for its merit of continuous discharge of spent spherical fuel elements without shutting down the reactor, which can increase the reactor operation availability.

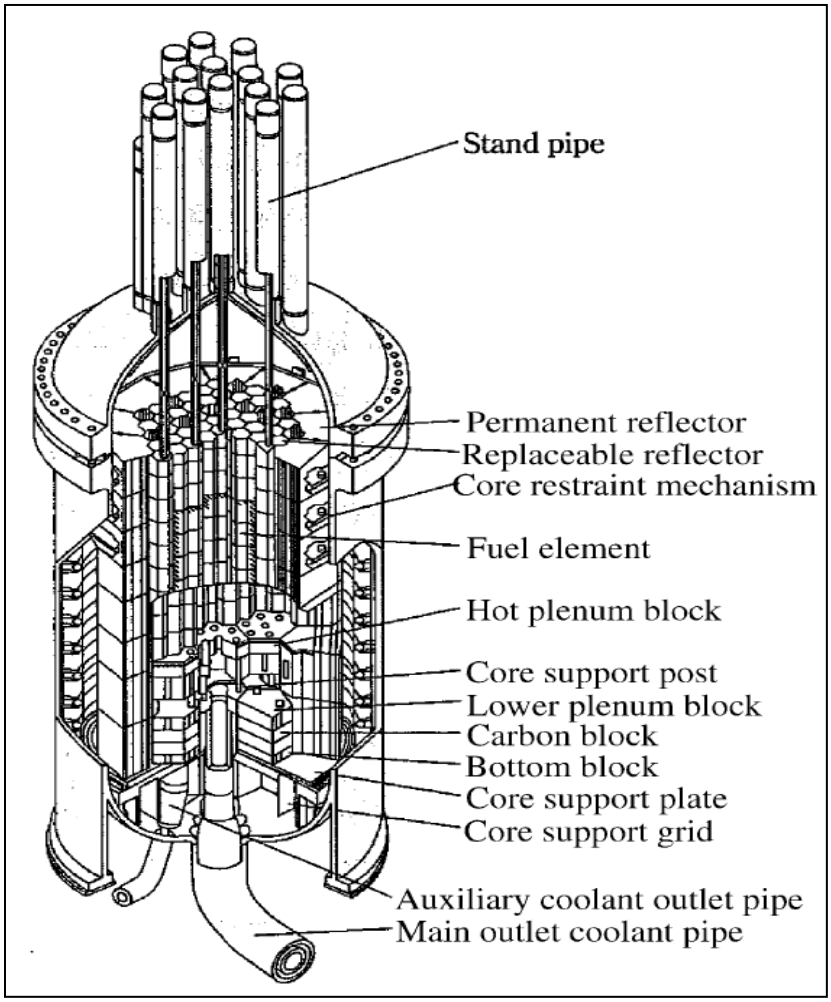

Figure 1.4. Reactor core structure of HTTR [16]

Helium gas coolant moves downwards through complex interconnected network of voids formed between pebbles and removes the heat from the fuel [21, 22]. The fuel pebbles drop into the reactor core and moves downward under the gravitational effect and then discharged from the bottom of the reactor. Then the fuel pebbles pass through defective fuel separator and the burn-up measurement facility one by one. The defective fuel elements and the scrap fragments should be sorted and dropped into the scrap contained. The fuel elements which have not reached the burn-up target (i.e., the amount of fissile materials in it) will be recirculated into the reactor core, and the spent fuel elements excessing the burn-up target will be discharged and transported into the spent fuel discharge tank.

The advantages and disadvantages of PBR are mentioned in Table 1.1. South Africa spent huge expenditures on pebble bed modular reactor (PBMR) before subsiding the project in 2009. The development of PBMR, proposed by Eskom, in South Africa was announced in 1998. The design features of the core are shown in Figure 1.5 The design features and operational experiences is similar to the features mentioned in previous parts for HTR-10 as China developed HTR-10 with guidance of AVR and PBMR [2, 23].

The PBMR is considered the reference design for NGNP pebble-based VHTR reactor configuration. The Gas Turbine Modular Helium Reactor (GT-MHR) is a nuclear fission power reactor design under development by a group of Russian enterprises (OKBM Afrikantov, Kurchatov Institute, VNIINM and others), an American group headed by General Atomics, French Framatome and Japanese Fuji Electric.

Table 1.1. Advantages and disadvantages of PBR [23]

Advantages	Disadvantages
The moving fuel pebbles provide variations in packing, physics, and heat removal.	Moving bed of complex-flow structure and path.
Inherent safety due to fuel type and gas coolant; hence a negative temperature coefficient is achieved, which means that if the temperature rises, the nuclear reaction is slowed and power is reduced.	Due to the system complexity, extremely complex transport and processes involved.
High outlet gas temperature yields higher thermal efficiency.	Accurate analysis of flow-field and heat transport in the dynamic core pose an extreme challenges to the efficient design and safe operation
High heat capacity and low power density.	
Unlike conventional nuclear reactors, pebble bed reactors do not need to be shut down in order to check the integrity and consumption of uranium and to de refueled, this is due to on-line refueling.	
Promises to generate less nuclear waste.	
The design produces a small reactor that can be built cheaply with short construction time and operated safety.	
The pebbles are supposed to survive at temperature of 1600 °C, far hotter than the worst foreseeable accident scenario.	

It is a helium cooled, graphite moderated reactor and uses TRISO fuel compacts in a prismatic core design. This reactor is considered the reference reactor for NGNP prismatic conceptual VHTR. The GT-MHR couples a gas-cooled modular helium reactor (MHR), contained in one vessel with a high efficiency Brayton cycle gas turbine (GT) which is contained in an adjacent vessel as shown in Figure 1.6 and core construction in Figure 1.7. The helium coolant is heated in the reactor core by flowing downward

through coolant channels in graphite fuel elements and then through the cross-vessel to the power conversion system. Heated helium from the reactor expands through the gas turbine to drive the generator and gas compressors.

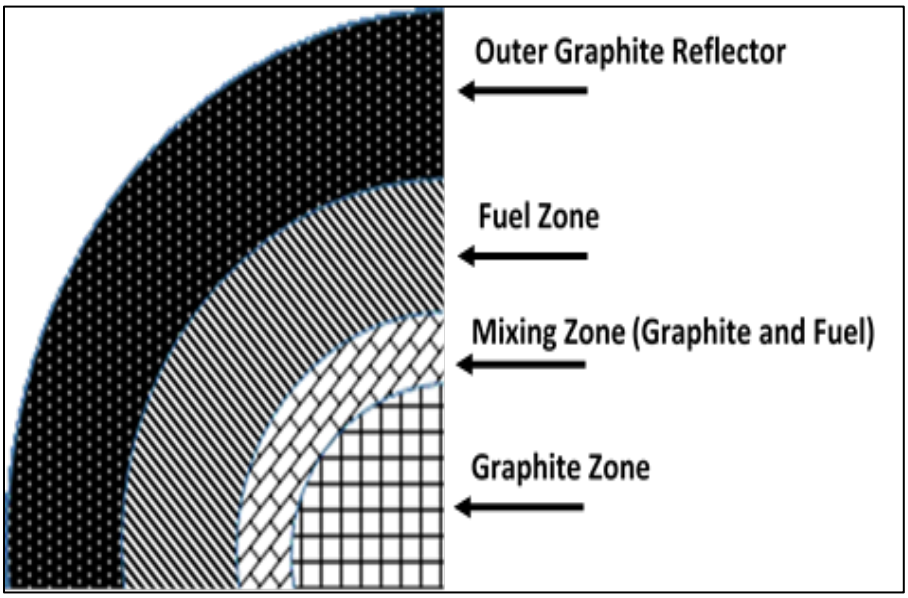

Figure 1.5. Core configuration of PBMR [23]

The use of Brayton cycle provides 48% efficiency which is higher than light water reactor nuclear plants. The GT-MHR has two active heat removal systems, the power conversion system and a shutdown cooling system that can be used for the removal of decay heat. The shutdown system is the reactor cavity cooling system (RCCS) surrounding the reactor vessel. The reactor was designed to permit the removal of decay heat via thermal radiation from the vessel, and conduction into the walls. More details about the GT-MHR is found in the [24-28].

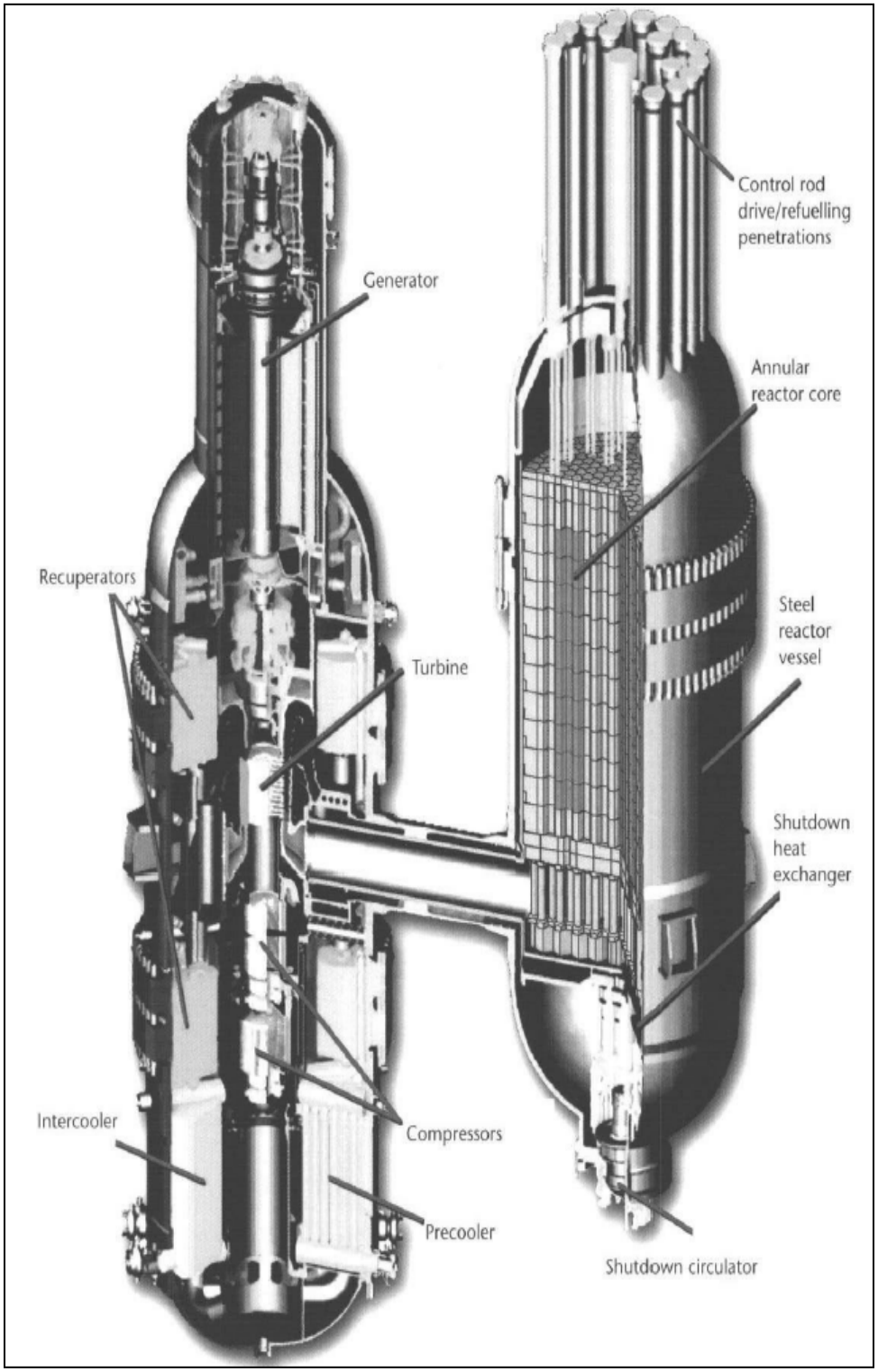

Figure 1.6. GT-MHR core design [24]

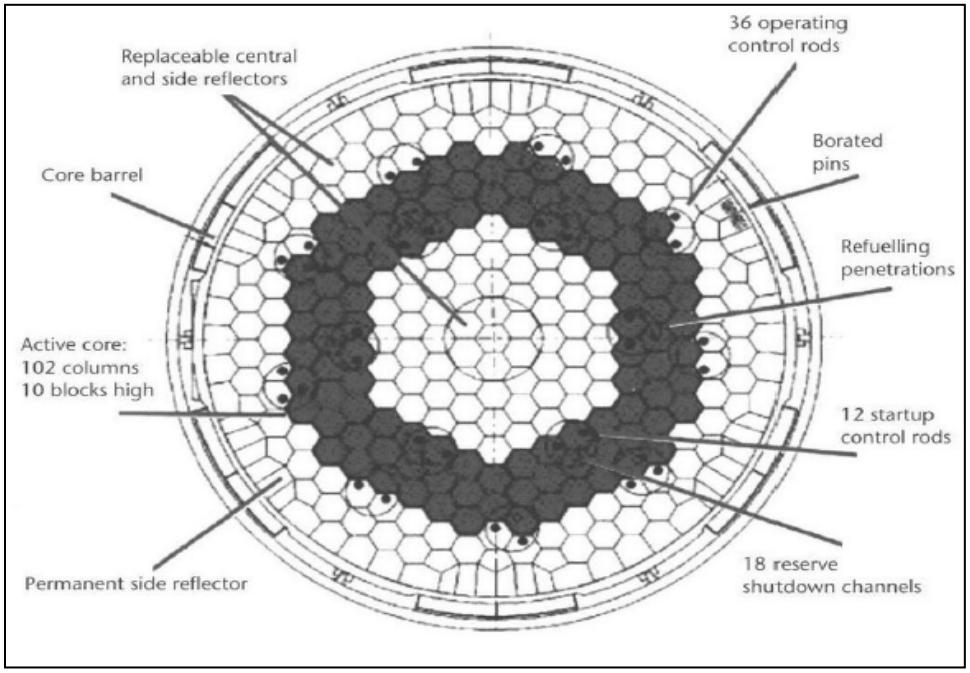

Figure 1.7. Core construction [24]

1.3. ACCIDENT ANALYSIS OF GAS COOLED REACTORS

The modular high temperature gas reactor depend strongly on passive decay heat removal in the case of accident scenario or in the case of absence of active heat removal system in which the core heat decay is transferred to and through pressure vessel and to RCCS (Reactor Cavity Cooling System) in reactor cavity by conduction, radiation , and natural convection. Important classification of accidents scenarios with all different reasons in parallel with recommended protection is presented in IAEA publication [29].

According to IAEA, accident analysis for modular high temperature gas reactors are classified in two categories based on frequency or by type.

- Classifications of events by frequency

The classifications of modular HTGR events by frequency can be investigated by two approaches based on the philosophy of safety margin. In the first approach which is

called deterministic approach, an event initiator is used as event frequency while the second approach is known as probabilistic approach (scenario frequency) that implement the event sequence and take in consideration the probability of failure and success of proposed events regarding the used equipment and operator in the plant [30-32]. Figure 1.8 shows a sample classification of events by frequency and consequence (dose) in which the events which have a high frequency uncertainties involve significant uncertainties in used models, data, and technical basis in analysis of accidents events. Both approaches; deterministic and probabilistic approach are common in safety analysis of modular high temperature gas reactor [32].

- Classifications by grouping of events by type

Individual accidents events that could be take place in the modular HTGR can come from combination of plant operational state (event sequence) or individual initiating event of the same type. The grouping can be built on dominating a phenomena taking place during accident scenario such as:

- Pressurized loss of forced convection
- Depressurized loss of forced convection
- Depressurized loss of forced convection with air ingress
- Core coolant bypass flow and crossflow
- Process plant coupling event
- Load change event
- Water steam ingress

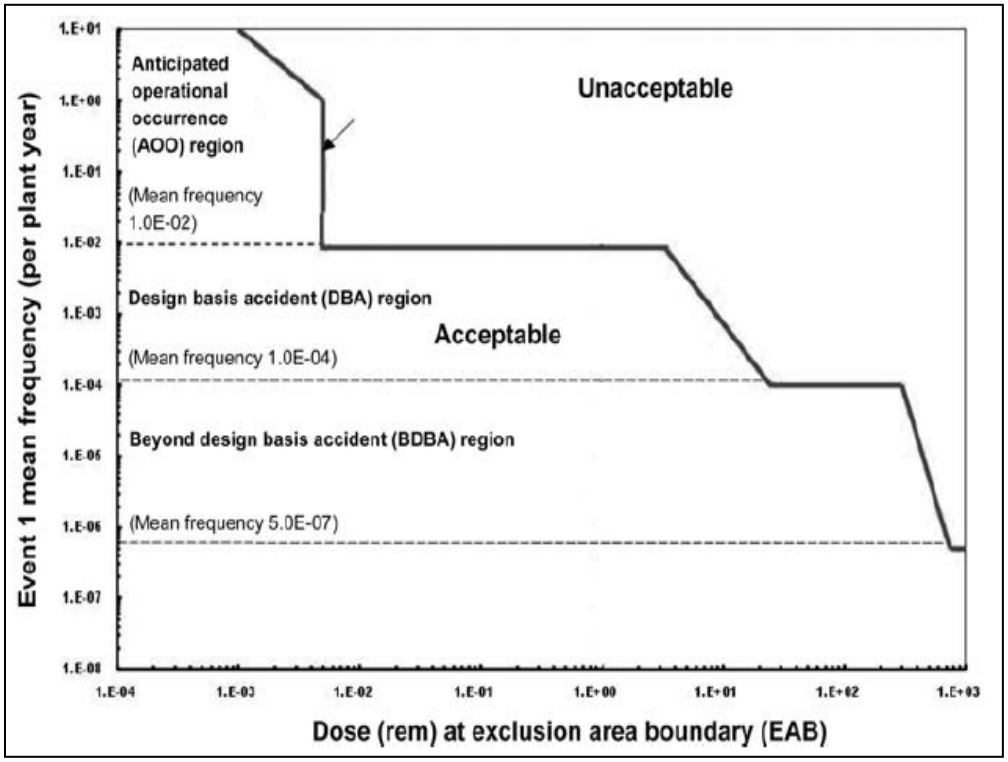

Figure 1.8. Sample classification of events by frequency and consequence (dose) [32]

1.3.1. Pressurized Loss of Forced Convection (P-LOFC or PCC). The PCC is an accident boundary remains close to normal operations and no depressurization or air ingress exists. Natural circulation is the primary mode of heat transfer during this event in the core which results in flow and temperature reversal. So PCC is the initiator of natural circulation [33, 34]. Natural circulation is the primary mode of heat transfer during this event in the core which results in flow and temperature reversal. So PCC is the initiator of natural circulation. PCC is associated with:

- Flow and temperature reversal (Due to natural circulation)
- Low flow
- Core coolant bypass flow

- Viscosity and friction effect for coolant
- The hottest region in the reactor will be in the upper plenum
- Radiant mode of heat transfer from upper plenum (top of core) to the vessel head
- Significant hot spots

There are many postulates that can be a reason for initiation the PCC scenario such as loss of power supply or loss of grid load, or failures of the primary circulating equipment (helium circulators or turbo machines):

- Complete loss of flow.

The PCC scenario is initiated by a complete loss of gas flow, where the forced convection through the core is lost. It is postulated that as the gas inertia decreases, the flow through some core channel will begin to reverse and move into a situation of intra-core recirculation. The flow pattern of the intra-core circulation is introduced in next sections.

- Outlet duct break.

This accident scenario is simulated by Oregon State University's HTTF facility by opening a valve between the inlet and the outlet ducts. This would allow a recirculation to establish. Results of this simulation is reported in the literature [34].

Failure of a single train of reactor cavity cooling system (RCCS) is single train RCCS failure is also simulated by HTTF. In this case, PCC is initiated by the loss of flow with failure of single train of PCC. HTTF RCCS is comprised of eight water cooling sections, where each section is considered as single train, each section is fed by its own inlet and outlet valve piping system. When one train is lost, this initiate the PCC

event leading to asymmetrical in core temperature. Results of these tests are also reported in INL/EXT-12-24701 [34].

1.3.2. Depressurized Loss of Forced Convection (D-LOFC or DCC). Loss of forced circulation with depressurization conditions may come from break in the pressure boundary of the system such as large leaks or ruptures in the piping and connection system. The D-LOFC involves some sort of reactor coolant system break which allow the primary coolant to leak into the cavity of the reactor. The D-LOFC with air ingress is classified a separate event because not all break in the pressure system with depressurization scenario can lead to significant air ingress in the core [35,36]. There are many reasons that can be consider the initiator for break of pressure.

- Double ended inlet-outlet crossover duct break.

The DCC event is initiated by the break of the concentric inlet and outlet ducts which allow for flow between both plena and the reactor cavity

- Inlet crossover duct break.

The DCC event is initiated by the break of the annular inlet duct which allows for flow between the upper plenum and the reactor cavity.

- Pressure relief valve break.
- Control rod drive nozzle break.

1.3.3. Depressurized Loss of Forced Convection with Air Ingress. The air ingress is a different scenario from DCC scenario. The air ingress is initiated by large enough break with a high enough rate of depressurization which consequently lead to air ingress into the vessel. The oxygen in the air oxidizes the graphite structure in the moderator and reflector and components within the vessel, and to the fuel particles

(TRIOS), and degrades structural integrity of the internal pressure vessel structure and the core through a chemical reaction with oxygen, this can lead to accumulation of explosive in the reactor and can potentially lead to a total damage. In addition to, the Air ingress events are categorized as low probability events [29, 33, 38-42] presented an example for simulation and investigation of air ingress scenario simulation for modular HTGR under different operating conditions and oxidation of graphite by oxygen. The reasons of air ingress:

- Double-ended inlet-outlet crossover duct break
- Break of the coaxial hot and cold ducts that connect the rector to the power system.

The types of air ingress [43]:

- Air ingress by lock-exchange flow

This type is initiated by flow of cold air to the bottom of hot duct to produce counter current flow through the hot duct in lower plenum to generate a cold plume which is responsible for a head waves that moves back and forth along bottom of lower plenum consequently promote mixing. As the times goes the lower plenum is filling with a cold air and interface with the hot helium in the core of reactor, this thermally interface is considered as the starting point of the molecular diffusion of air into the helium as shown in Figure 1.9.

- Air-ingress by molecular diffusion

The molecular diffusion comes subsequent to the lock-exchange flow due to the thermal interface between the cold air and the hot helium which stays above stagnant volume of air. Over time the cold air will diffuse into the hot helium and similarly the hot

helium will diffuse into the cold air so we have a mixture of helium-air mixture which is lighter than the cold air alone. The mixture will travel by counter-current flow through the top of hot duct and flows out to the environment as shown in Figure 1.10.

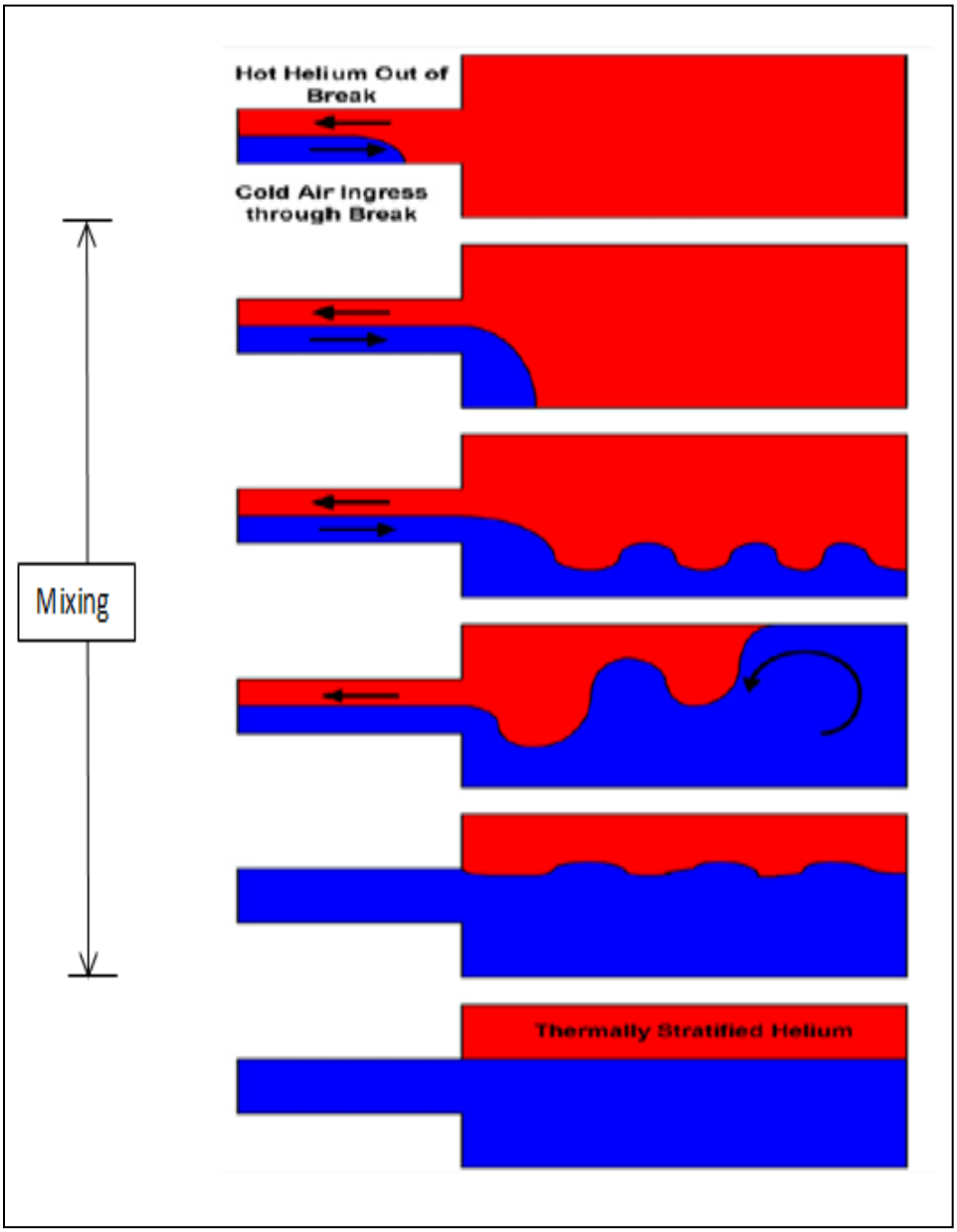

Figure 1.9. Lock-exchange mixing in VHTR [43]

1.3.4. Core Coolant Bypass Flow and Crossflow. The types of core coolant bypass accident scenario in very high temperature reactors will discussed in following section.

1.3.4.1. Core coolant bypass. One of the most importance phenomena that could take place in the core of prismatic VHTR is coolant bypass flow which takes place in the interstitial regions among blocks of fuel and reflectors due to presence of gaps between the neighboring fuel and reflector blocks.

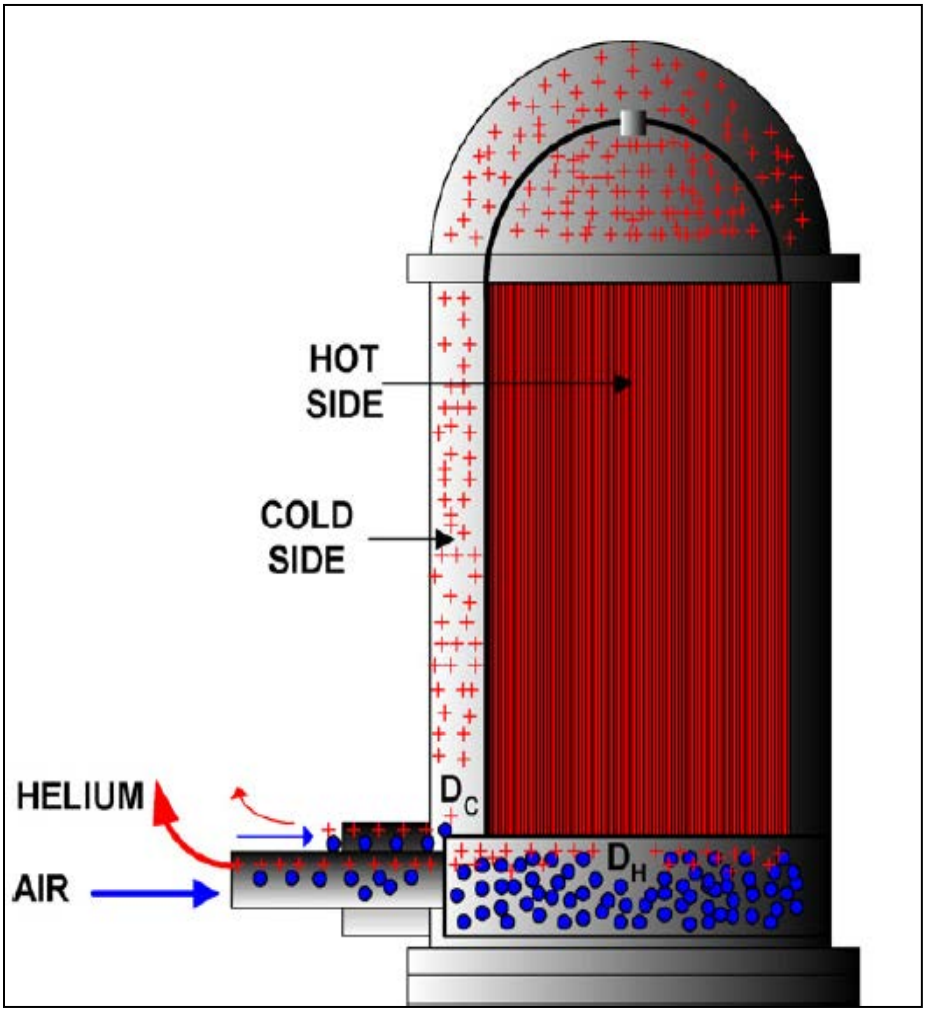

Figure 1.10. Air ingress by molecular diffusion on the hot and cold side of VHTR [43]

These gaps come from tolerances in fabrication and installation of the graphite blocks, in addition to, thermal expansion and radiation effect has a significant effect on geometry change of blocks and producing gaps. Flow in these gaps are called bypass flow and are significant for reactor safety analysis.

1.3.4.2. Cross flow. Groehn [44] was the first one to do experiment to investigate the cross flow in the gap region and he found out that the cross flow could lead to 72% reduction in coolant flow. There are a lot of studies conducted focusing on the cross flow and bypass and their effect on fuel cooling and hotspots in the core of VHTR [45-57]. Figure 1.11 shows the side view for bypass and cross flow in two blocks of prismatic VHTR.

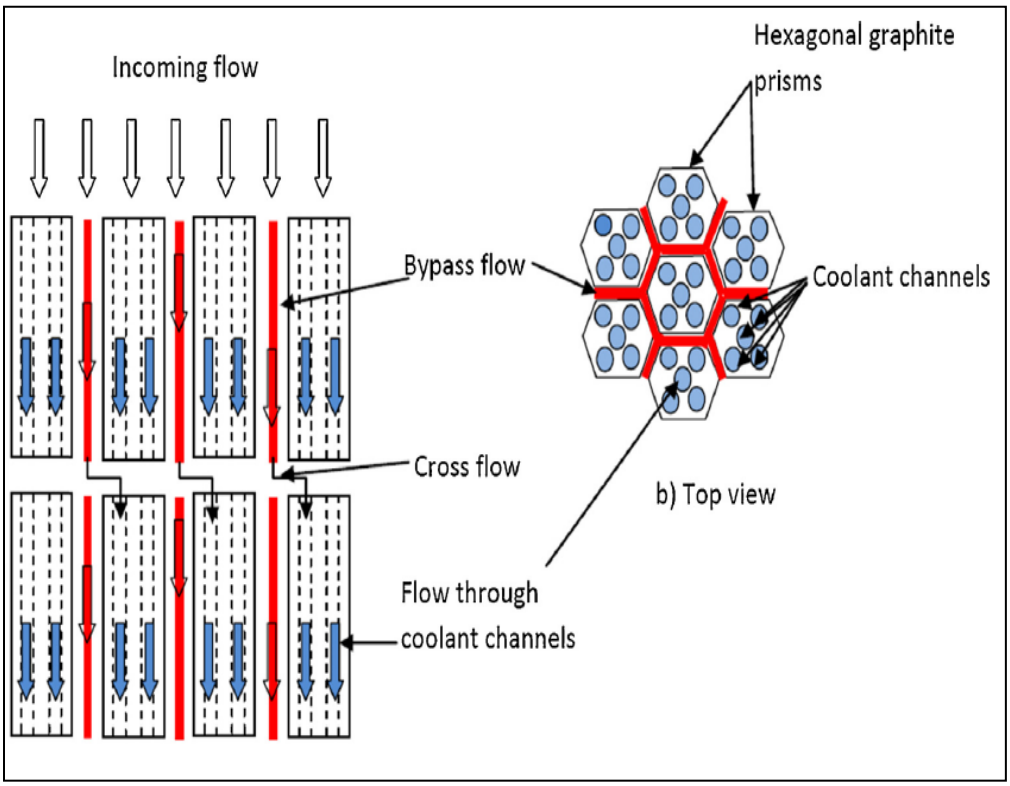

Figure 1.11. Side of prismatic core VHTR in case of bypass and cross flow [55]

1.3.5. Process Plant Coupling Event. In the coupling of VHTR with a chemical plant for producing hydrogen as an example, there are a lot of new risks resulting from operation of VHTR reactor and from chemical plant of producing hydrogen or other explosive and/or flammable products as well as toxic products. Due to all these risks CEA put a specific safety approach that demonstrate the expectable accidents [58]. There are two event to be considered in coupling VHTR with Hydrogen production plant as an example, one is called 'internal event or internal accidents' which take in consideration the change in mass and energy transferred between two plants in parallel with loss of physical boundaries between the VHTR and chemical plant which is represented by transients and break in pipes and in heat exchangers that taking place in the coupling circuit. The other type of events is called 'External event or external accident' this type takes in consideration the integrity of various equipment in plant such as emergency cooling system and VHTR containment , this type induce an external impacts on boundaries between two plants. There are few studies which focusing on coupling event of VHTR with hydrogen production plant [59-61].

1.3.6. Load Change Event. Load change event can be included in normal operation, and can be classified into two categories according to change in flow of coolant, one is accompanying with transient flow and other with steady flow, during this event the reactor trip does not occur and there is no failure in power conversion system which connected to reactor system, this will lead to core power increase or decrease:

- Load change associate with transient flow:

This event is initiated by reduction in flow of coolant or increase in the flow of coolant by coolant (Helium) inventory or turbine by pass flow control. The load change

due to reduction of flow is raised by 20% reduction in primary flow of coolant consequently reduces the power of the core due to raise in average core temperature and core outlet temperature will change and this promote the hot spots [62]. In addition to, the load change event can be generated by an increase of the primary flow of the helium (coolant) which increases the power of the core [63].

- Load change associate with steady flow:

This event is initiated due to flow symmetry in upper and lower plena, in which the core power reaches the steady state level and is balanced by reactivity feedback and control rod, this event is characterized as steady power operation [63].

1.3.7. Water Steam Ingress. Water ingress into the core of the reactor is one of the most important accident scenario for high temperature gas-cooled reactor during failure of steam generator. The water-steam ingress is initiated by break in the steam generator i.e. the steam generator loose its integrity, as a result of this the core filling with moisture and is transported by circulating helium, in which the steam –water mixture enters the side reflector and then passes to the top reflector and the reactor core. The water-steam ingress has a two significant effects on the performance of the reactor, the first effect is related to the corrosion of graphite of the reactor core and reflector which is classified as long-term effect, which is effected by mass of water ingress. The second effect is the positive reactivity insertion due to water ingress into the sub moderated reactor core which is classified as short term effect. Positive reactivity insertion is determined by the rate of water ingress into the reactor core [64]. Water-steam ingress accident is classified as rapid and severe accident due to high pressure difference between the primary and secondary circuit and positive reactivity.

There are two probabilities for the location of rupture in the steam generator; subcooled section or superheated section. The most common place of the break in the steam generator is the subcooled section [64] based on concepts of thermodynamics and heat transfer. Subcooled break will lead to flashing of the water into the primary circuit of reactor, the subcooled water ingress could cause a temperature reduction close to the break and consequently temperature and pressure reduction in the primary circuit. As time progresses, the continuous flow of water will make the water in the primary circuit to reach the saturation state in which the temperature decrease and the partial pressure will increase after this the water starts to evaporates and a mixture of water and steam flows to the core of reactor, but if the break occurred in the superheated section of steam generator, we will have a different situation where the pressure and temperature will increase in the primary circuit and steam remains in its state and flows to core. Siemens Interatom studied the water ingress into the core of reactor through one tube double ended rupture in the steam generator, they found out that this action produces 600 kg water ingress into the primary circuit in the VHTR module [65,66]. The total water inventory in the primary circuit can be limited to 3000 Kg for all possible break size in modular high temperature gas reactor. Several studies investigated the water-steam ingress for high temperature gas-cooled reactor [65-70].

1.4. LITERATURE REVIEW

1.4.1. Normal Scenario. Nakano et al. [45] presented three-dimensional thermal and hydraulic analyses to show how a VHTR with an outlet temperature of 950 °C would function. They found that it requires 90% fuel flow fraction to function

properly. Fuel flow fraction is defined as the core flow distribution in which the flow in few moderator channels is upward while the flow in the rest of moderator channels is downward.

Sato et al. [46] introduced a 3D computational fluid dynamic analysis conducted on a 1/12 sector of a prismatic block of the core of a VHTR. This was done in order to investigate the effect of the gaps within the blocks on the temperature distribution within the reactor. They found that increasing the size of the block gaps decreases the outlet temperature of the helium and increases the temperature gradient within the graphite blocks [46].

The correlation $N_u = N_{u_{FD}}$ [1+ 0.57e$^{-0.20(z/D)}$] was tested for model helium flow and heat transfer in the coolant channels by Travis and El-Genk [48]. They found when accounting for helium that flows through the gaps between fuel elements, or accounting for helium flowing into the holes for the control rods, the edge temperature is reduced, but the maximum temperature was observed close to the center of the fuel element due to less helium flow in central cooling channels. [48].

Sato et al. [50] used three dimensional CFD calculations to see how inter-column gap-width, turbulence model, axial heat generation profile, and geometry change from irradiation-induced. They found that as the gap between fuel blocks increase, amount of bypass flow increases. This causes hot spots to form in the reactor, which can increase the maximum core temperature and the temperature variation throughout the reactor [50].

Simplified models have been proposed by Tak et al. [52] to calculate the temperature of the fuel, graphite fuel blocks, and helium coolant. They found that there are large temperature variations when there is a uniform power distribution throughout

the fuel assembly. They also found that the unit cell approach was accurate when the coolant flow between the fuel blocks is small. If the coolant flow between the blocks increases, then the unit cell model greatly underestimates the reactor temperature [52].

Numerical simulation and turbulent convection heat transfer correlation for coolant channels in a Very-High-Temperature Reactor is introduced by Travis and El-Genk [53]. They used a 3-D computational fluid dynamics numerical calculations to develop a turbulent convection correlation for helium coolant flow in channels of a prismatic core very high temperature reactor. They found that the local turbulent heat transfer coefficient increases near the entrance of the coolant stream, but its effect diminished once the coolant travels up the channel [53].

Wang et al. [55] introduced CFD analyses simulating the Texas A&M University scaled down model of the GT-MHR to analyze only the fluid flow and mass flow rates. The main thing to note is that as gap width between blocks increases then the mass flow rate in the bypass flow significantly decreases and flow in the coolant channels significantly increase [55].

Valentin et al. [71] investigated how the forced convection of the helium gas in the VHTR changed between upward flowing stream and a downward flowing stream. They found that a downward flow of the gas caused higher upstream temperatures and lower downstream temperatures than an upward flow. This was because buoyancy-induced heat mixing caused higher convection heat transfer and lower wall temperatures in the downstream for a downward flow [71].

Valentín et al [72] investigated helium flow laminarization at high temperature and high pressure in a graphite flow channel. They found that there can be a significant

reduction in the Reynolds's number between the inlet and outlet of the channel. They also found that flow laminarization occurs when the local Nusselt number decreased 20% below the Nusselt number predicted by the modified Gnielinski correlation [72].

1.4.2. Pressurized Conduction Cool Down (PCC) and Depressurized Conduction Cool Down (DCC) Accidents Scenario. The current work deal with the experimental simulation of PCC and DCC, therefore there accident scenarios will be discussed in little detail. Haque et al. [73] represent an earlier attempt at constructing a thermal analysis of the VHTR using CFD code THERMIX. They found in all simulated cases that peak fuel temperature would not exceed 1600 °C. However, for DCC peak fuel temperature were much closer to 1600 °C which is considered as the design limits. For this reason, subsequent work was focused on DCC. They also performed analyses with varying inlet and outlet temperature to see how that would affect results. It appears that raising the inlet or outlet temperature has a similar effect in raising the peak fuel temperature. Neither inlet nor outlet temperature primarily control peak fuel temperature, it is the combined effect of both [73].

Kim et al [35] investigated how changes in graphite properties would affect maximum fuel and reactor pressure vessel temperatures. They found that reactor pressure vessel maximum temperature is much less sensitive to graphite properties than core temperature. In PCC accidents, changes in conductivity created greater response whereas in DCC volumetric heat capacity was more sensitive parameter. The most interesting result was that the reactor pressure vessel's maximum temperature was positively correlated with graphite conductivity. This observation is because heat transfer to the

reactor pressure vessel RPV increases with conductivity more quickly than heat transfer in a radial direction [35].

The Oregon State University (OSU) constructed a High Temperature Test Facility (HTTF) as a scaled down model of the Modular High Temperature Gas Reactor (MHTGR) [74]. The main purpose of the experiment was to compare the data during DCC from the HTTF to the MHTGR. Further, they tested the RELAP5-3D computer code to see if it accurately modeled the HTTF. The goal was that all predictions and scaling would be accurate so that the HTTF could be used as an effective model for MHTGR experiments. The results found that the HTTF had a few key failings in its ability to simulate the MHTGR. Namely, it lost heat at a much higher scaled rate than the MHTGR. Also, at the beginning and end of the diffusion phase of DCC, HTTF did not provide accurate simulation. However, HTTF did provide many valid simulations for natural convection phase, and gave good estimates of temperature profiles and peak temperatures during these listed phases (despite the additional heat loss). The RELAP model worked well in these cases using separate effects tests, but it was concluded that the Integrated Effects Tests model needed improvement [74].

The AREVA HTR (High Temperature Reactor) reactor is designed to produce high temperature steams [75]. AREVA facility essentially investigated safety of the initial design, in the case of depressurized conduction cool down (DCC) accident. Primarily, the goal was to make sure that the material choices and design are acceptable, and that running the reactor at 625 MWt will be safe. The study uses Star-CD as its CFD software. It studies 4 cases for DCC. There is the nominal case, which is just the expected case, and then 3 cases that take into account further things that could make the scenario

less safe, such as higher decay heat, higher inlet temperature, and less conductive graphite (due to radiation). In all cases, the results were within the acceptable limits. This effort allows for further detailed analysis to be performed as the design is finalized, knowing that the initial design choices were functional [75].

Odmaa and Obara [76] considered the impact of placing a prismatic HTGR (high-temperature gas-cooled reactor) below or above ground and how that choice would affect the design considerations, as the conduction through soil or convection through air works differently. It was found that changes in structural materials had the same affect in either location. However, above ground the primary variable affecting reactor building minimum size was reactor temperature. For below ground the size was most influenced by the power of the reactor [76].

Tung and co-worker [77] investigated the circulation of coolant during normal operations and during a loss of flow accident (LOFA). During normal operations, the coolant is forced to circulate throughout the reactor and the flow is turbulent, but during a LOFA the flow is significantly slowed down. Using computational fluid dynamic calculations they investigated the initial turbulence of the natural circulation effects on natural circulation of the coolant during an accident scenario. They found that a slower initial circulation resulted in fewer recirculation zones, and the number of recirculation zones increased as the turbulence of the initial coolant flow increased. It also found that larger recirculation zones lead to effective passive cooling of the reactor core under LOFA [77].

Valentin et al. [78] presented numerical analysis to study the effectiveness of the passive cooling in a VHTR. It is important to ensure that passive safety can keep the

reactor from overheating in the event of an accident. This cooling is caused by the natural convection of the coolant as it circulates throughout the reactor vessel. The thermal conductivity of the graphite in the core also effects the passive cooling in the VHTR. They found that increasing the viscosity of the coolant increases the average temperature of the reactor wall. They also found that the average wall temperature decreased as the radius of the cooling channel decreased. This is because a greater mass of graphite in the reactor means that more energy is required to raise the temperature of the reactor's walls. The results concluded that an optimal radius of the cooling channel must be chosen to balance the cooling effect of the forced circulation during normal operations and the passive cooling during LOFA [78].

Before the Very High Temperature Reactor (VHTR) can be built, certain scenarios must be studies which have been shown to cause hot spots in the reactor. These phenomena include degraded heat flow, the effect of bypass flow, and non-uniform heating in the core. A test facility was designed to study the effects of these phenomena during transient conditions [79]. Valentin et al. studied the effect of two phenomena on the heat transfer in the reactor. They looked at flow laminarization and non-uniform heating in the reactor core. They found that the amount of heat transferred by convection decreases from the inlet to the outlet of the reactor. They could not make a strong conclusion on the effects of non-uniform heating, because graphite's high thermal conductivity cause an even distribution of heat throughout the reactor core [79].

Bertrand et al. [60] reported a study of additional risks that would come from coupling a VHTR with a hydrogen production plant (HYPP). Under normal operation, the heat from the VHTR provides the energy needed to drive the chemical reactions of

hydrogen production. The accident scenarios were divided into two cases. The internal case, where problems in the HYPP lead to problems for the VHTR through the coupling. One case important is where part of the HYPP need shut down or operates under reduced capacity. The VHTR produces a fixed power, so extra energy needs to be used up in some other way (a secondary heat exchanger) or be dumped out. Other internal cases are when hydrogen makes its way through the coupling pipes into the reactor building of the VHTR due a pipe rupture. External accidents come from things like hydrogen explosions or SO2 release from the HYPP. They concluded that a safety distance of 100 m between the HYPP and VHTR could provide sufficient safety in these scenarios. Their mainly focused was on outlining problems and providing some solutions, they didn't go into much detail on the CFD analysis of the solutions [60].

It is important to study the passive safety systems of small and medium sized reactors. This will allow us to see how reactors behave in an accident scenario. Previous studies have found that when a reactors shifts from forced convection as a cooling method for normal operation to natural convection, the ability of the coolant to remove heat can be significantly reduced. Wibisono et al. [80] studied single phase gas, water, and liquid metal reactors with passive safety features. They found that a reactor with a single phase coolant system will lose its ability to remove heat once forced convection is stopped. The water cooled reactor was found to still have its ability to remove heat when forced convection was stopped if the reactor was large. This ability was weakened as the size of the reactor decreased. The liquid metal system was found to be safer in an accident scenario than the water system, but further research is needed. Liquid metal system's ability to passively remove heat also weaken as the size decreases [80].

Conceptual design for a small modular district heating reactor for Mongolia has been introduced by Sambuu and Obara [81]. They discussed a small high temperature gas cooled reactor design that could be built in Mongolia to help meet rising energy demands in the country. Such a reactor must have a long core life and must have the ability to passively remove heat in the event of any accident. The core was chosen to have a diameter of 8 m, a height of 8 m, which can generate 330 MW of power. It was proposed to be able to run for 16 years with 20 wt% enriched uranium. Sambuu and Obara proved that a nuclear reactor could help provide the much needed energy to Mongolia by designing a small reactor that is relatively cheap, lasts a long time, and has passive safety features. The prismatic HTTR designed by Japanese scientists meets these criteria. Figure 1.12 shows the core temperature changes after shutdown of reactor surrounded by reflectors ((a) design limit, (b) 8.72 × 9.16 m core, (c) 8 × 8 m core). This reactor has a core life of 16 years without refueling, and should be able to generate 330MWth of power [81].

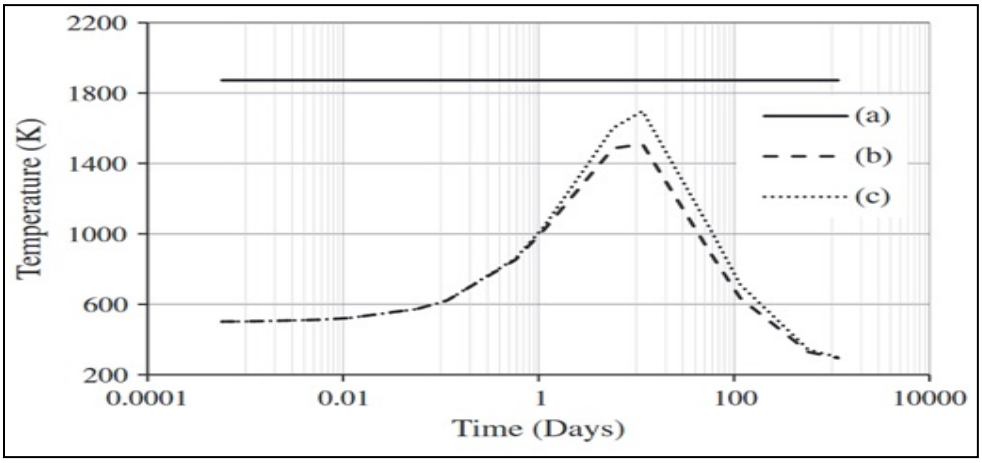

Figure 1.12. Core temperature changes after shutdown of reactor surrounded by reflectors [81]

Valentin et al. investigated the abnormal heat transfer and flow in VHTR core [82]. The purpose of their experiment was to find the conditions which would cause abnormal heat transfer phenomena to occur in the very high temperature reactor with a prismatic core. They tried to find what could cause flow laminarization to occur in this reactor. A 2.7 m long graphite test section was created and used to study the natural and forced circulations of helium, nitrogen, and air in a high pressure and temperature situation. They found that a turbulent gas flow leads to greater heat being transferred by convection in the reactor. They concluded that the coolant became less turbulent between the inlet and the outlet of the reactor model. They also found that turbulence decreased as the temperature of the reactor increased. As the turbulence of the gas decreases, the heat transfer by convection also decreased. They also found that importance of heat transfer by radiation increased as the thermal conductivity of the graphite decreased [82].

The scaling analysis of the High Temperature Test Facility HTTF was investigated at Oregon State University [83]. They found that due to the quicker heat removal, the HTTF would not show a peak temperature after the PCC began, but fuel temperature would monotonically decrease. They suggested some ways to make the HTTF behave more like MHTGR, one way would be to restrict designed mass flow rates further to limit heat removal. Another possibility would be to decrease core power more slowly after PCC started to simulate the slower decay heat and hopefully see a temperature peak. The HTTF materials could also be modified for more accurate thermal conductivity scaling [83].

Valentín et al. [84] presented an analysis of the heat transfer in the Very High Temperature Reactor with a prismatic core during an accident scenario. They looked at

the role of conduction, forced and natural convection, and radiative heat transfer during accident scenarios that lead to pressurized conduction cooling, depressurized conduction cooling, and forced convection cooling. COMSOL Multiphysics code was used to model the reactor and examine the radiative heat transfer between the reactor's graphite core and surrounding graphite blocks. They found that this radiative heat transfer could account for 20-30% of heat removed from the center block during normal operation, and it could become the primary heat transport mode during an accident situations. They used a computer simulation to see how heat is removed from the reactor's graphite core during an accident scenario. They found that the amount of heat transferred from the core to the graphite blocks surrounding the core was quite significant in an accident scenario. As much as 42% of the core's heat was removed through radiative heat transfer. This process is very important in preventing the reactor from overheating [84].

Valentín et al. [85] looked at both numerical and experimental results dealing with the thermohydraulic behavior of the coolant in a VHTR under steady state, transient, and accident scenarios. The experiment was carried out using a 2.7m long graphite channel equipped with four 2.3kW heaters. They looked at how heat was transferred within the column under these conditions as well as looking at how turbulent flow effected the transfer of heat within the column. They concluded that the Reynolds number decreased by 35% between the inlet and the outlet of the channel. They also concluded that natural circulation of the coolant will occur in an accident scenario in the VHTR because of differences in fluid temperatures and densities [85].

The GAMMA+ code was used to model a LOFA with a failure of the reactor cavity cooling system (RCCS) in a prismatic core gas cooled reactor by Kim et al.[86].

They found that the maximum core temperature could exceed 1600 °C within 50 hours during LOFA with the failure of the RCCS. They concluded that the maximum temperature of the core and the vessel increased as the variation of the thermal conductivity of the graphite increased. They also found that without an insulating layer in the reactor vessel it is very difficult to calculate the maximum reactor temperature. It can be concluded that the structure of the reactor and the materials surrounding it can have a significant impact on the maximum temperature of the reactor [86].

Computer models have been used to study the prismatic gas cooled very high temperature reactor ability to prevent a meltdown during a loss of flow accident because of its ability to naturally circulate the gas coolant in a situation where the forced coolant is stopped by Tung et al. [87]. But most models have only looked at a small section of the core. They looked at the laminar and turbulent flow in a 1/12 section of the reactor core using a computational fluid dynamic analysis. They found that the temperature distribution within the fuel core is not symmetrical during normal operating conditions or during a loss of flow accident. They also found a lack of symmetry in the heat transfer throughout the channels and in the flow of the coolant in the upper plenum [87].

2. STUDY THE EFFECT OF THE OUTER SURFACE TEMPERATURE OF THE DOWN-COMER CHANNEL AND UPPER PLENUM

As the world searches for an energy source with high energy density, clean, abundant, and storable nature to avoid global warming issues, very high temperature reactor (VHTR) seems to be a promising solution, particularly the possibility of producing hydrogen. VHTR is a gas-cooled and graphite-moderated reactor designed to accomplish future energy needs. VHTR is considered as a Generation IV reactor with higher safety and thermal efficiency and lower operation and maintenance costs, and due to high temperature helium coolant, it could possibly produce hydrogen through thermo-chemical methods. There are two versions of VHTR: pebble bed reactor (PBR) and the prismatic modular reactor (PMR), which are promising candidates [88]. In last decade, extensive studies on VHTR applications were focused on high temperature outlet and hydrogen production. For industrial heat source as well as high efficiency electricity production, very high temperature steam ranging from 700 °C to 850 °C seems to be very attractive requiring additional studies focusing on VHTR. VHTR coupled with direct gas cycle gas turbine systems has superiority for high efficient electricity generation [89] in addition to possible hydrogen production. General Atomics' Energy Multiplier Module (EM2) is the most promising PMR design for a gas-cooled reactor with an outlet temperature of 850 °C. With its modular design and small size, it is characterized as a small modular reactor (SMR), making it an attractive Generation IV contender. Prismatic design is comprised of hexagon-shaped graphite blocks containing fuel rods with dispersed Tristructural-isotropic (TRISO) particles as the nuclear fuel (Figure 2.1, 2.2) [90,91]. Graphite blocks also contain coolant flow channels for helium (coolant) from

upper plenum to the lower plenum for normal operations. However for accident conditions, such as pressurized conduction cool down (PCC) scenario, natural circulation is used as a passive safety mechanism.

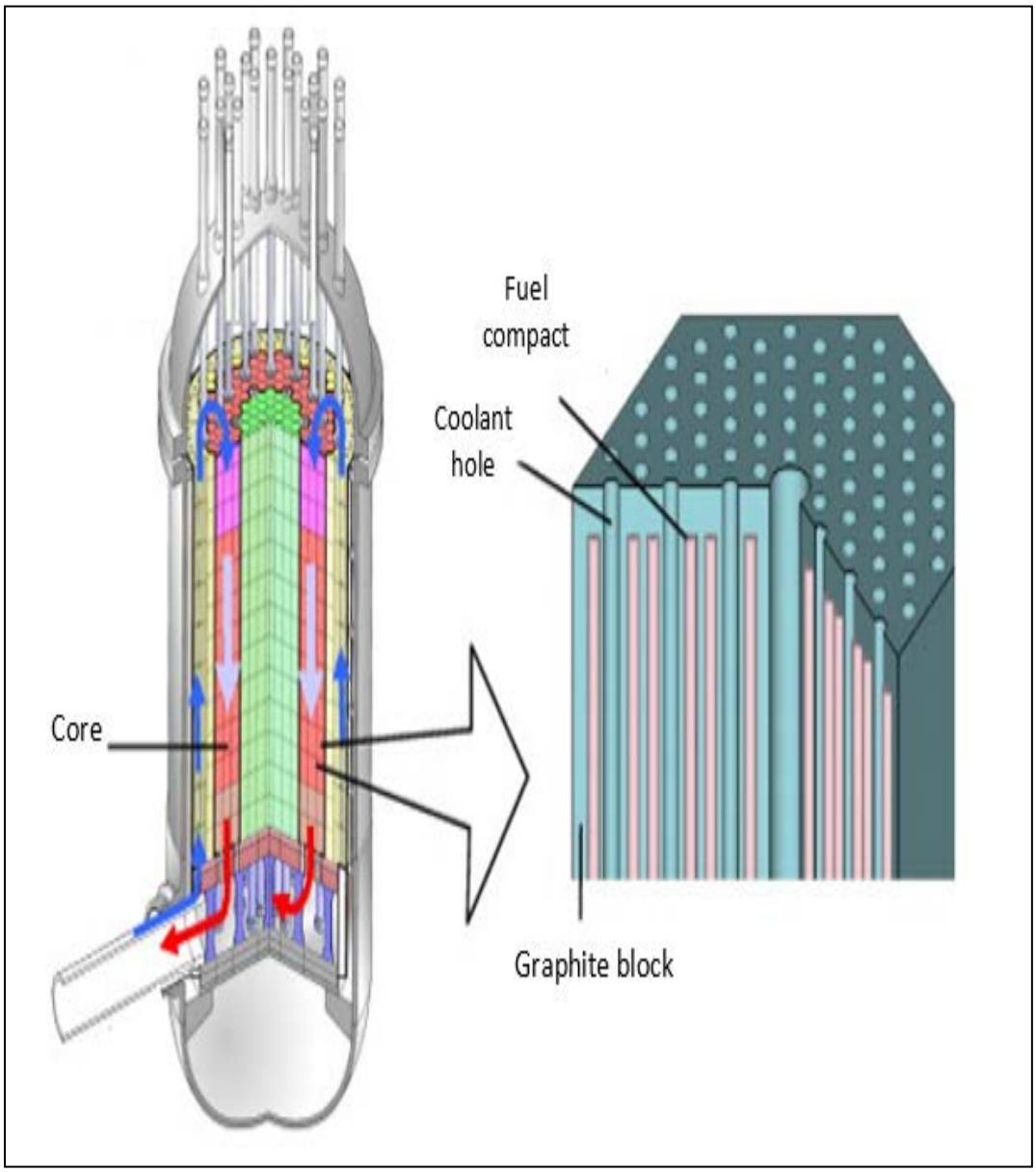

Figure 2.1. Core internal structures of PMR

For PPC, which means the loss of cooling has occurred but the primary pipe still remains at full pressure, the hotter coolant channels will have helium flowing upwards and returning from the cooled channels.

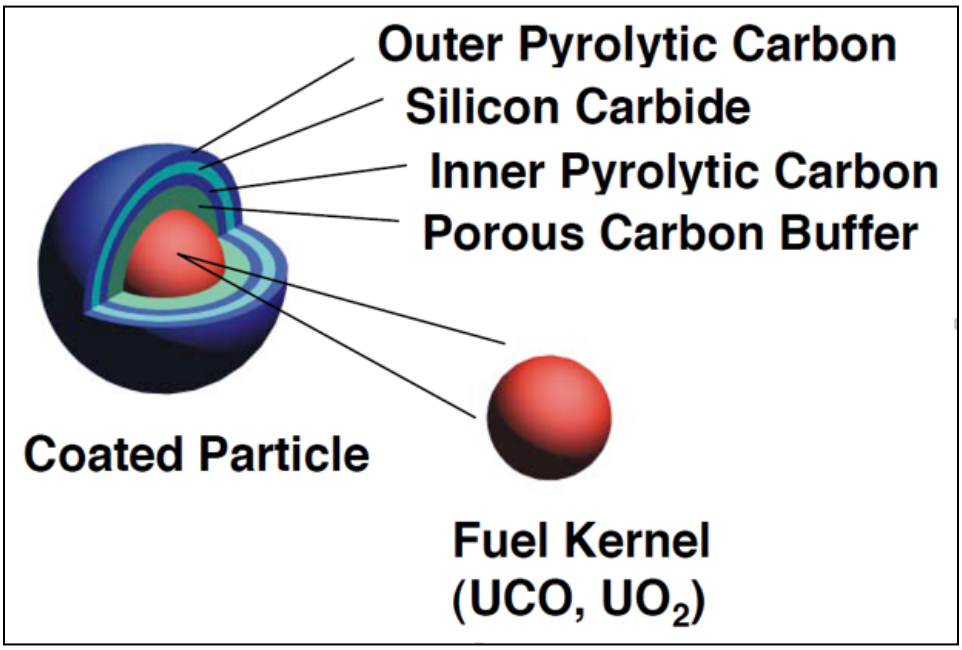

Figure 2.2. Coated Tristructural-isotropic (TRISO) particles

The second possible scenario could be that of depressurized conduction cooling (DCC), which means a primary pipe rupture accident occurred and the system pressure is dropped down immediately. In this case, gas coolant is expected to enter the reactor pressure vessel from the breach. Earlier studies demonstrated that it is possible to prevent a core meltdown by natural flow of heat under both PCC and DCC conditions [92]. Many studies have been conducted to investigate heat transfer in PMR and VHTRs [93]. There are extensive computational studies in the literature regarding the natural circulation within the PMR under accident scenario. Kao et al. performed the natural flow conditions

in plenum to plenum and identified streamline and velocity variations in the upper plenum and the two channels at given initial conditions for two different cases of 0.8 MPa and 4.2 MPa [94]. Yu-Hsin Tung et al. performed CFD calculations of natural circulation at high temperature following a postulated pressurized circulation shutdown and presented results to demonstrate the potential for natural circulation loop establishment between the core itself and the upper and lower plena. Flow paths in the gaps between the graphite blocks that allow bypass flow to occurred was also observed in their results [95]. Moreover, the influence of several parameters on key phenomena related to degrade heat transfer in a VHTR was performed by Valentín et al. [85]. They found significant reductions of up to 35% in Reynolds and Nusselt numbers between the test section inlet and outlet, and they concluded that due to fluid temperature and density differences between the hot fuel zone and cooler reflector zone, natural circulation flow is expected to establish in VHTR under PCC and DCC conditions. Takeda et al. performed experiments and numerical analysis of a control method for natural circulation with air and helium when injected during DCC conditions. Their study suggests that the velocity of the natural circulation of air can be reduced by injecting helium gas into the top of the channel. Moreover, the ordinary natural circulation of air could be controlled by injecting a small amount of helium gas. All these efforts were focused on the overall velocity and temperature measurement, and no effort is reported in the literature when detailed velocity and temperature profiles are reported. Hence, there is a real need to provide benchmarking heat transfer data within a representative geometry under natural circulation [96]. Said et al. experimentally investigated the effect of the outer surface temperature of the upper plenum and cooled channel in a scaled-down dual channel

facility in mReal in Missouri S&T by using air as a coolant [97]. In VHTR system, helium gas is considered as coolant; therefore, additional emphasis is placed on generated heat transfer data for helium. The current study is significant particularly because heat capacity of the helium is much greater than the heat capacity of the air, which will have profound effects on natural convection/circulation phenomenon. In this paper, experimental results and analysis are provided for natural circulation with helium using advanced instrumentation detailing heat transfer data in terms of temperature fields (centerline helium and inner wall surface temperatures) and heat transfer coefficients under natural circulation. The effect of the outer surface temperatures of the upper plenum and downcomer channel at steady state are investigated for helium at 413.685 kPa. The collected data in this study can provide the necessary benchmark data to validate thermal hydraulic codes such as; RELAP5-3D, CFD-STAR-CCM1, CFD-Fluent, and so forth.

Since the inception of the passive safety concept for nuclear reactors, natural convection has been extensively investigated [98,99]. Basu and co-authors summarized the status of single phase natural circulation studies for nuclear application [100]. Another publication by Beeny and Vierow investigated the passive safety and natural circulation features of Gas-cooled reactor [101]. Vijayan presented the results of an experimental study on natural circulation with through analysis of the results [102]. Velocity characterization of natural circulation flow was also reported in the literature [103]. In general natural circulation has found its application in many other fields. For example, Budihardjo and co-workers reported a new correlation for natural circulation in a solar system [104].

2.1. EXPERIMENTAL WORK

2.1.1. Missouri S&T Prismatic Scaled-Down Dual Channel Facility. Oregon State University (OSU) supplied a ¼ geometrically scaled-down experimental facility named High Temperature Test Facility (HTTF) based on the modular high temperature gas-cooled reactor (MHTGR) design specifications. The HTTF is capable of simulating the important thermal hydraulic behavior during accident PCC and DCC scenarios for the MHTGR. The similarity between HTTF and MHTGR has been assessed via computational investigations carried out to determine how the HTTF simulates the hot helium coolant gas flowing into the upper plenum during accident scenarios. Despite scaling distortions caused by the complexity of the phenomena encountered in the VHTRs, these investigations have shown a strong similarity between HTTF and MHTGR, which is why Missouri S&T adopted the same geometrical scaling ratio utilized by OSU in developing the first phase of the Missouri S&T facility, which is considered a scaled-down separate effects test facility. The two plena of the current facility are ¼ scaled down (i.e., axially and radially) with reference to the HTTF. The core (i.e., channels) is ½ axially scaled down relative to the HTTF core dimensions, while channels diameter is kept the same as HTTF as shown in the table below. The dimensions of the S&T facility are compared with OSU's HTTF in Table 2.1. Also, an extensive computational work has been performed to guide the design and experiments in terms of matching thermal hydraulic parameters between the current work and OSU-HTTF [94].

Table 2.1. Dimensions of S&T Facility with Reference to OSU-HTTF

Parameter	S&T Facility	OSU-HTTF
Tube diameter (m)	0.016	0.016
Coolant channel length inside block (m)	1	2
Core diameter (m)	0.3	1.2
Upper plenum height (m)	0.239	0.956
Outer vessel diameter (m)	0.381	1.524
Number of channels	Two channels (one upward flow and other downward flow)	- 516 coolant channels - 210 Heater rod - Six inner gap channels - 36 outer gap channels

2.1.2. Test Facility Description. The mReal research team at Missouri University of Science and Technology (S&T) has designed, developed, and tested a scaled-down dual-channel facility with reference to Oregon State University-High Temperature Test Facility (OSU-HTTF). The height of the current setup is 1.62 m tall with a 0.305 m diameter grid plate. Figure 2.3 shows the layout of the seven prismatic graphite blocks in the PMR and the relative locations of the two channels modeled in the current study. Each graphite block makes up a single nuclear fuel channel (shown as a heating rod) surrounded by six coolant channels. A picture of the Missouri S&T scaled-down facility is shown in Figure 2.4 a. In its current design, it is comprising of two channels; for the center block is a single riser channel (heated) for upward flow, while the outer block is a downcomer channel (cooled) for downward flow (Figure 2.4 b). The riser channel's outlet is mixed in the upper plenum and goes back via the downcomer channel to the lower plenum (Figure 2.4 a). This investigation used helium as the working fluid to conduct natural flow experiments. All experiments were conducted at a pressure of

413.685 kPa. A pressure gauge (PERMA-CAL INDUSTRIES, INC., CAGE 59018) with an accuracy of ± 1% has been used to measure the operating pressure.

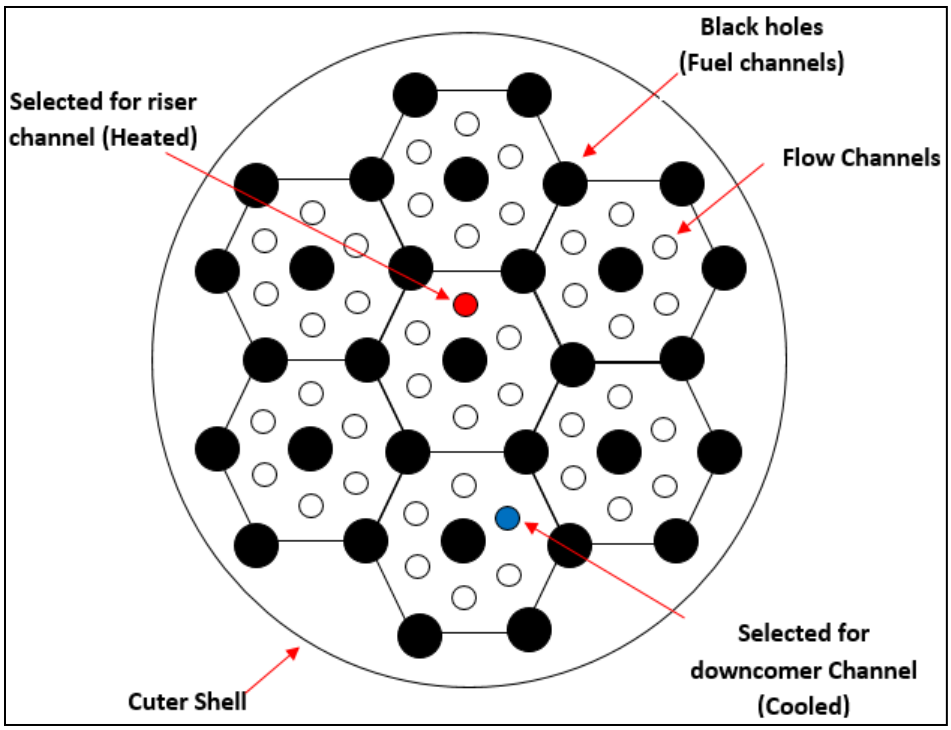

Figure 2.3. Schematic diagram of top view of the seven blocks

The Missouri S&T facility is comprised of a stainless steel alloy with a thermal conductivity of 16.2 W/m K. Stainless steel was selected for the system to withstand high pressures of up to 1034.21 kPa and temperatures up to 533.15 K. The upper plenum of the S&T facility has been designed and built using an external cooling jacket containing chilled water that surrounds the entire upper plenum. So the outer surface temperature of the upper plenum is controlled by chiller water supplied from a chiller.

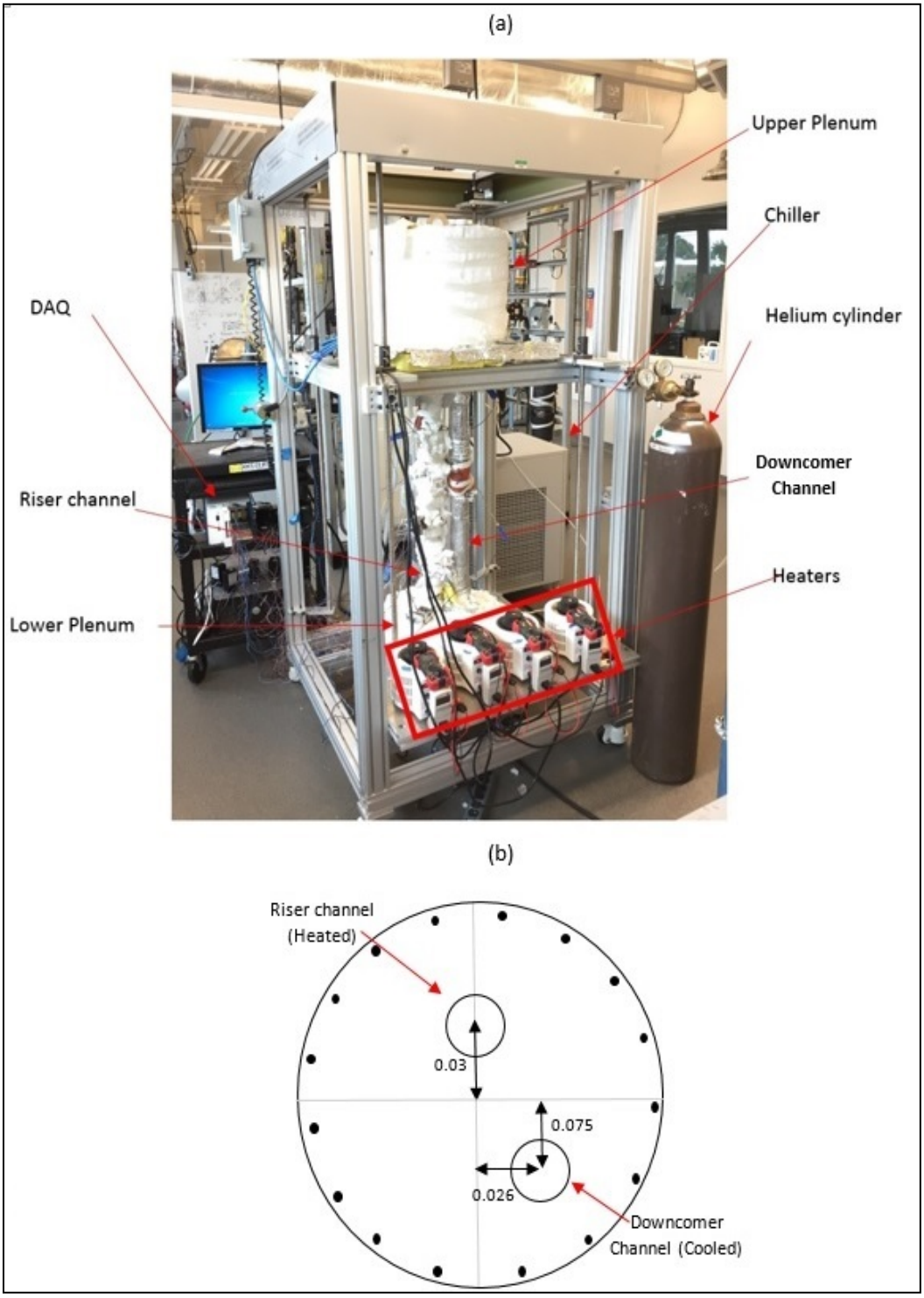

Figure 2.4. Physical picture of the current facility at S&T and the top view position of the channels at the lower plenum

In addition, helical coil is wrapped around the downcomer channel to act as a heat exchanger and maintain the external surface temperature of the downcomer at the desired value. The downcomer channel's helical coil heat exchanger uses 3.5 mm diameter high thermal conductivity copper tube with a Fine wall thickness of 0.85 mm. To improve the thermal contact between the copper cooling tube and the downcomer, high thermal conductivity silicone paste is used that can withstand high temperatures. This paste ensures good thermal contact and efficient heat transfer between the chiller water and the downcomer gas. A high-capacity chiller (Applied Thermal Control Ltd, K4 chiller) is used to provide the water at desired pressure of 275.8 kPa. This chiller is comprised of both pressure and temperature controllers. Based on the flow of helium inside the downcomer channel, the chilled water comes out of the chiller and goes upward (counter-current). The upper plenum's cooling jacket is also attached to the chiller to regulate the upper plenum's outer surface temperature. Therefore, both the outer surfaces temperatures of the upper plenum and downcomer channel are maintained constant at the desired values throughout the experiments. The upper plenum's outer surface and downcomer channel temperatures are the key study variables for this work. Four electrical heaters of 0.0254 m and 2.438 m (width and length, respectively) are wrapped in a continuous manner around the riser channel to create uniform heating around the channel. A variable voltage regulator having a span of 0-130 volts plus a digital power reader (0.2% precision) is attached to each electrical heater to regulate and monitor the intensity of the power supplied to the riser channel. The riser's external surface has been accurately insulated using a ceramic fiber blanket of 0.05m in thickness with a low thermal conductivity of 0.07 W/m K in order to reduce the heat loss to the environment.

Similarly, the upper and lower plena plus the cooled channel are thermally insulated using a ceramic fiber blanket. More details regarding the design criteria and experimental setup can be found in [105-111].

2.1.3. The Heat Transfer Coefficient Probe. To measure heat transfer data, enhanced flush-mounted heat transfer foil sensors (6.35 mm x 17.78 mm x 0.08 mm) from RdF Corporation (model no. 20457-1), with accuracy of 2.5% of the sensor reading, are installed at the inner wall of the channels. There are six heat flux sensors for the riser and three for the downcomer assemblies as a data acquisition block. In addition, for each heat flux measurement location, a T-thermocouple (diameter of 1.6 mm), with uncertainty of 0.75% of the reading, is mounted along the axis to track temperature variations. Figure 2.5 shows the location of the data acquisition blocks in the facility. Details of the measurement setup can be found in earlier publications [97, 105-107, 112, 113]. The foil sensor is capable of concurrently measuring the surface temperature and local heat flux using a thermocouple built into the foil sensor's surface. mReal and others [97, 105-107, 112, 113] have utilized such flush-mounted heat transfer methods to differentiate the coefficients of heat-transfer in single and multiphase flow systems. The current study considers the application of three axial positions along the downcomer channel (Z/L=0.044, 0.5, 0.956) and six axial positions along the riser channel (Z/L=0.044, 0.279, 0.409, 0.591, 0.773, 0.956) for the purposes of gathering data for the experiment. Riser and downcomer channels are divided into small sections. The foil sensors are mounted at the inner surface using high-temperature glue. The axial location's centerline temperatures are measured using a T-thermocouple (1.6 mm) placed

in front of the foil sensor at the channel's centerline (same axial location). It is important to note that the foil sensor has the ability to detect the heat transfer direction.

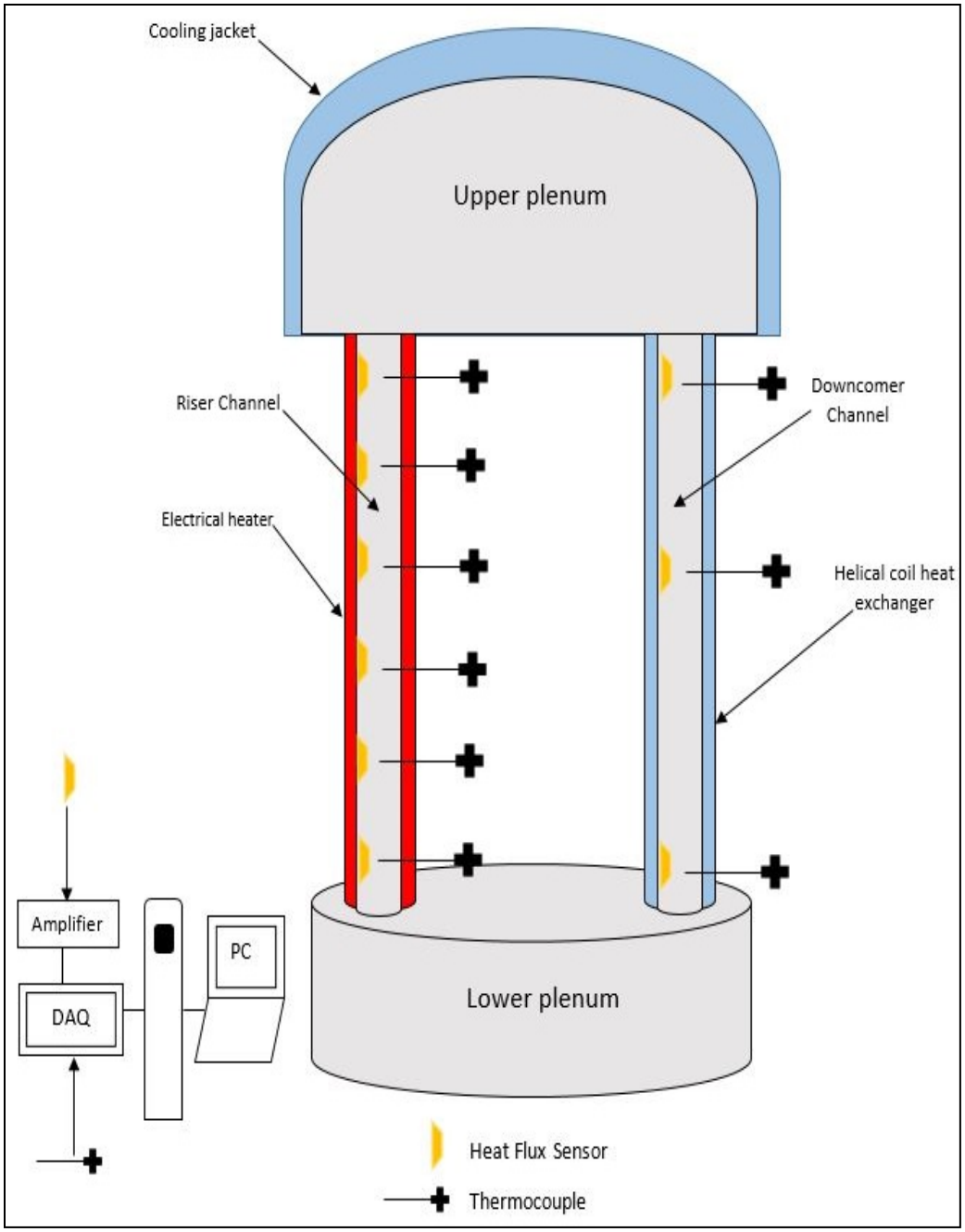

Figure 2.5. Schematic diagram of the illustrated technique in S&T facility with data acquisition system

Positive signals indicate the heat transfer is from the channel's inner wall to the adjacent fluid, while a negative signal shows the heat transfer from fluid to the channel's inner wall. By conducting a simultaneous measurement of the heat flux (qi) and surface temperature (Ts) via the heated foil sensor, and using Equations 1 and 2, the local time-averaged heat-transfer coefficients (havg) and the instantaneous heat-transfer coefficient (hi) can be obtained for N data sample. In this study, N= 2000 was selected to attain stable values.

$$h_i = \frac{q_i}{(T_{S,i} - T_{b,i})} \tag{1}$$

$$h_{avg} = \frac{1}{N}\sum_{i=1}^{i=N} h_i \tag{2}$$

The sampling of thermocouples and heat flux signals is done simultaneously at 40 Hz for 50 s. The selection of sampling frequency is based on preliminary tests with diverse frequencies that indicates no variation in the time-averaged heat-transfer coefficients. In the present study, we focus on the measurement of the riser channel's heat transfer coefficients under various cooling conditions. Figures 2.6, 2.7, and 2.8 show selected samples of data that were measured for heat flux, surface temperature, and centerline temperature, respectively, of axial position Z/L=0.409 and outer surface temperature of 298.15 K.

2.1.4. Uncertainty Analysis. In general the uncertainty of experimental data depends strongly upon the uncertainty of the individual measuring instruments that used in the experiments. In the current work a differential approximation method was used

which reported by J.P. Holman [114]. The uncertainty in results R that is given function of independent variables Y_1, Y_2, Y_3, ….. Y_n, thus R = R (Y_1, Y_2, Y_3, ….. Y_n), if there are uncertainty W_1, W_2, W_3, ….. W_n in the independent variables and W_R is the uncertainty in the proposed experimental results with the same odds, then the uncertainty in the experimental result can be given as:

$$W_R = \left[\left(\frac{\partial R}{\partial Y_1} W_1\right)^2 + \left(\frac{\partial R}{\partial Y_2} W_2\right)^2 + \ldots\ldots + \left(\frac{\partial R}{\partial Y_n} W_n\right)^2\right]^{\frac{1}{2}} \quad (3)$$

$$W_h = \left[\left(\frac{\partial h}{\partial q} W_q\right)^2 + \left(\frac{\partial h}{\partial T_S} W_{T_S}\right)^2 + \left(\frac{\partial h}{\partial T_b} W_{T_b}\right)^2\right]^{\frac{1}{2}} \quad (4)$$

It was found that the max uncertainty in the local heat transfer coefficient equal to ± 0.527 %. Tables 2.2 and 2.3 show the uncertainty of experimental instruments and parameters.

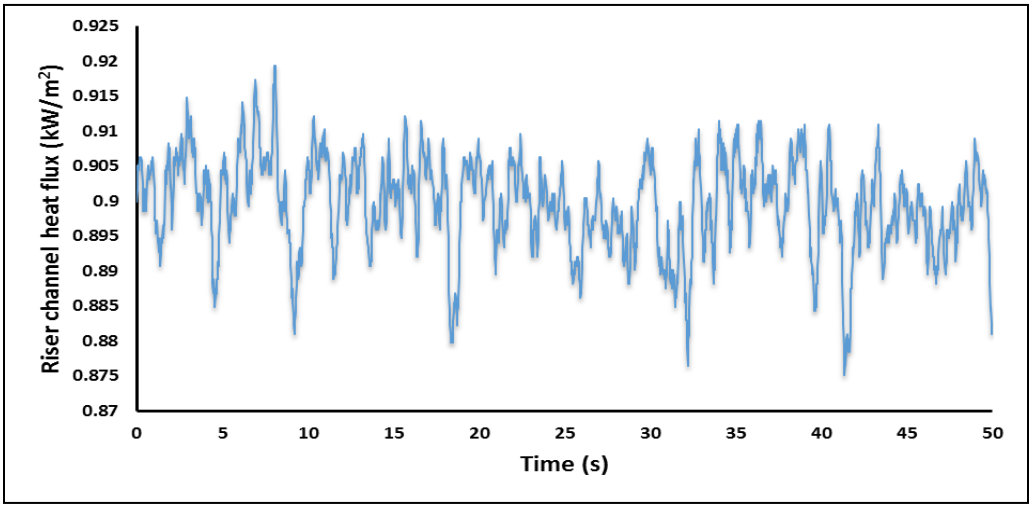

Figure 2.6. Riser channel heat flux data

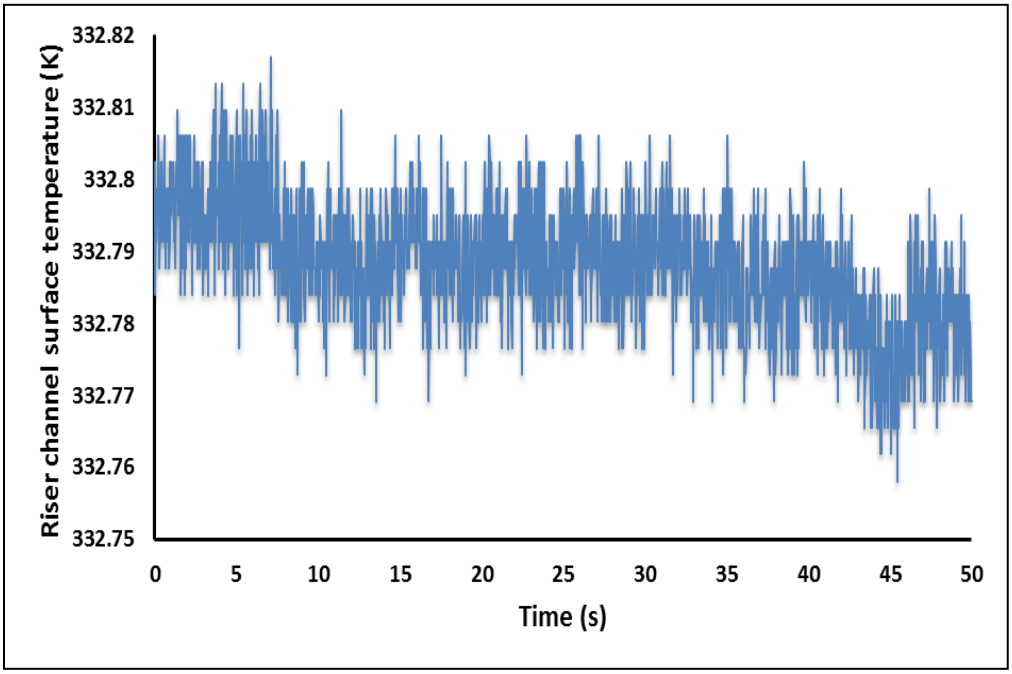

Figure 2.7. Riser channel surface temperature data

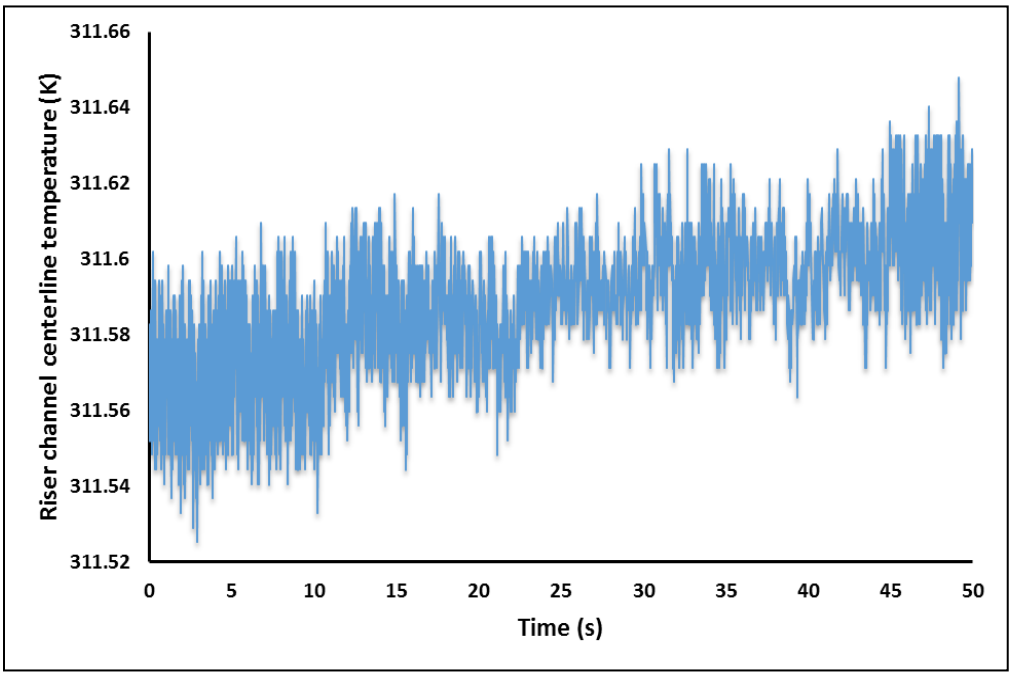

Figure 2.8. Riser channel centerline temperature data

Table 2.2. Uncertainties of experimental instruments

Name of instrument	Range of instrument	Variable measured	Uncertainty
T-Thermocouple	133 to 370 °C	Centerline temperature	± 1 °C or 0.75%
Heat flux foil sensor	No range	Heat flux	2.5%
	0 to 260 °C	Inner surface temperature	± 1 °C or 0.75%

Table 2.3. Uncertainties of parameters

S. no.	Variable name	Uncertainty error
1	Heat transfer coefficient, h	0.527 %
2	Inner surface temperature	± 1 °C or 0.75%
3	Centerline Temperature	± 1 °C or 0.75%

2.2. EXPERIMENTAL PROCEDURE

The scaled-down dual channel was pressurized of ultrapure helium gas at absolute pressure of 413.685 kPa for this set of experiments. The effect of the outer surface temperatures of the upper plenum and downcomer channel on the intensity of natural circulation is investigated using four outer surface temperatures (278.15, 288.15, 298.15, and 308.15 K). This range of temperatures is restricted with the capability of the current chiller. Each run was repeated three times to ensure data quality for each outer surface temperature of the upper plenum and the downcomer channel fixed at desired cooling

temperature during the experiment. On the other hand, the riser channel was kept at a uniformly constant heat flux of 2.12 kW/m^2. The steady state of the current system was tested by Said et al. [97, 105-107], and they concluded that the system takes approximately four hours to reach steady state. Steady state was achieved when temperature readings did not vary by more than 0.5 K and the local heat transfer coefficient was within ±0.8 W/m^2 K for a 30-minute observation. We implemented the same criterion for achieving steady state as Said et al. [97, 105-107] for our helium experiments. Four hours was more than sufficient to achieve steady-state conditions for all operating conditions investigated in this study.

2.3. RESULTS AND DISCUSSION

2.3.1. End Effect and Heat Flux Distribution. The end effect in terms of heat flow reversal and reduction in temperature fields is observed in two different axial positions along the riser channel (Z/L = 0.773 and 0.956). At Z/L = 0.773, the end effect was observed with high outer surface temperatures (288.15, 298.15, and 308.15 K) and was not observed at lower outer surface temperature (278.15 K). Figures 2.9 and 2.10 show the reversal in the heat direction (negative signals of heat fluxes) from the adjacent helium to the inner wall for Z/L = 0.773 and 0.956. The negative signals of heat fluxes in Figures 2.9 and 2.10 explained the heat was transferred from helium gas to the inner wall of riser channel, while positive heat fluxes are observed for the remaining axial locations. Figure 2.11 shows all positive heat fluxes for Z/L=0.591. It is worth mentioning that Said et al. [97] observed this end effect only at Z/L= 0.956 in riser channel with air as a cooling fluid. Results presented here indicate the role of thermal capacity of working

fluid (helium in this case verses air in the previous work [97]) on the axial location of heat flow reversal and the end effect zone. This end effect at the end of the riser channel could be attributed to heat conduction between the two channels through the upper flange which results in temperature variation along the riser channel. The second reason for the end effect is the interaction between hot plumes of rising helium (lighter) and denser helium in the upper plenum, which descends due to higher density. Moreover, negative heat fluxes are observed along the downcomer channels for all operating conditions, confirming the downward flow and establishment of natural circulation between upper and lower plena.

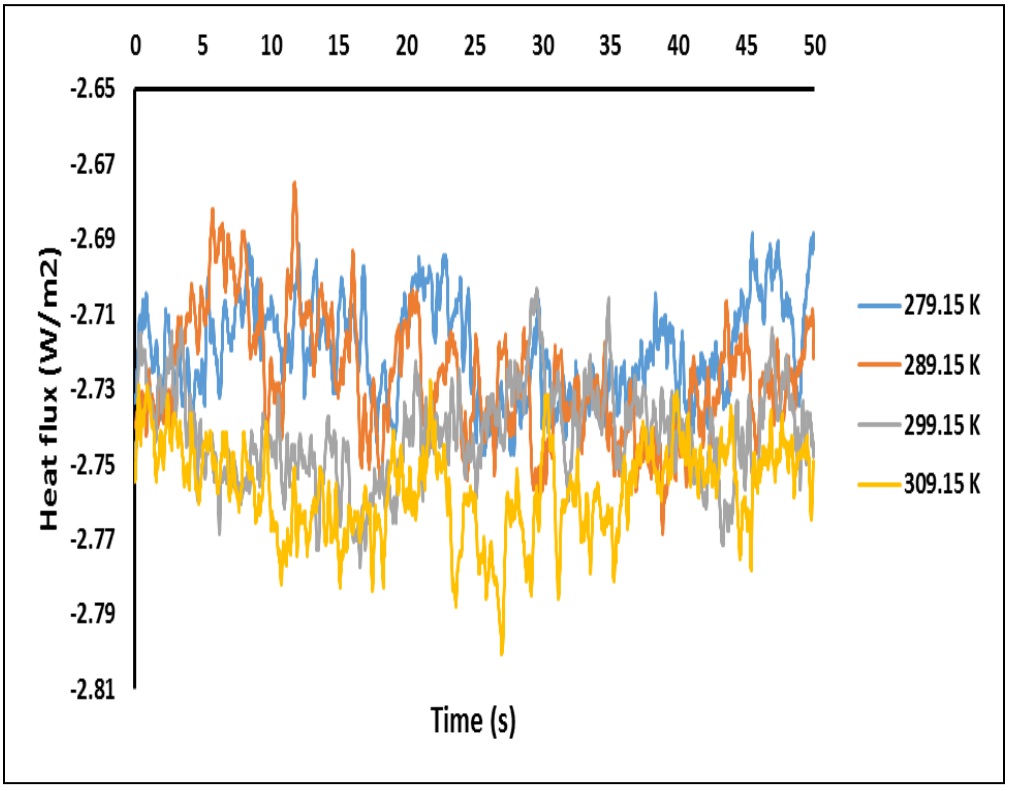

Figure 2.9. End effect at riser channel position Z/L=0.956

2.3.2. Axial Variation of Inner Surface Temperature along the Flow Channels.

Figure 2.12 a shows the temperature variations along the inner surface of the riser channel at different axial positions (Z/L= 0.044, 0.279, 0.409, 0.591, 0.773, and 0.956), and a significant (7.4%) reduction of surface temperature is observed with decreasing

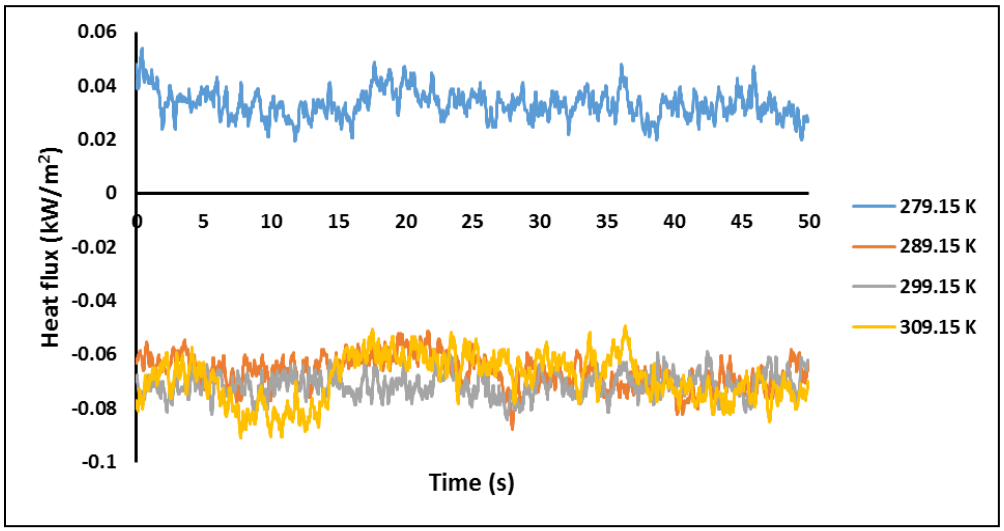

Figure 2.10. End effect at riser channel position Z/L=0.773

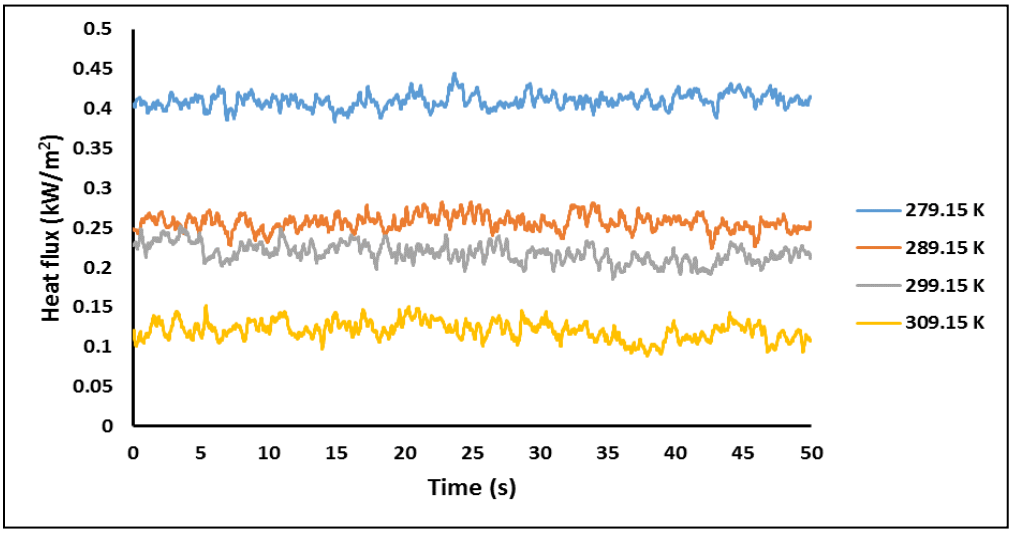

Figure 2.11. End effect at riser channel position Z/L=0.591

outer surface temperature of the upper plenum and downcomer channel from 308.15 K to 278.15 K. Maximum temperature is observed at Z/L= 0.773 and not at Z/L = 0.956, which as discussed earlier is attributed to the reversal of the heat flow and buoyancy-induced motion that has a significant effect in phenomenon of natural circulation [107, 115, 116]. In addition, the phenomenon of back-mixing is also possible for this setup and hence can be a concern for VHTR. Back-mixing is caused by the interaction of the rising plume from the heated channel and the fluid in the upper plenum, which in turn results in decreasing of the inner surface temperature of heat flow direction reversal past Z/L= 0.773. Figure 2.12 b shows the temperature variations along the inner wall surface of the downcomer channel. A decreasing trend in the temperature from Z/L= 0.956 (inlet) to Z/L= 0.044 (outlet) is observed, which confirms the establishment of natural circulation and downward flow.

2.3.3. Axial Variation of Centerline's Helium Temperature along the Flow Channels. Figure 2.13 a shows an axial variation of the centerline's helium temperature along the flow channel. It is found that, with decreasing the outer surface temperature of the upper plenum and downcomer channel from 308.15 K to 278.15 K, the average centerline's helium temperature decreased by 10.14%. Also, a reduction in the centerline helium temperature is observed close to the exit of the riser channel where a plateau is observed (Figure 2.13 a). Similar results were reported by Barnes [117]. This plateau could be attributed to the end effect. On the other hand, the helium centerline temperature along the downcomer channel is observed to be decreasing throughout from Z/L= 0.956 (inlet) to Z/L= 0.044 (outlet), as shown in Figure 2.13 b.

(a)

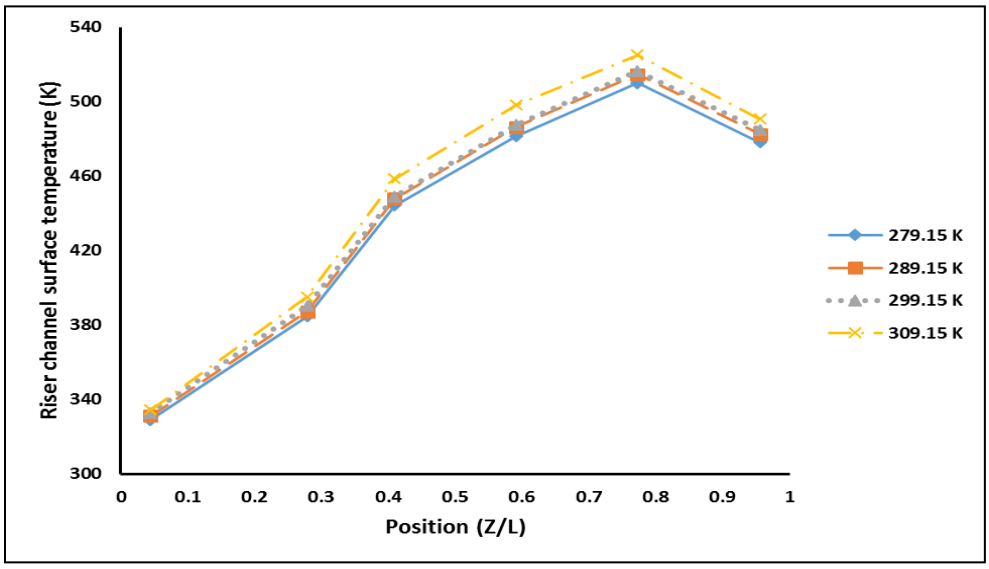

(b)

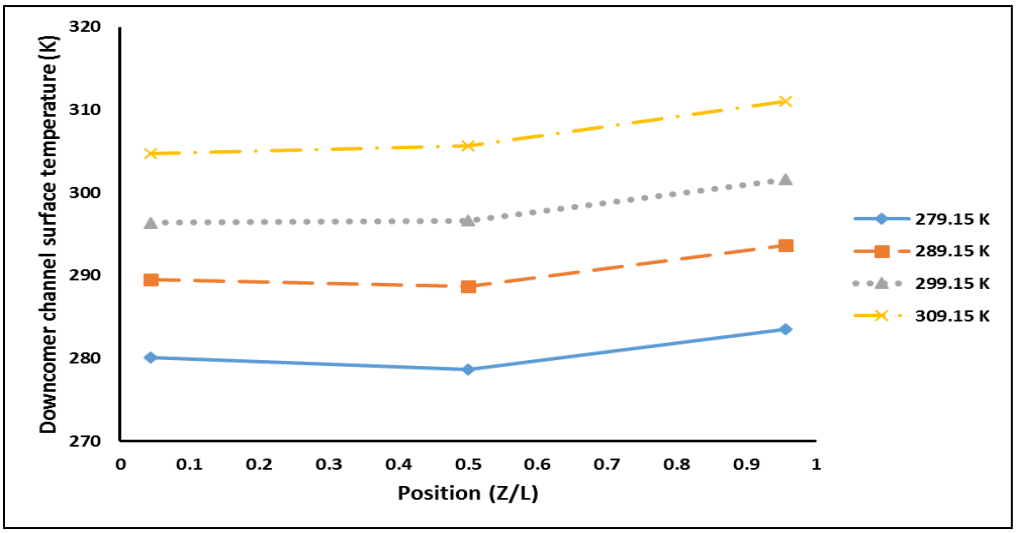

Figure 2.12. Axial variation of inner surface temperature along the flow channels

No significant end effects are observed for the downcomer. Figure 2.14 shows riser channel temperature difference (gain) from inlet (Z/L=0.044) to outlet (Z/L=0.956) for centerline and inner wall surface for four chiller temperatures (278.15, 288.15, 298.15, and

308.15 K). One can observe that the temperature difference between gas and surface is much larger for lower (278.15 K) outer surface temperatures than for higher (308.15 K) chiller/outer wall temperature.

(a)

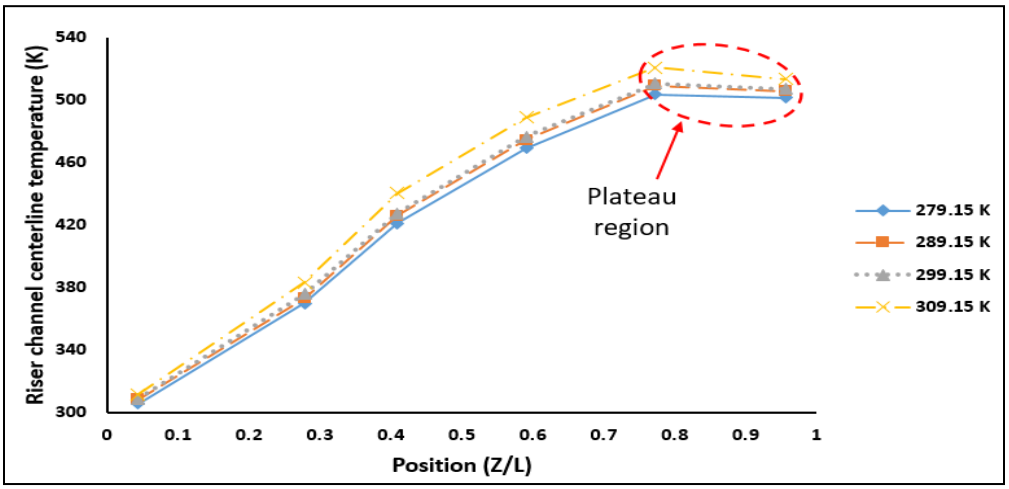

(b)

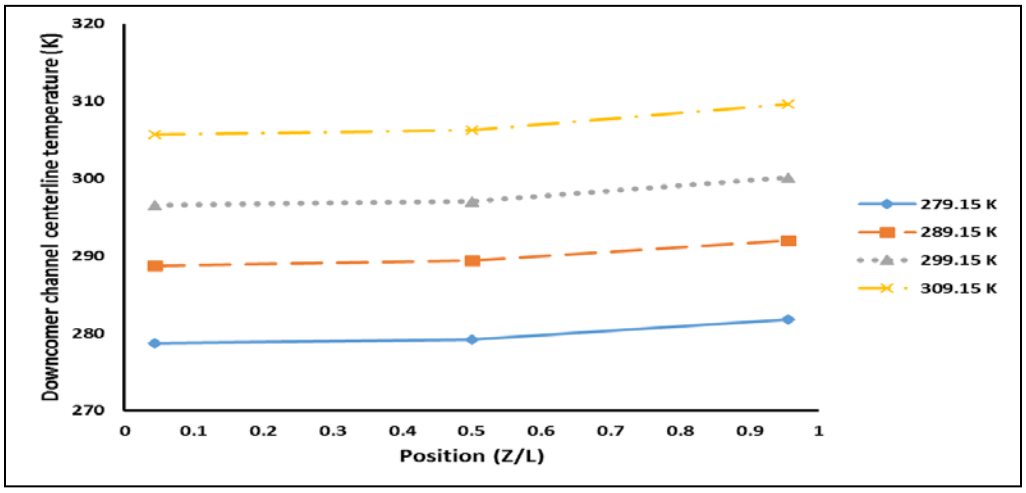

Figure 2.13. Axial variation of helium centerline temperature along the flow channels

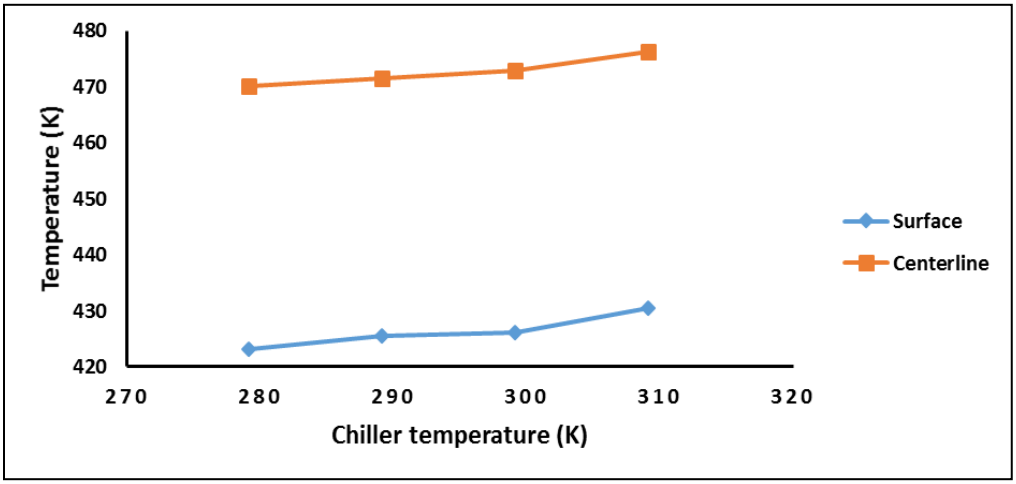

Figure 2.14. Difference temperature across riser channel surface and helium centerline temperatures

This observation is further discussed in the next section. The film/bulk temperature of the coolant gases (helium and air) is calculated for each axial location by taking the time average of the surface and gas centerline temperatures and then taking the average of the averaged surface and averaged centerline temperatures (T_f) as Equation (5). Average film temperature (T_f) is used to determine the physical properties of the gas, such as thermal conductivity and thermal diffusivity [115]:

$$T_f = \frac{\bar{T}_S + \bar{T}_b}{2} \tag{5}$$

Figure 2.15 shows the comparison of air and helium film temperatures for various chiller temperatures. As shown in the Figure 2.15, after axial position of Z/L=0.279, the average film temperature for helium increases by 29%, and this can possibly be attributed to the higher thermal conductivity and thermal diffusivity of the helium than air.

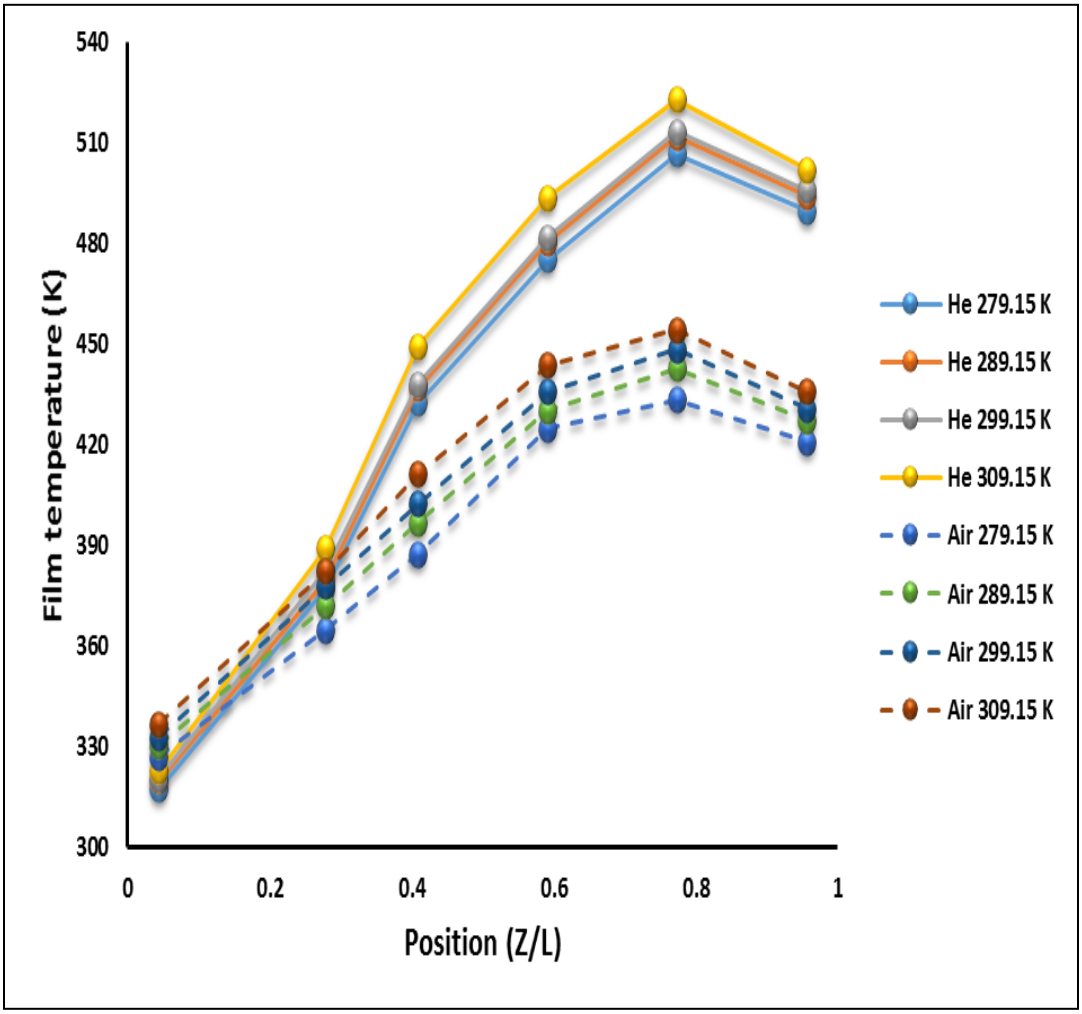

Figure 2.15. Film temperature profile of helium and air across riser channel positions

Figures 2.16 (a & b) and 2.17 (a & b) show the axial variations of the thermal conductivity and thermal diffusivity of helium [118] and air [97] along the riser channel, respectively. It is clear that the appearance of a plateau instead of a sharp reduction for helium close to the exit of the riser channel in terms of centerline helium temperature could be attributed to the five time higher specific heat of helium as compared to air.

(a)

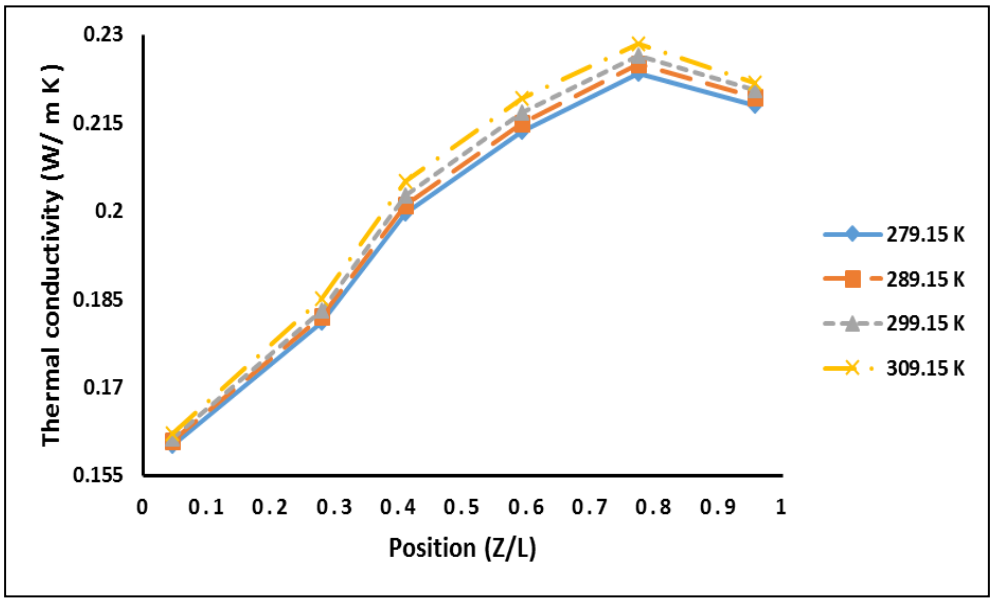

(b)

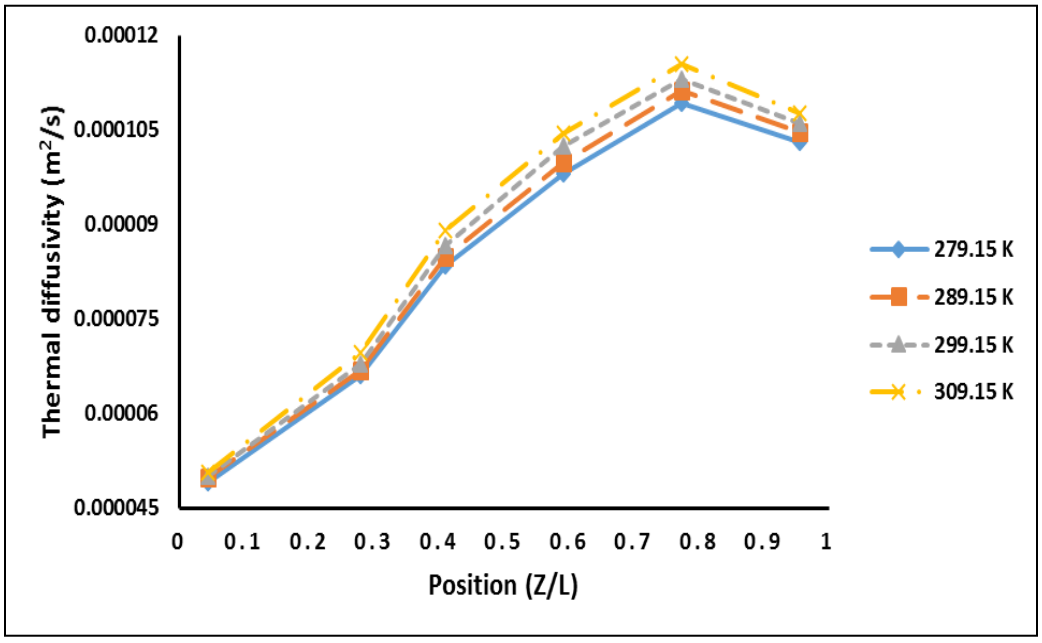

Figure 2.16. Helium physical properties

(a)

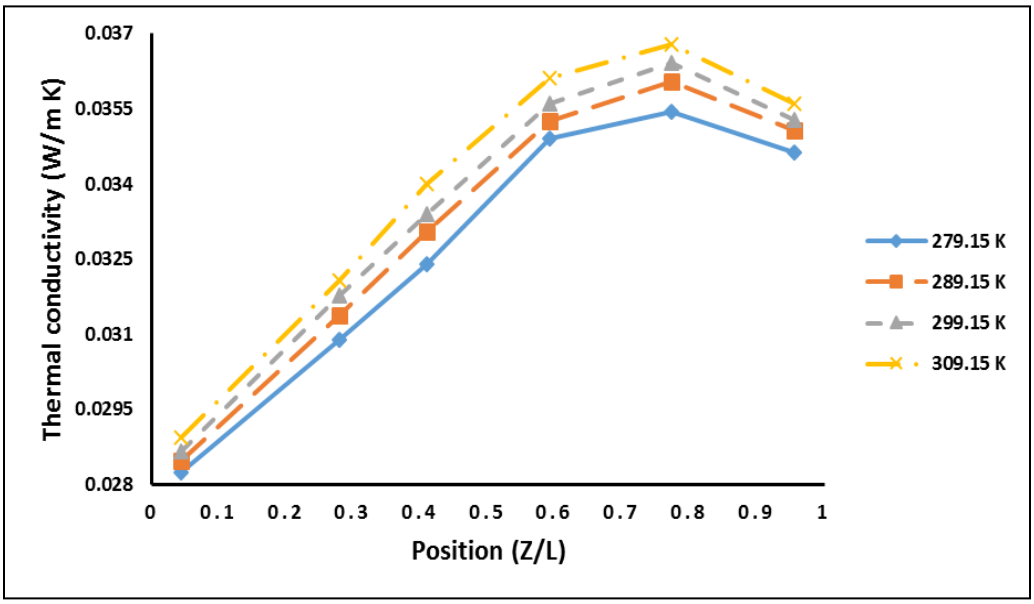

(b)

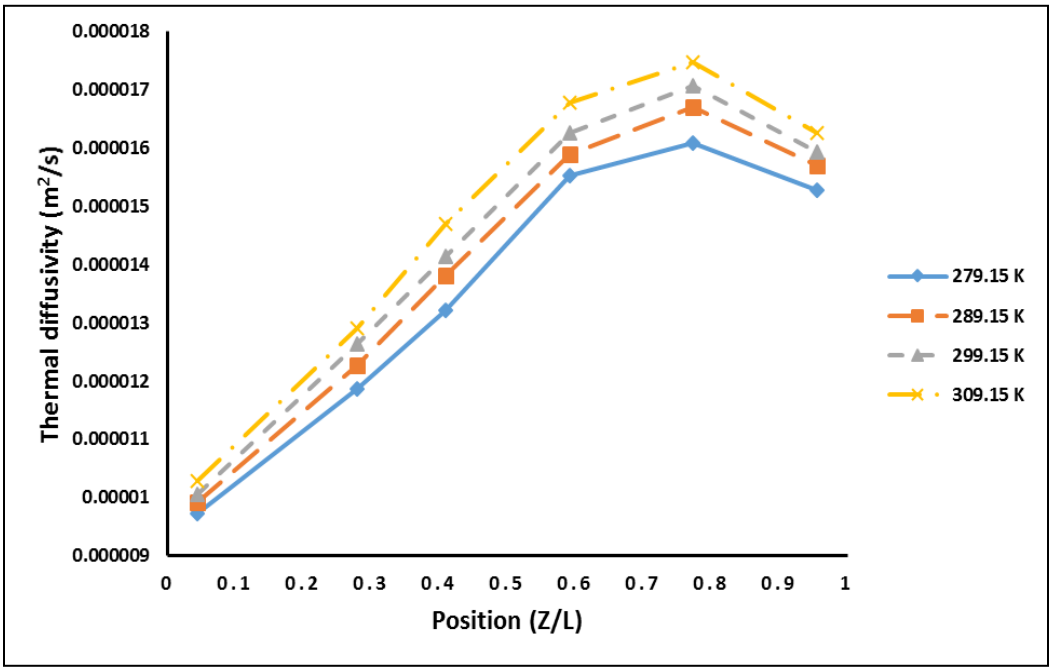

Figure 2.17. Air physical properties for Said et al. [97]

2.3.4. Axial Variation of Heat Transfer Coefficient along the Riser Channel.

Heat transfer coefficient is a quantitative characteristic of convective heat transfer efficiency between flowing coolant (helium in this case) and the heated surface. Figure 2.18 shows the variations of the local heat transfer coefficients along the riser channel from the inlet (Z/L = 0.044) to the outlet (Z/L = 0.956).It is clear that the heat transfer coefficients decreases from the inlet (Z/L = 0.044) to (Z/L = 0.279), this could be attributed to the developing of hydrodynamic and thermal boundary layers. An increase in the values of the heat transfer coefficients is observed after Z/L = 0.279 to Z/L = 0.591 due to the laminarization effects [119]. The influence of end effect is very clear on values of the local heat transfer coefficients after Z/L=0.591 in terms of a decreasing trend.

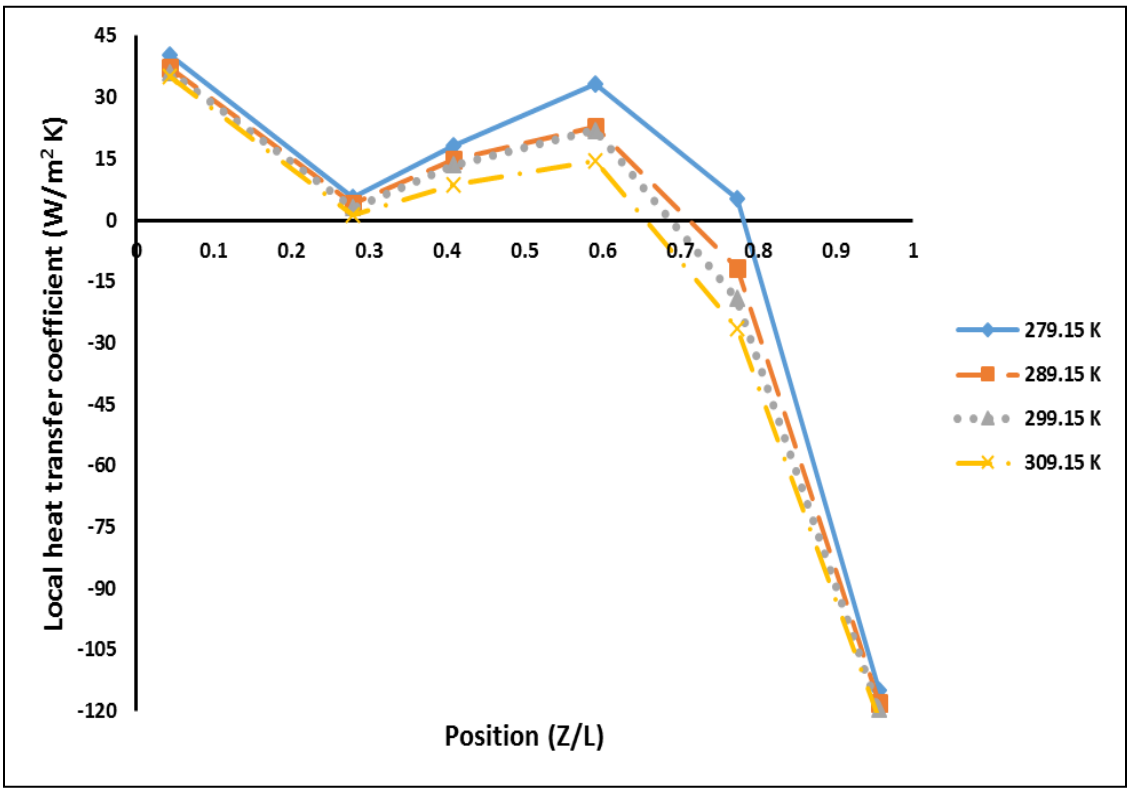

Figure 2.18. Local heat transfer coefficient along the riser channel

Also, negative heat transfer coefficients are observed for 288.15, 298.15 and 308.15 K at Z/L = 0.0.773 and beyond, but for the case of 278.15 K only negative heat transfer is observed at only Z/L=0.956. Another important observation is the fact that heat transfer coefficient is higher for all locations for the 278.15 K case and decreases in the order of upper plenum wall temperature (lowest for 308.15 K). For lower plenum and downcomer temperature, the intensity of natural convection would be higher giving rise to enhanced convection. The experimental observations of Figure 2.18 support this argument.

2.3.5. Comparison between Helium and Air Data. An earlier study by Said et al. [97] reported the effect of outer surface temperatures of the upper plenum and downcomer channel on the intensity of natural circulation using air as a working fluid. It is worth mentioning that the proposed coolant for prismatic modular reactor is helium rather than air. The thermal performance of helium is significantly better than air [116], and that is what motivated us to investigate the role of helium as well as the outer surface temperatures on the intensity of natural circulation. Said et al. [97] observed experimentally the end effect only at Z/L= 0.956 in the riser channel, while in the current study the end effect has been extended lower down the channel to Z/L=0.773 for three higher outer surface temperatures (288.15, 298.15 and 308.15 K) experiments. This end effect is possibly due to the role of lower coefficient of thermal expansion for helium ($\beta \cong 0.002/K$) as a coolant in comparison to air ($\beta \cong 0.0034/K$).

Furthermore, helium has higher specific heat will lead to lower temperature rise (the gas will be able to absorb more heat) both the lower expansion coefficient and higher specific heat will lead to smaller change in the density of helium. Consequently, the jet

will be suppressed and the downward flow from the upper plenum will penetrate deeper into the channel. These results can be seen in Figure 2.15, where the film temperature of helium is higher than that of air due to faster thermal response of air. Moreover, a plateau was observed at position Z/L=0.773 in the current study as shown in Figure 2.13 a, while for air heat transfer data [97] showed a sharp reduction in air's centerline temperature at position Z/L=0.773. In addition, more comparisons between Said et al. [97] and the current study, are shown in Figures 2.19 and 2.20, and these figures explain the differences between air and helium as working fluid in the system. Figures 2.19 and 2.20 show an increase in the inner surface and centerline temperatures along the riser channel for helium than air, which suggests that helium would be a better coolant than air. The centerline end effects are suppressed for helium, and the exit temperature is higher. Both of these observations are desirable, and hence helium is a better choice for coolant under natural circulation.

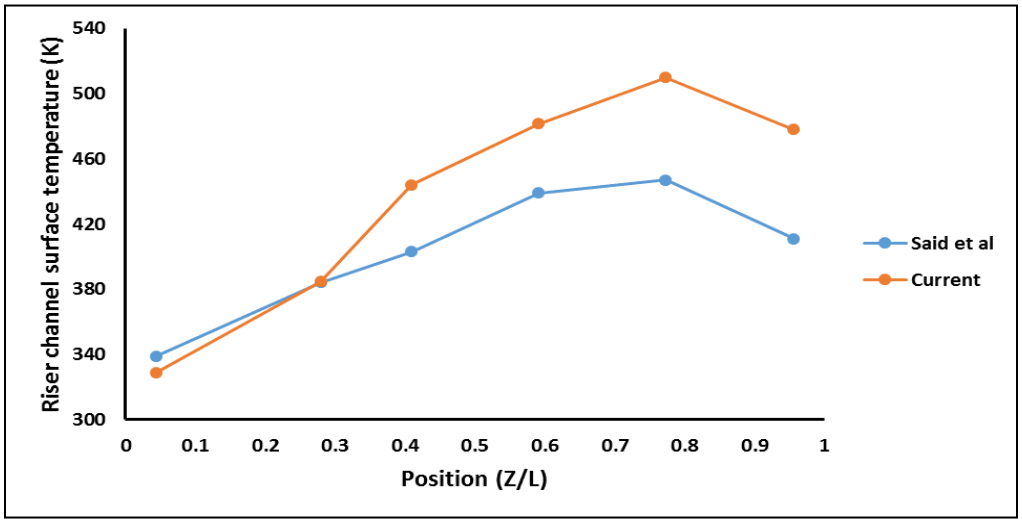

Figure 2.19. Comparison of inner surface of the riser channel between current study (Helium) and Said et al (air) [97]

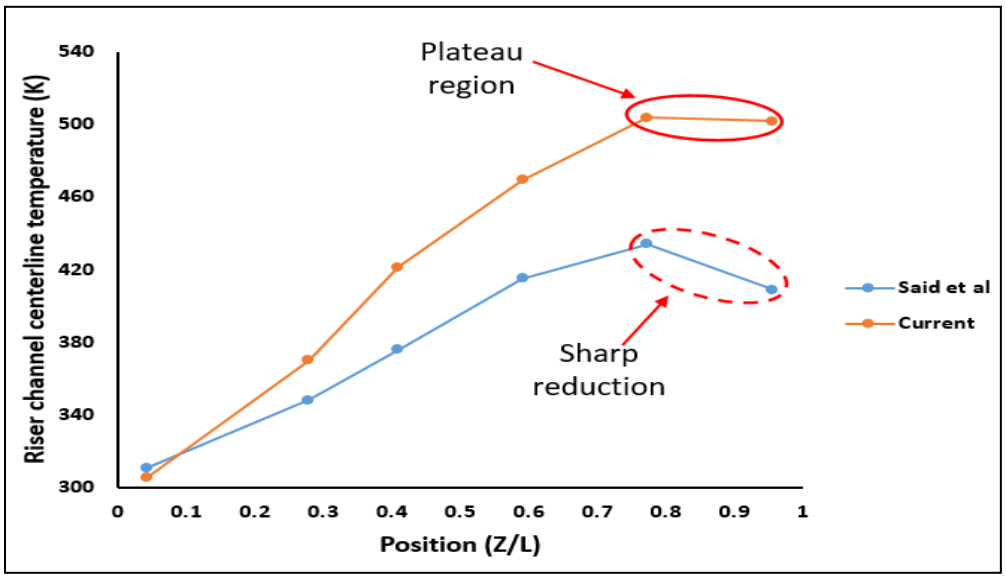

Figure 2.20 Comparison of centerline of the riser channel between current study (Helium) and Said et al. (Air) [97]

3. THE INFLUENCE OF NONUNIFORM HEATING ON NATURAL CIRCULATION HEAT TRANSFER IN A PRISMATIC DUAL-CHANNEL CIRCULATION LOOP

Focus of many past and current studies, has been directed in conducting investigations on natural convection heat transfer and flow dynamics in diverse geometries and operating conditions. Researchers have given much attention to natural convection for natural systems, as well as engineering applications. The implementation of natural convection in nuclear reactors comes in the form of an engineered feature to accomplish passive safety [74, 120]. Natural convection is one of the major passive safety phenomena in gas-cooled reactors such as prismatic very high-temperature reactors (VHTRs) used as a safeguard under the loss of flow accidents (LOFA) [77]. Because of density differences, the natural circulation will subsequently be established so that the decay heat coming from the core can be removed. There is reversal of coolant flow direction during LOFA, and two different possibilities for the direction of flow that may take place inside the flow channels in the core as a result of large variation in temperature. The flow of the coolant would be upward in the high heat sections/channels of the core, while the flow would be downward in the relatively cooled section, thereby establishing the natural circulation loop as a result of buoyancy force. The upward flow channels and the downward channels act as riser channels and downcomers respectively. The decay heat coming from the reactor core is transported by natural convection currents through fluid plumes from the reactor core to the reactor cavity cooling system, thereby preventing the possibility of core meltdown and localized hot spots. Standard computational fluid dynamics (CFD) codes integrated with heat transfer calculations like

CFD-STAR-CCM+, as well as CFD-Fluent and thermal hydraulic codes like RELAP5-3D are capable of generating crucial heat transfer data used in conducting majority of the reactor safety analyses studies. Reports of the existence of extensive natural circulation computational studies in the prismatic very high temperature reactor (VHTRs) are made in the open literature [74,77,87,92,95,120-122]. But little consideration has been given to nonuniform heat flux axially variation effect on the flow field, heat transfer coefficient, and temperature profile in VHTR [123-127]. In a typical nuclear reactor we expect to see a cosine shaped axial power profile peaking in the center of the core. Therefore, effect of axial power shape must be investigated for natural circulation. Most numerical and experimental studies on natural convection heat transfer in the open literature are limited to uniform heat flux [128-134]. Thus, a unique scaled-down experimental setup with two flow channels with separate effects was designed, constructed, and tested at Missouri University of Science and Technology (Missouri S&T) by the research team in Multiphase Reactors Engineering and Applications Laboratory (mReal) [97,105-107,110,111]. The mReal's facility incorporated advanced non-invasive heat flux sensors, T-thermocouple sensors (1.6 mm in diameter) in an innovative manner for axially heat transfer coefficient and temperatures measurement along the flow channels. Most of the studies in the scaled-down dual-channel setup at Missouri S&T investigated the flow field, heat transfer coefficient, and temperature profile under uniform heating condition. As discussed earlier, in a VHTR system, power distribution in the core is nonuniform. Therefore, additional emphasis is placed on generated heat transfer data for nonuniform heating. The current study is significant particularly because nonuniform heat distribution demonstrates the natural convection of the real VHTR system, which

will have profound effect on natural convection/circulation phenomenon. Using advanced instrumentations, detailed heat transfer data in terms of temperature fields (centerline coolant and inner wall surface temperatures) and heat transfer coefficients under natural circulation are presented here. The effects of the nonuniform heat distribution in the riser channel at steady state are discussed using air at 60 psi of air as coolant. The collected data in this study can provide the necessary benchmarking to validate thermal hydraulic codes such as; RELAP5-3D, CFD-STAR-CCM1, CFD-Fluent, and so forth. Several experimental measurements were executed on the natural convection for a loop of two flow channels (riser and downcomer channels) with upper and lower plena under nonuniform heat flux distribution. Therefore, the main objective of the current work is to experimentally investigate the phenomenon of the natural convection in terms of heat transfer coefficients and temperature fields (coolant and wall surface temperatures) at different operating power with air as a working fluid using the newly developed facility and the novel techniques. Though this work only uses two channels for coolant flow, the study can be extended to multiple channels and different working fluid.

3.1. METHODOLOGY

The experimental setup is considered to be a scaled-down separate effects facility that utilizes stainless steel alloy with 16.2 W/m K thermal conductivity in handling high temperature and pressure. The Missouri S&T scaled-down setup's schematic diagram is shown in Figure 3.1. It consists of two plena-upper and lower and having two channels in the reactor core for coolant flow. The upward and downward flows inside the reactor core with regard to the LOFA are mimicked by two channels: one riser channel (heated)

for upward flow, and one downcomer channel (cooled) for downward flow. The flow channels' diameter is maintained at 16 mm, and the channel height is 1 m.

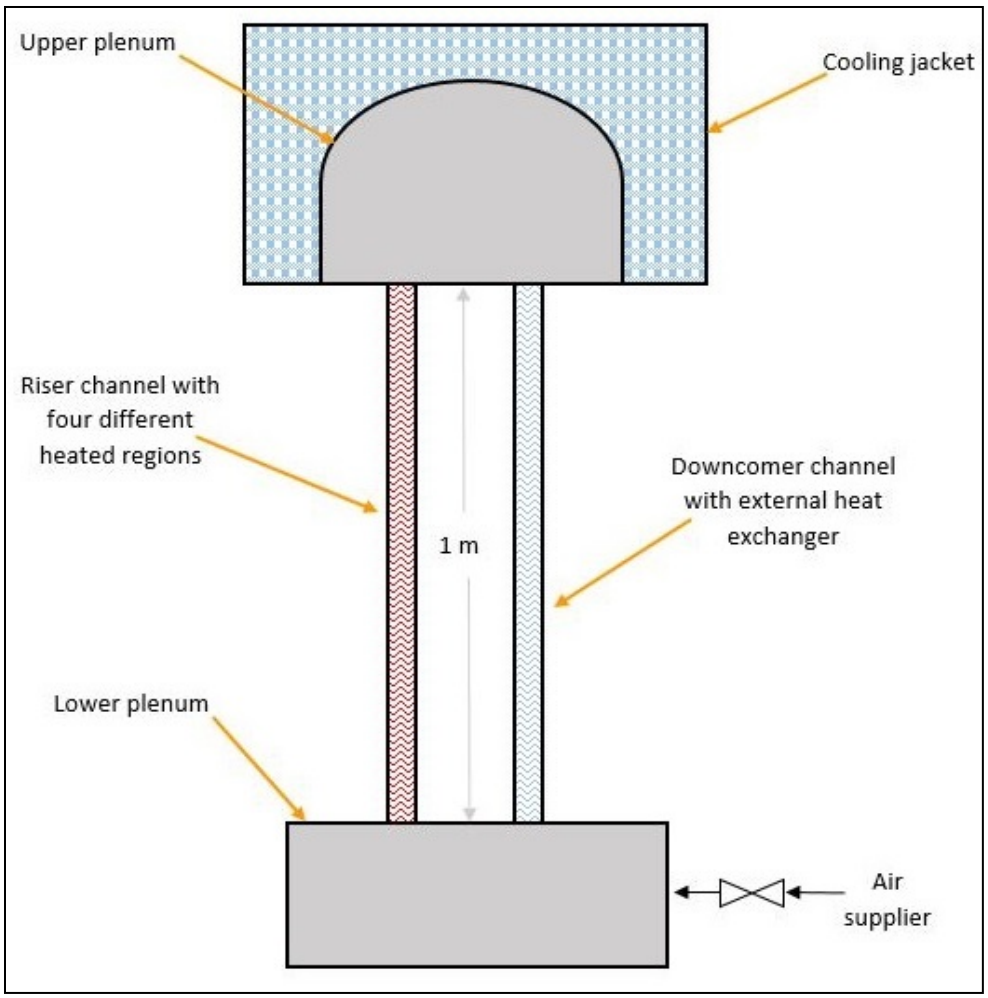

Figure 3.1. Missouri S&T scaled-down facility schematic

Four heavily insulated Duo-Tape electrical heaters (50.8 × 609.6 mm), with heating capacity of 312 W at 120 V each are used to heat the riser channel electrically and simulated the upward flow in the riser channel for the reactor core as shown in physical picture, Figure 3.2 ((a) setup, (b) data acquisition, (c) radial temperature

adjuster). An individual connection of each electrical heater to a variable voltage regulator that has a digital power reader maintains the heater wattage of the riser channel under fine control. Downward flow in the downcomer channel is accomplished by cooling for the channel outer surface by chilled water mimicking VHTR natural circulation. For downcomer cooling, helical coil carrying chilled water is wrapped around the downcomer channel. In order for the upper plenum outer surface temperature to remain at a constant value, the upper plenum outer surface is equipped with a cooling jacket. An automatic chiller (Applied Thermal Control Ltd, K4 chiller) that has temperature and pressure controllers is used to ensure that chilled water is made available to the cooling jacket and helical coil heat exchanger for downcomer at the required temperature. Thus, throughout this experiment, the upper plenum's outer surface temperatures and downcomer channel are maintained at a constant temperature of 5 °C. Only less than 1.5 K temperature difference was observed between the chilled water inlet and outlet across the cooling jacket and the heat exchange. Thus, it is fair to assume constant wall surface temperature thermal boundary condition for both the downcomer channel and the upper plenum. The maintenance of the lower plenum walls are at adiabatic conditions through the use of thick ceramic fibre blanket. In order for the heat losses to the environment to be reduced, the entire setup was thermally insulated by using ceramic fibre blanket. Additional details and explanation of the experimental setup, together with the design considerations are provided elsewhere [97,105-107,110,111]. The significant study variables are the nonuniform heating distribution that comes in the form of stepwise-reducing and stepwise-increasing along riser channel. Electrical heater of width 0.0254 m and length 2.438 m are wrapped around the riser channel in a

continuous manner, for heating the channel. The electrical heater is attached to a variable voltage regulator with a span of 0-130 volts control through a digital power reader of 0.2% precision for the regulation and monitoring of the power intensity supplied to the riser channel. A ceramic fibre blanket with a thickness of 0.05 m and a thermal conductivity of 0.07 W/m K is used to carefully insulate the riser external surface to reduce any heat loss coming from the heater to the environment.

(a)

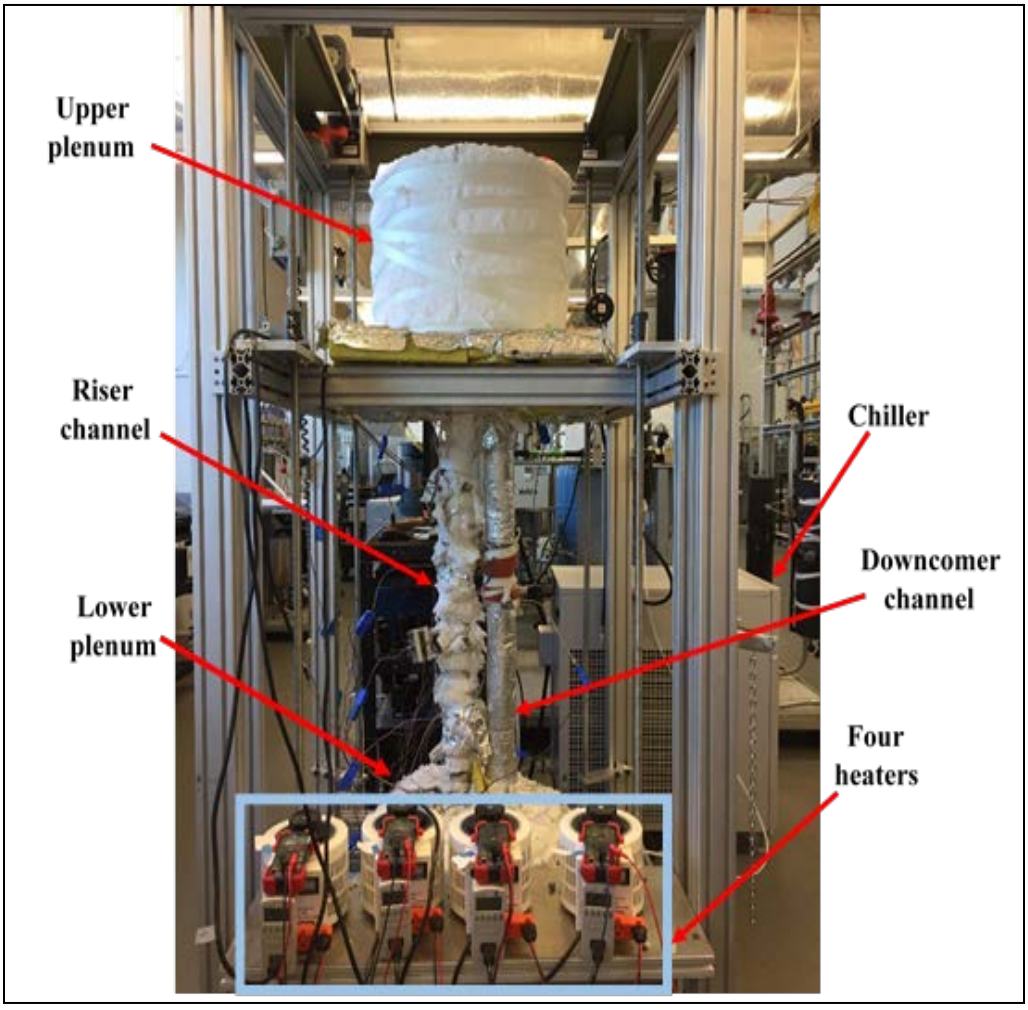

Figure 3.2. Physical picture of the current facility in Missouri S&T

(b)

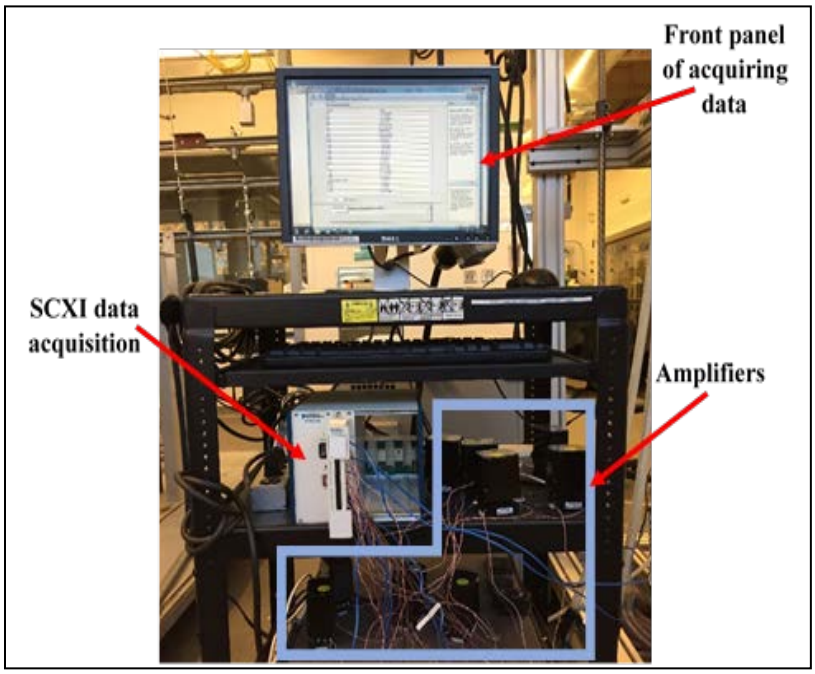

(c)

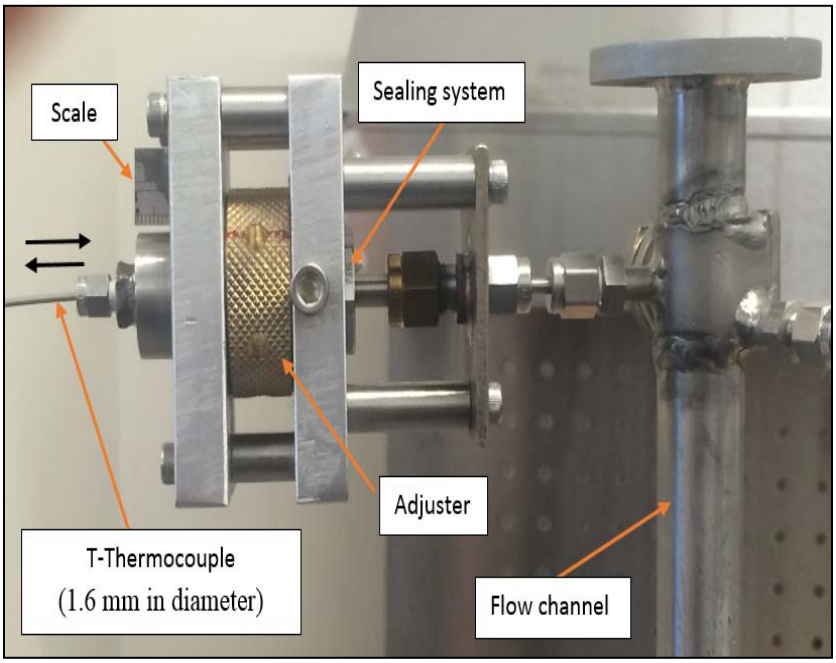

Figure 3.2. Physical picture of the current facility in Missouri S&T (Cont.)

The creation of an improved integrated fast-response heat transfer method was undertaken, and it is made up of flush-mounted heat transfer foil sensors (6.35 mm x 17.78 mm x 0.08 mm) installed on the inner wall of the channel. Several 1.6 mm T-thermocouple are mounted along the axis of riser and downcomer channels for monitoring temperature fields and heat flux variations along the channel. The foil sensor utilizes the thermocouple built into the foil sensor surface to provide the heat flux measurements. Simultaneous measurement of surface temperature and local heat flux at mReal lab has enable us to acquire heat-transfer coefficients in single as well as multiphase flow systems [97,105-107,110-113]. Three axial positions along the downcomer channel (Z/L=0.044, 0.5, 0.956) and six axial positions along riser channel (Z/L=0.044, 0.279, 0.409, 0.591, 0.773, 0.956) are used for collecting data for this present study. A connection block is utilized for gathering data at each location along the heated and cooled channels. High-temperature glue is used to securely install the foil sensors at the channel inner surface. A T-thermocouple (1.6 mm) is placed exactly in front of the foil sensor (same axial location) measure centreline coolant temperature. The ability of the foil sensor to measure heat transfer direction is essential for these experiments. The heat transfer from the channel inner wall to the adjacent fluid indicates positive signals, while heat transfer from the adjacent fluid to the inner wall of the channel indicates a negative signal. The sampling of thermocouples and heat flux signals is performed simultaneously at 40 Hz for 50 s. The sampling frequency selection is performed based on preliminary tests with varied frequencies. At 40 Hz no variation in the time-averaged heat-transfer coefficients was observed.

3.2. UNCERTAINTY ANALYSIS

The accuracy of the experimental data depends strongly upon the accuracy of the individual measuring instruments used in the experiments. In the current work, a differential approximation method was used, which was reported by J.P. Holman [114]. Suppose we need to evaluate the uncertainty in results R which is a function of independent variables Y1, Y2, Y3, ….. Yn, thus R = R (Y1, Y2, Y3, ….. Yn). If the uncertainties in independent variables are W1, W2, W3, ….. Wn respectively, the uncertainty in the results WR is given by equation (4)

It was found that the max uncertainty in the heat transfer coefficient for stepwise-reducing and stepwise-increasing is ± 0.9206 % and ± 0.3836%, respectively. Tables 3.1 and 3.2 show the uncertainty of experimental instruments and heat transfer coefficients.

Table 3.1. Uncertainties of experimental instruments

Name of instrument	Range of instrument	Variable measured	Uncertainty (%)
Thermocouple	133 to 370 °C	Centerline temperature	±1 °C or 0.75%
Heat flux foil sensor	No range	Heat flux	2.5
	0 to 260 °C	Inner surface temperature	±1 °C or 0.75%

Table 3.2. Uncertainties of heat transfer coefficients

Case	Variable name	Uncertainty error,%
Stepwise reducing	Heat transfer coefficient, h	0.9206 %
Stepwise increasing	Heat transfer coefficient, h	0.3836 %

3.3. PROCEDURE

The scaled-down dual-channel setup was pressurized by air as coolant at 413.685 x 10^3 Pa (60 psi). The chiller was started to maintain a constant temperature of 5 ^oC at the outer surface temperatures of the upper plenum and the downcomer channel fixed for the entire duration of the experiment. It is worth mentioning that the riser channel is divided into four sections (0.25 m increment). Each section is connected with a separate electric heater (Figure 3.2 a). The riser channel is nonuniformly heated in the form of stepwise - reducing and stepwise-increasing with reference to an average uniform isoflux heating, as shown in Figures 3.3 and 3.4 ((a) stepwise-reducing, (b) stepwise-increasing.) Table 3.3 also shows the corresponding nonuniform heat flux distributions along the riser channel. The current setup takes approximately four hours to reach steady state.

3.4. RESULTS AND DISCUSSION

By implementing the heat flux foil sensors in measuring the local heat flux (q_i) and surface temperature (T_S) simultaneously, the local time-averaged heat-transfer coefficients (h_{avg}) and the instantaneous heat-transfer coefficient (h_i) can be obtained through Equations 1 and 2 [97,105-107,110-113] at 40 Hz for 50 s over 2000 data points.

The average values of the heat transfer coefficient ($\bar{h}_L$) and the average Nusselt number ($\overline{Nu}_L$) along the riser channel for the positive signals of heat fluxes from Z/L = 0.044 to Z/L = 0.591 can be calculated as follows:

$$\bar{h}_L = \frac{1}{L}\int_{L=0}^{L=0.591} h_{avg}\ d(L) \tag{6}$$

$$\overline{Nu}_L = \frac{\bar{h}_L\ l}{k} \tag{7}$$

Equations 8, 9, and 10 present the axial average inner surface temperature ($\overline{T}_S$), axial average bulk temperature ($\overline{T}_b$), and the average film temperature ($\overline{T}_f$) for the positive signals of heat fluxes, which are used to calculate the average heat transfer coefficient of Equation (6) along the riser channel:

$$\overline{T}_S = \frac{1}{L}\int_{L=0}^{L=0.591} T_S\ d(L) \tag{8}$$

$$\overline{T}_b = \frac{1}{L}\int_{L=0}^{L=0.591} T_b\ d(L) \tag{9}$$

$$\overline{T}_f = \frac{\overline{T}_S + \overline{T}_b}{2} \tag{10}$$

3.4.1. Inflecting Zone. Reversal of heat flow direction and reduction in temperature fields are observed within the riser channel close to the exit. This behavior is known as the inflecting zone (end effects) [97,105-107,110,111], and this thermal behavior was observed in the current study in two different axial positions along the riser

channel (Z/L = 0.773 and 0.956) with inflecting in terms of negative heat flux signals occurring at (Z/L = 0.773 and 0.956) for both stepwise-reducing and stepwise-increasing nonuniformly heating experimental runs as shown in Figures 3.5 and 3.6.

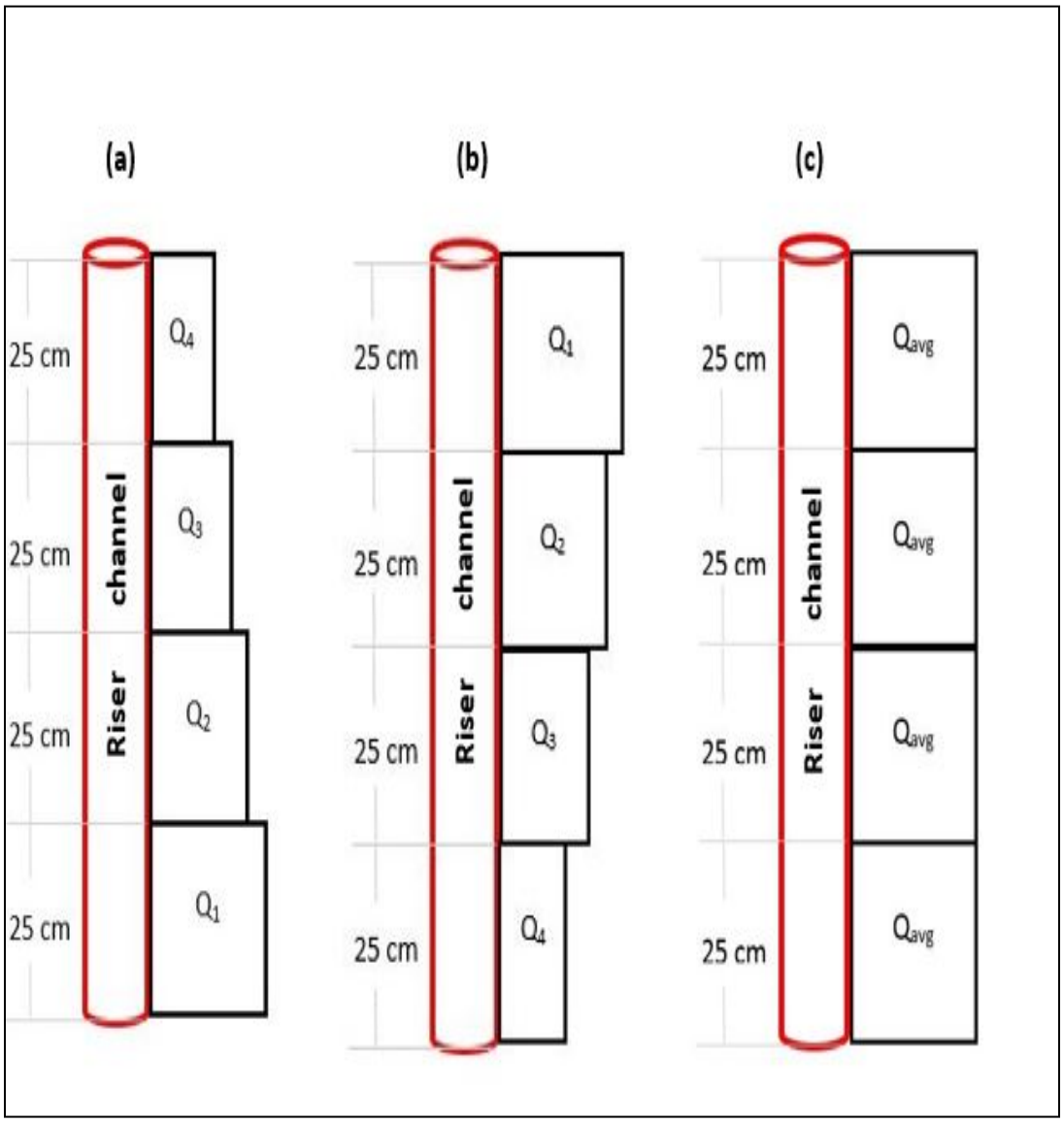

Figure 3.3. Heat flux distributions around riser channel

(a)

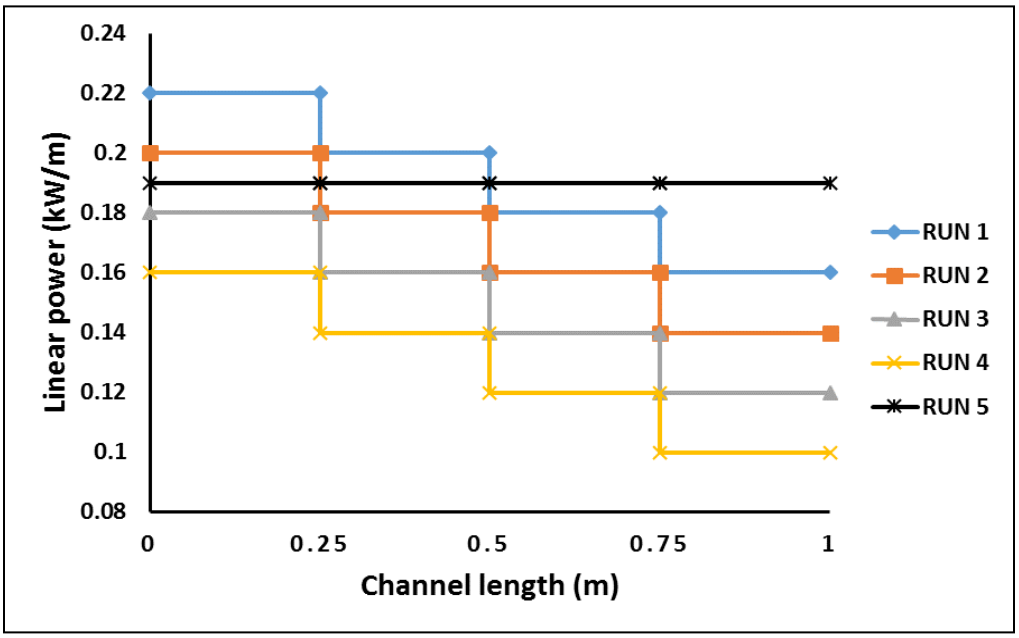

(b)

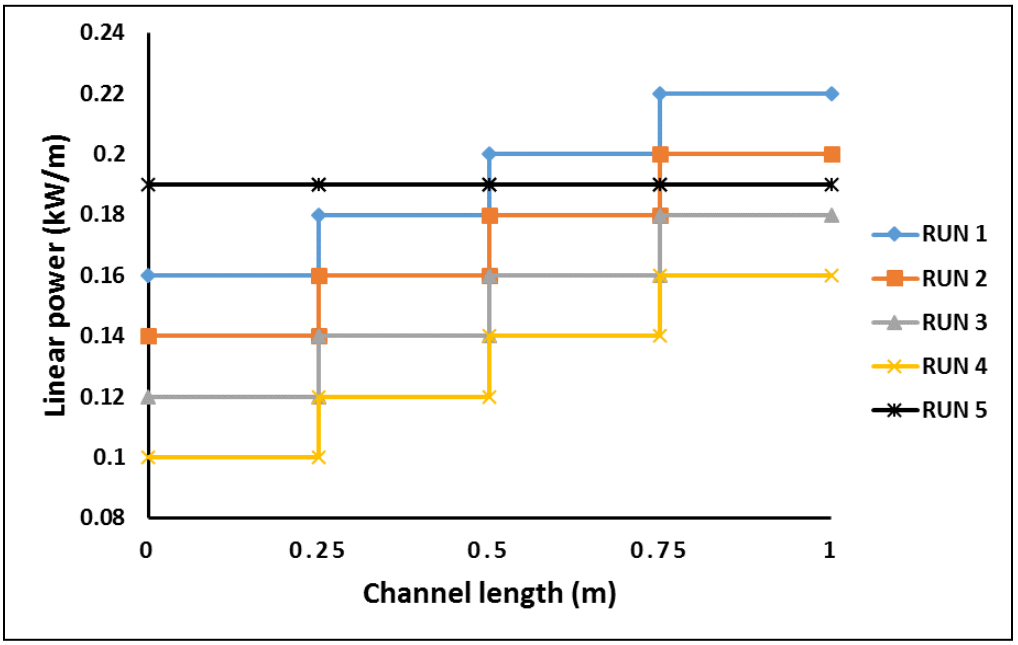

Figure 3.4. Power distribution around riser channel

The positive signals of heat fluxes were observed from Z/L = 0.044 up to Z/L= 0.591 (non-inflecting zone) as shown in Figures 3.5 a and 3.6 a for selected condition of Z/L= 0.591, while Figures 3.5 b, 3.5 c show negative signals of heat fluxes for Z/L= 0.773 and 3.6 b, 3.6 c show the for selected conditions for Z/L=0.956. These results show that the heat flow direction was reversed (from the flowing coolant air to the inner surface of the riser channel) for axial locations close to the exit. It is worth mentioning that the previous study [97] observed this end effect only at Z/L= 0.956 in riser channel with air as a coolant fluid under uniform isoflux heating. It is clear from the comparison of the current work with the other study [97] that the inflecting zone under nonuniform heating can be extended down into the riser channel. One can remarks from Figures 3.5 and 3.6 ((a) free of end-effect at Z/L=0.591, (b) initial of end-effect at Z/L= 0.773, (c) strong of end-effect at Z/L=0.956) a significant interaction and co-circulation in terms of heat fluxes in a descending reorder from Z/L = 0.773 to Z/L = 0.956 was observed in the current study. These observations could be attributed to nonuniform heating in terms of secondary flow [128] as well as heat conduction between the two channels through the upper plenum flange. In addition, the nonuniform heat flux distributions along riser channel create a density difference in the fluid [126], and the interaction between hot plumes of rising fluid (lighter) and denser fluid in the upper plenum which descends due to higher density. Negative heat fluxes are observed along the downcomer channels for all operating conditions. This confirms the downward flow and establishment of natural circulation between upper and lower plena.

(a)

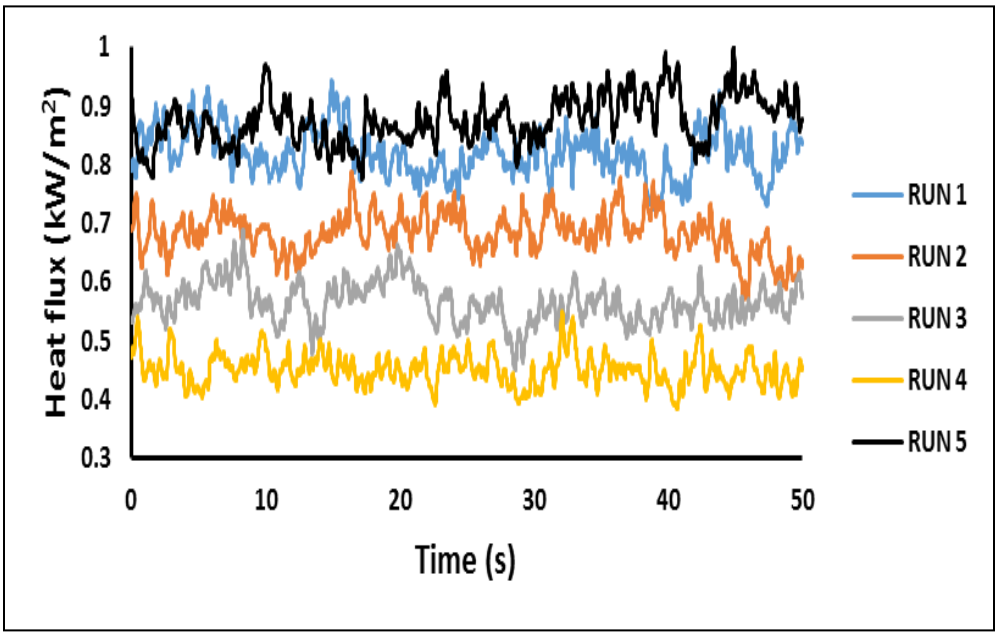

(b)

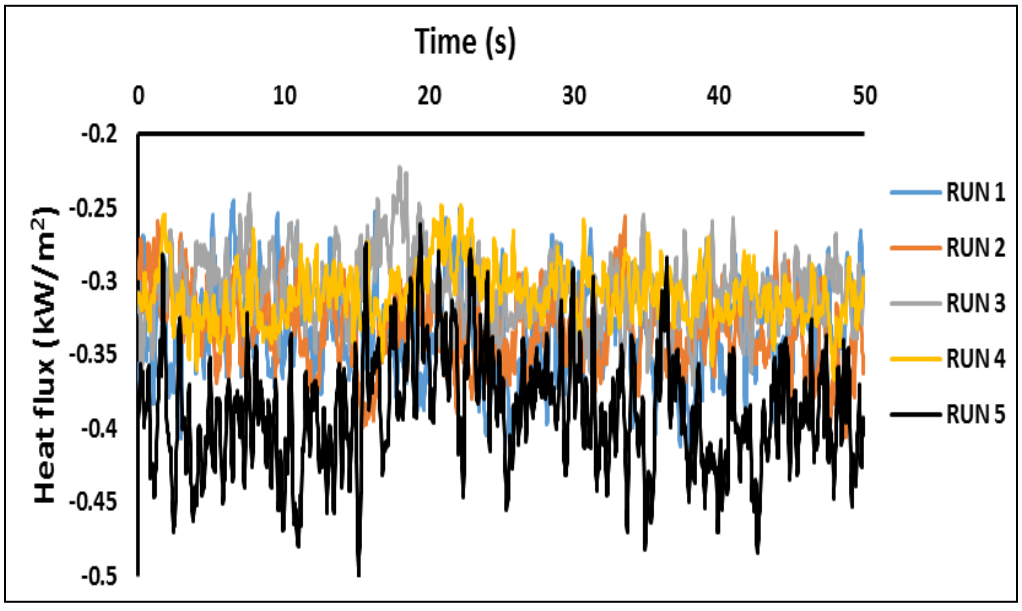

Figure 3.5. Stepwise-reducing, heating end-effect

(c)

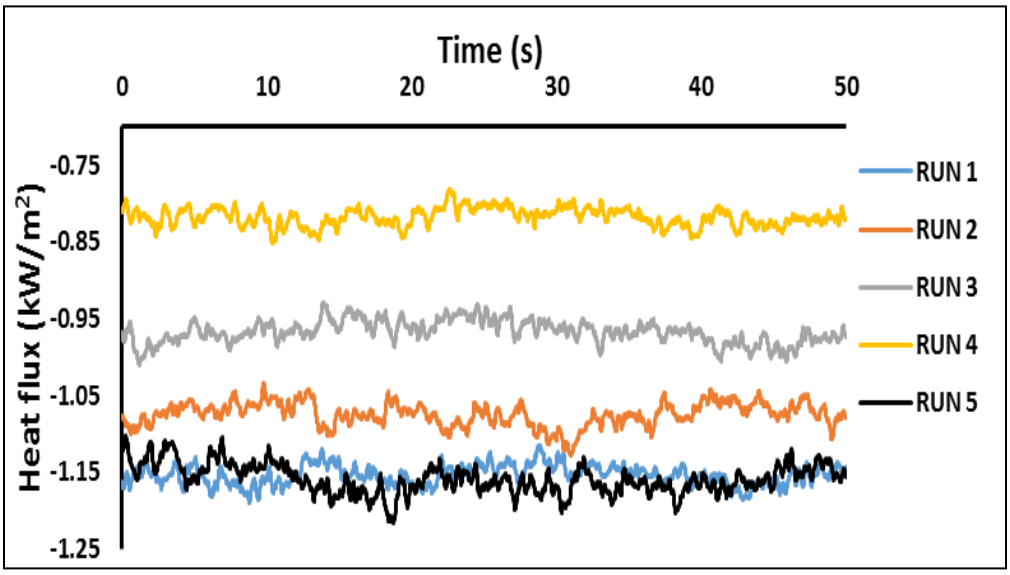

Figure 3.5. Stepwise-reducing, heating end-effect (Cont.)

(a)

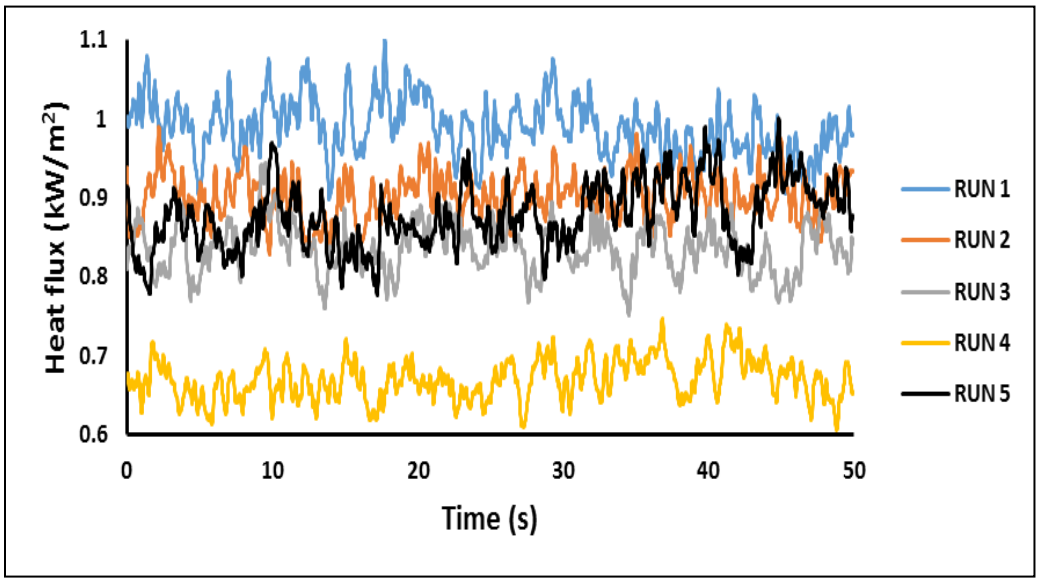

Figure 3.6. Stepwise-increasing end-effect

(b)

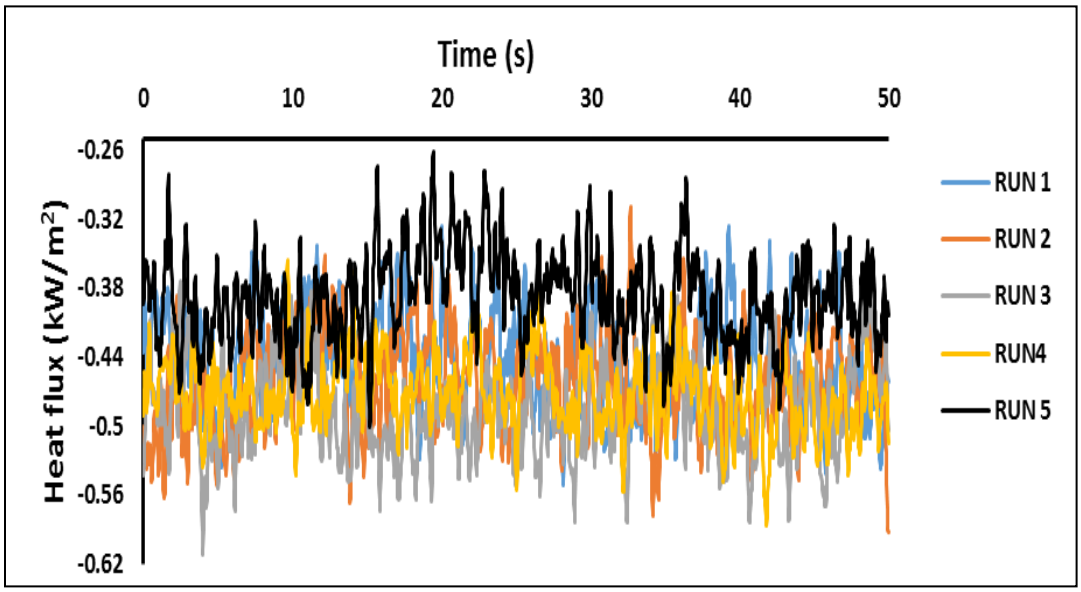

(c)

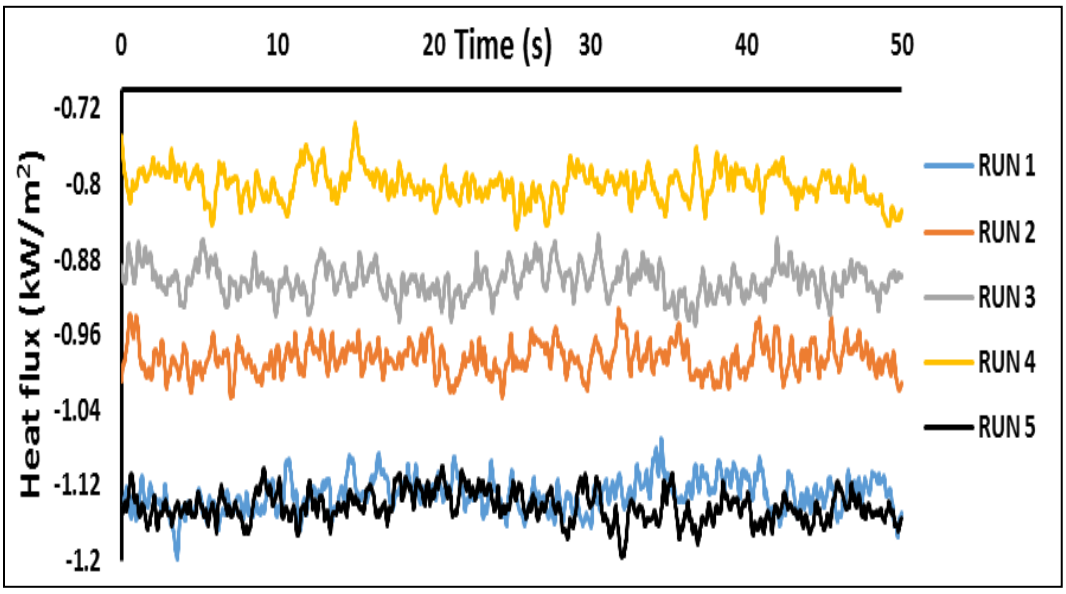

Figure 3.6. Stepwise-increasing end-effect (Cont.)

3.4.2. Temperature Field Profiles along the Flow Channels (Circulation Loop).

Next section will discuss the results of temperature distribution along flow channels and the effect of heat flux form that was applied around riser channel.

3.4.2.1. Stepwise-reducing-heating flux distributions. Figure 3.7 shows the axial temperature profiles along the circulation loop for stepwise-reducing heating for the inner wall surface and centerline air temperatures ((a) inner wall surface, (b) air centerline), and a sharp reduction for stepwise-reducing heating (runs 1 to 4) is observed compared to a uniform heating (run 5) for all experimental conditions. A significant reduction of the field temperatrures along the riser channel is observed to be 24.5% and 22.4% for inner surface and air centerline temperatures, respectively, from run 1 to run 4. One can notice that the axial distribution of the centerline air temperature is slightly different from the inner wall surface temperature as follows: 1) the maximum centerline air temperature is observed at Z/L=0.773, while the maximum surface temperature is observed at Z/L =0.591 2) A small plateau is observed for inner wall surface temperature between Z/L = 0.591 and Z/L=0.773, while no plateau is observed for the centerline air temperature, as shown in Figure 3.7 a and 3.7 b. This thermal performance in terms of field temperatures could be attributed to an increase in the air thermal conductivity, and that creates less resistance and an increase in the viscosity, causing radial flow of the hotter layers of air close to the surface toward the tube center. Moreover, with the nonuniform heating, the surface temperature reaches to the maximum value to develop the thermal boundary layer faster due to the buoyancy affected by nonuniform heating variation. This behavior is observed in open literature [128, 130, 135]. For uniform heating, the maximum temperature is at Z/L= 0.773 for both inner surface and air

centerline. This maximum temperature could be attributed to the reversal of the heat flow and buoyancy-induced motion, which has a significant effect in this phenomena [97,105-107,110,111,115,116,119,136,137]. The phenomenon of back-mixing is also possible for this setup and hence can be a concern for VHTR. Back-mixing is caused by the interaction of the rising plume from the riser channel and the fluid in the upper plenum, which in turn results in decreasing of the inner surface temperature of heat flow direction reversal. Downcomer channel during stepwise-reducing heating decreased from the inlet (Z/L=0.9560) to the outlet (Z/L=0.044), confirming the establishment of natural circulation and downward flow. A significant reduction in downcomer channel temperature profile is observed with decreasing the stepwise-reducing heating by 25.7% and 24.8% for inner surface and air centerline, respectively, for stepwise-reducing experimental heating runs.

3.4.2.2. Stepwise-increasing-heating flux distributions. In stepwise-increasing experiments, the results in Figure 3.8 ((a) inner wall surface, (b) air centerline) shows the axial temperature profiles along the circulation loop for stepwise-increasing heating for the inner wall surface and centerline air temperatures. A significant reduction of riser channel temperature is observed with decreasing stepwise-increasing heating by 25.6% and 23.1% for the inner surface and air centerline temperatures, respectively. The maximum temperature was observed at Z/L=0.773 for the inner surface and air centerline for stepwise-increasing and uniform heating runs and this phenomenon could be attributed to reversal of heat flow and back- mixing. The downcomer channel region showed a decreasing from the inlet (Z/L=0.9560) to the outlet (Z/L=0.044), which confirms the establishment of natural circulation and downward flow.

(a)

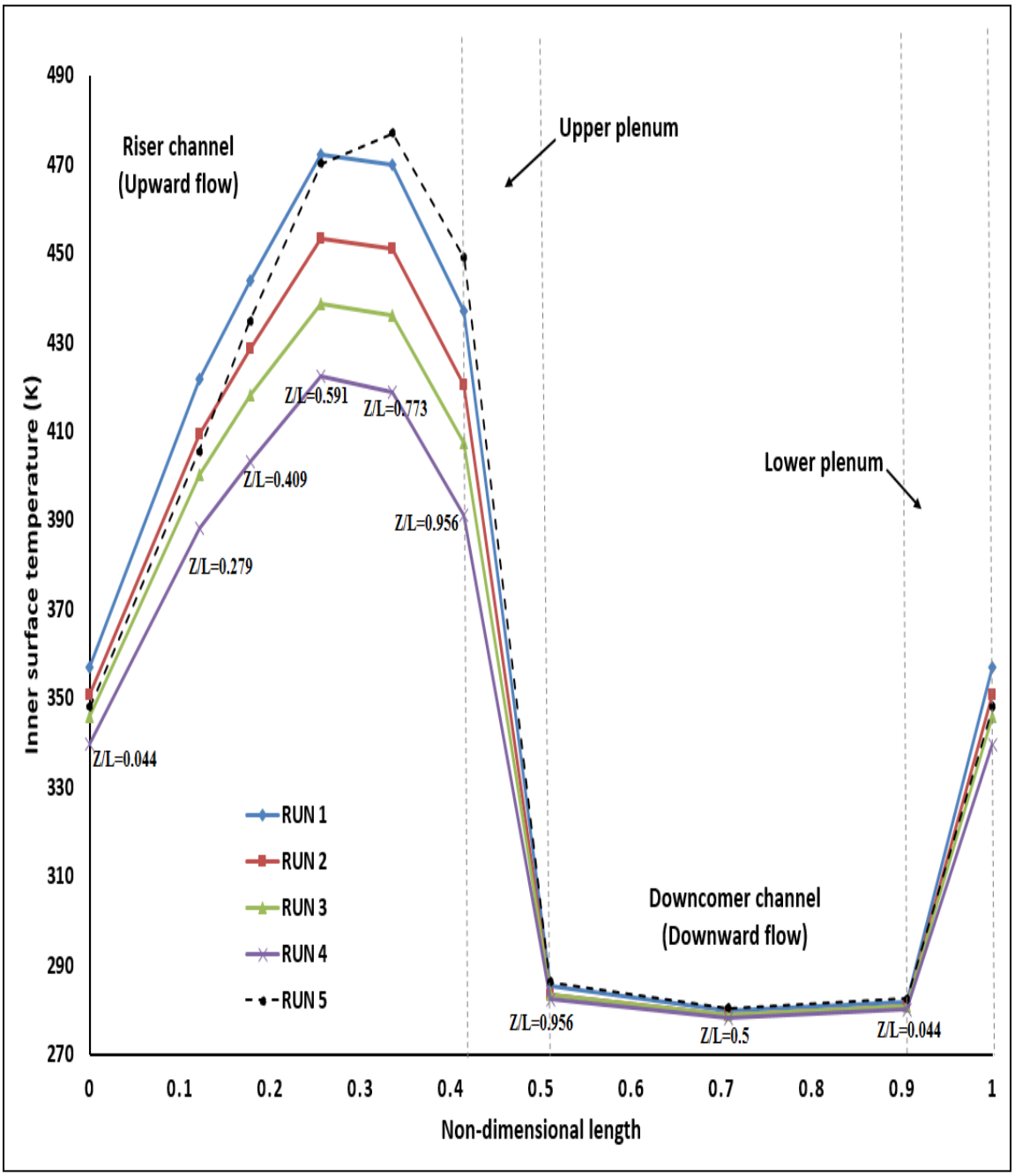

Figure 3.7. General steady-state temperature profile along the circulation loop for stepwise-reducing heating

(b)

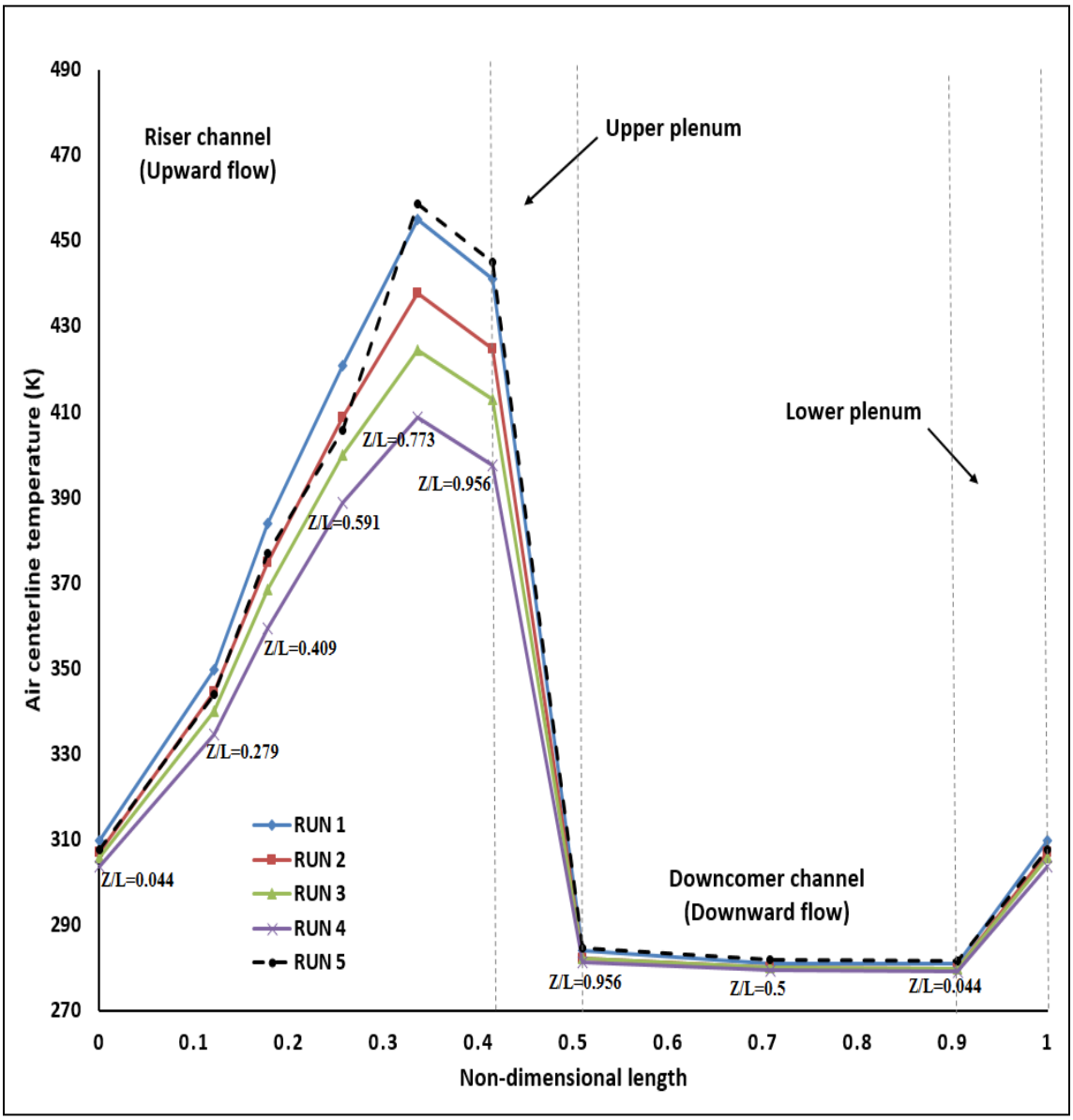

Figure 3.7. General steady-state temperature profile along the circulation loop for stepwise-reducing heating (Cont.)

A significant reduction in downcomer channel temperature profile is observed with decreasing stepwise-increasing heating by 14.1% and 14.8 % for inner surface and air centerline temperatures, respectively.

(a)

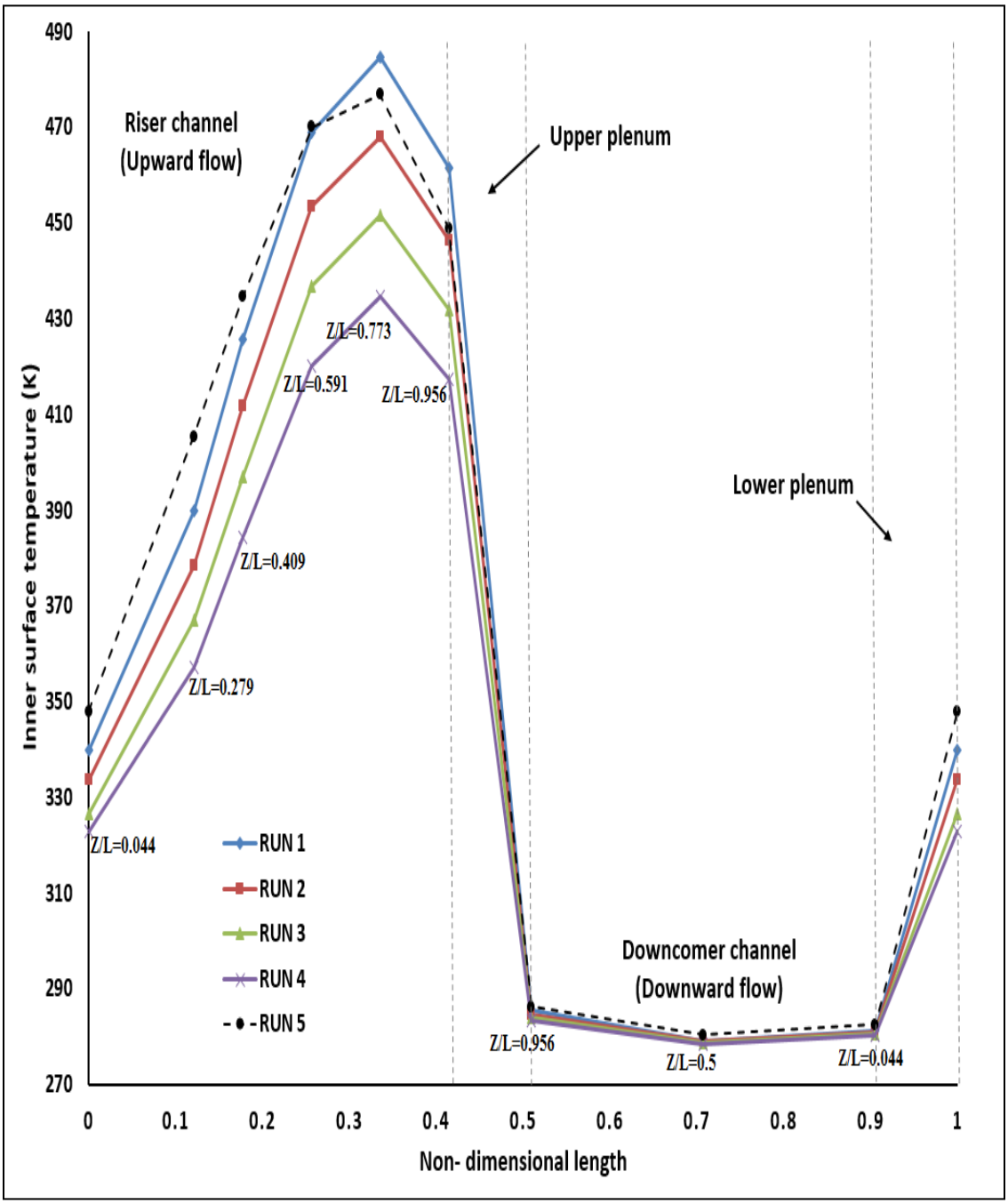

Figure 3.8. General steady-state temperature profile along the circulation loop for stepwise-increasing heating

(b)

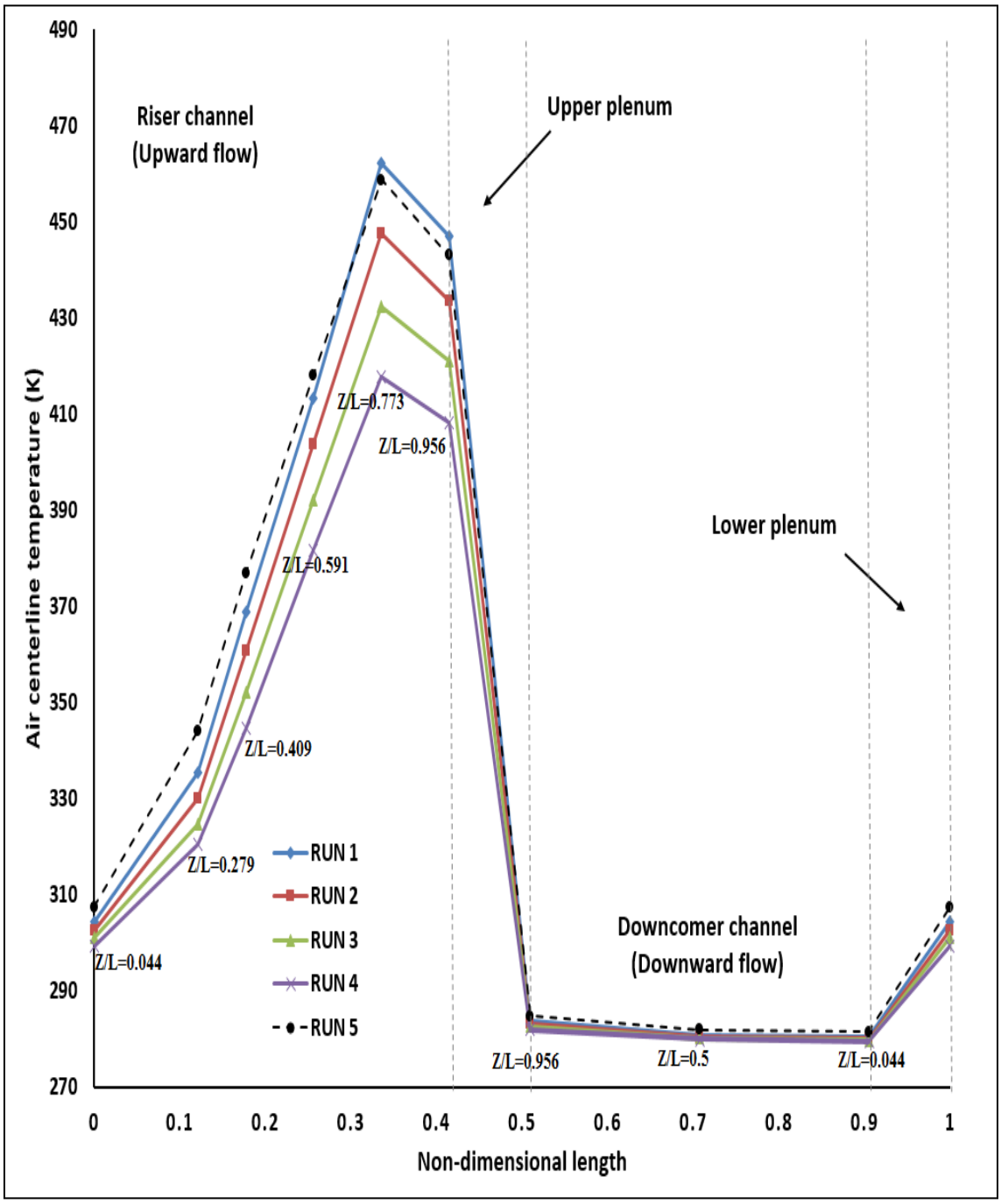

Figure 3.8. General steady-state temperature profile along the circulation loop for stepwise-increasing heating (Cont.)

3.4.3. Heat Transfer Coefficients along the Riser Channel. Next section will discuss the results of temperature distribution along flow channels and the effect of heat flux form that was applied around riser channel.

3.4.3.1. Stepwise-reducing-heating flux distributions. Figure 3.9 shows the results of heat transfer coefficient for stepwise-reducing heating. Figure 3.9 (a) shows the heat transfer coefficient along riser channel (Z/L= 0.044 to Z/L= 0.956) and the heat transfers from the adjacent air layer to the inner wall started after Z/L=0.591. This reversal in the direction of heat transfer could be attributed to the downward axial cooling conduction inside the solid wall of the riser channel from the upper plenum and co-circulation at the top section of the riser channel as reported in the literature [97,105-107,110,111, 138, 139]. The flipping (change in the order of the runs) is shown again in Figure 3.9 (a) to confirm the results in end–effect section in Figure 3.5 (c), which presents the strong end-effect that had occurred at Z/L= 0.956. Figures 3.9 (b) and 3.9 (c) present the variations of the heat transfer coefficient for Z/L= 0.044 to Z/L= 0.773 and from Z/L= 0.044 to Z/L= 0.591 along riser channel, respectively. It is clear from the results that for all cases heat transfer coefficients decrease from the inlet (Z/L = 0.044) to (Z/L = 0.279); this could be attributed to the development of hydrodynamic and thermal boundary layers. An increase in the values of the heat transfer coefficients is observed after Z/L = 0.279 to Z/L = 0.591 due to the laminarization effects [115,116,136,137]. At (Z/L= 0.409), the heat transfer coefficient is increasing by 40.8% in stepwise-reducing heating (runs 1and 2) with respect to the uniform heating, and decreasing by 21.3% for runs 3 and 4. The influence of end effect is very clear on values of the local heat transfer coefficients after Z/L=0.591 in terms of a decreasing trend.

(a)

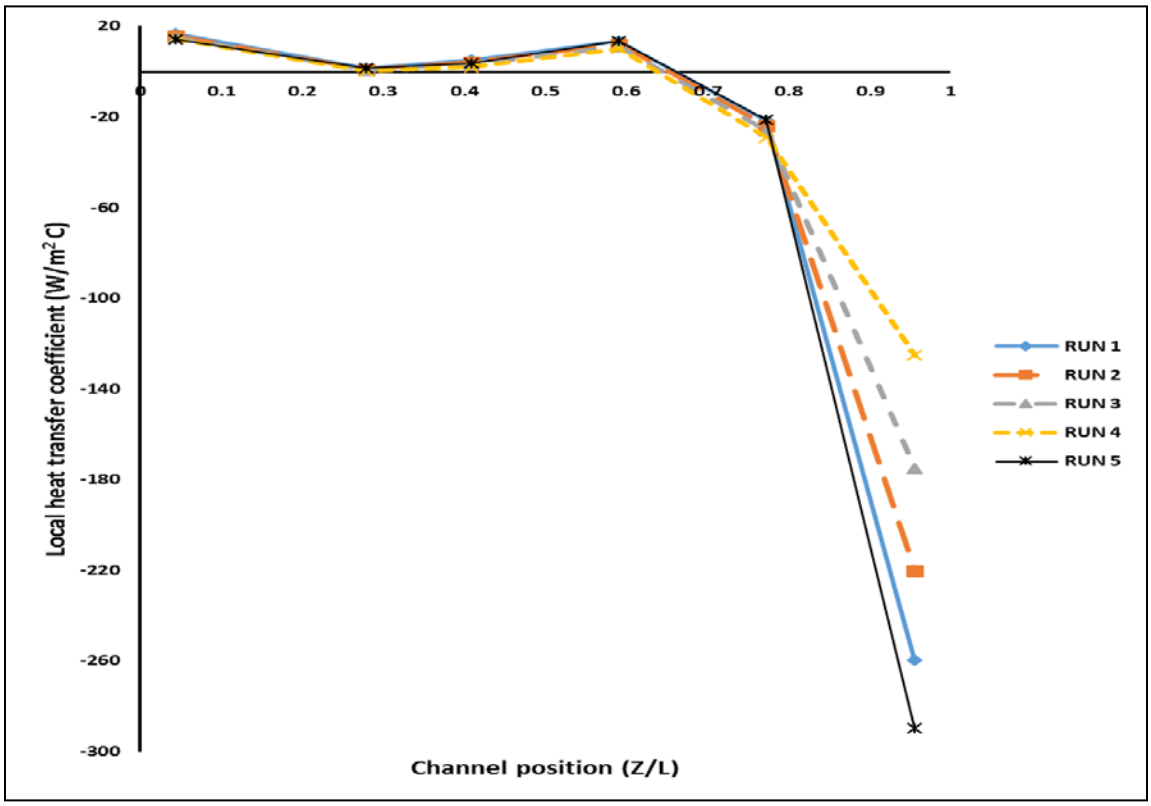

(b)

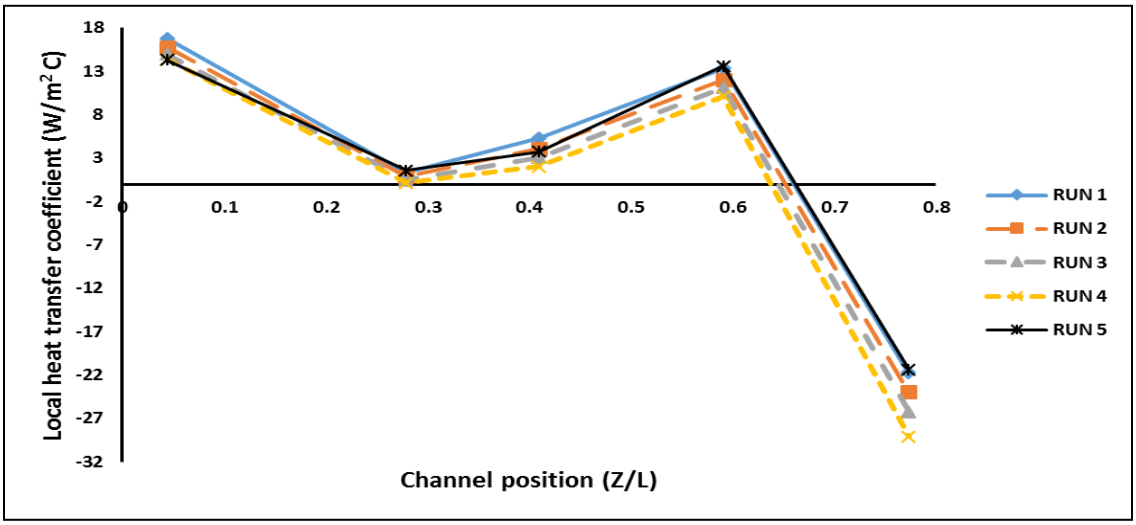

Figure 3.9. Stepwise-reducing heating heat transfer coefficient

(c)

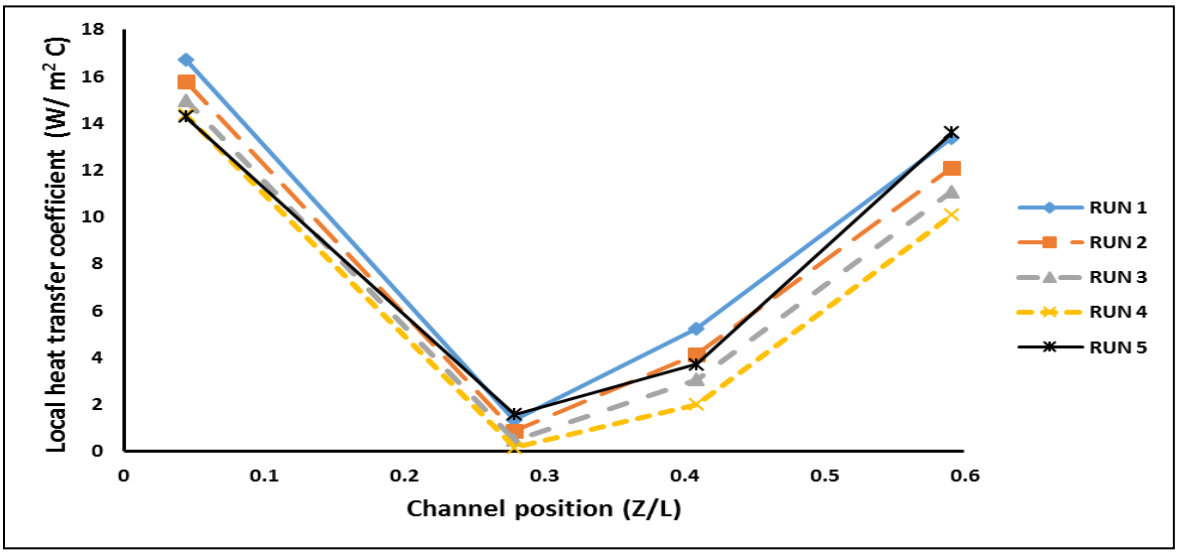

Figure 3.9. Stepwise-reducing heating heat transfer coefficient (Cont.)

3.4.3.2. Stepwise-increasing-heating flux distributions. Figures 3.10 shows the results of heat transfer coefficient for stepwise-increasing heating. Figure 3.10 a shows the heat transfer coefficient along riser channel (Z/L= 0.044 to Z/L= 0.956) and the heat transfers from the adjacent air layer to the inner wall started after Z/L=0.591. This reversal in the direction of heat transfer could be attributed to the downward axial cooling conduction inside the solid wall of the riser channel from the upper plenum and co-circulation at the top section of the riser channel as reported in the literature [119, 138]. The flipping is shown again in Figure 3.10 (a), confirming the results in the end-effect section in Figure 3.6 (c), which presents the strong end-effect that had occurred at Z/L= 0.956. Figures 3.10 (b) and 3.10 (c) present the variations of the heat transfer coefficient for (Z/L= 0.044 to Z/L= 0.773) and (Z/L= 0.044 to Z/L= 0.591) respectively along riser channel. It is clear that the heat transfer coefficients decrease from the inlet (Z/L = 0.044)

to (Z/L = 0.279); this could be attributed to the development of hydrodynamic and thermal boundary layers. An increase in the values of the heat transfer coefficients is observed after Z/L = 0.279 to Z/L = 0.591 due to the laminarization effects [97,105-107,110,111, 115,116,136,137]. At (Z/L= 0.591), the heat transfer coefficient is increasing by 11.1% in stepwise-increasing heating (runs 1and 2) with respect to the uniform heating, and decreasing by 1.1% for runs 3 and 4. The influence of end effect is very clear on the values of the local heat transfer coefficients after Z/L=0.591 in terms of a decreasing trend for all runs.

(a)

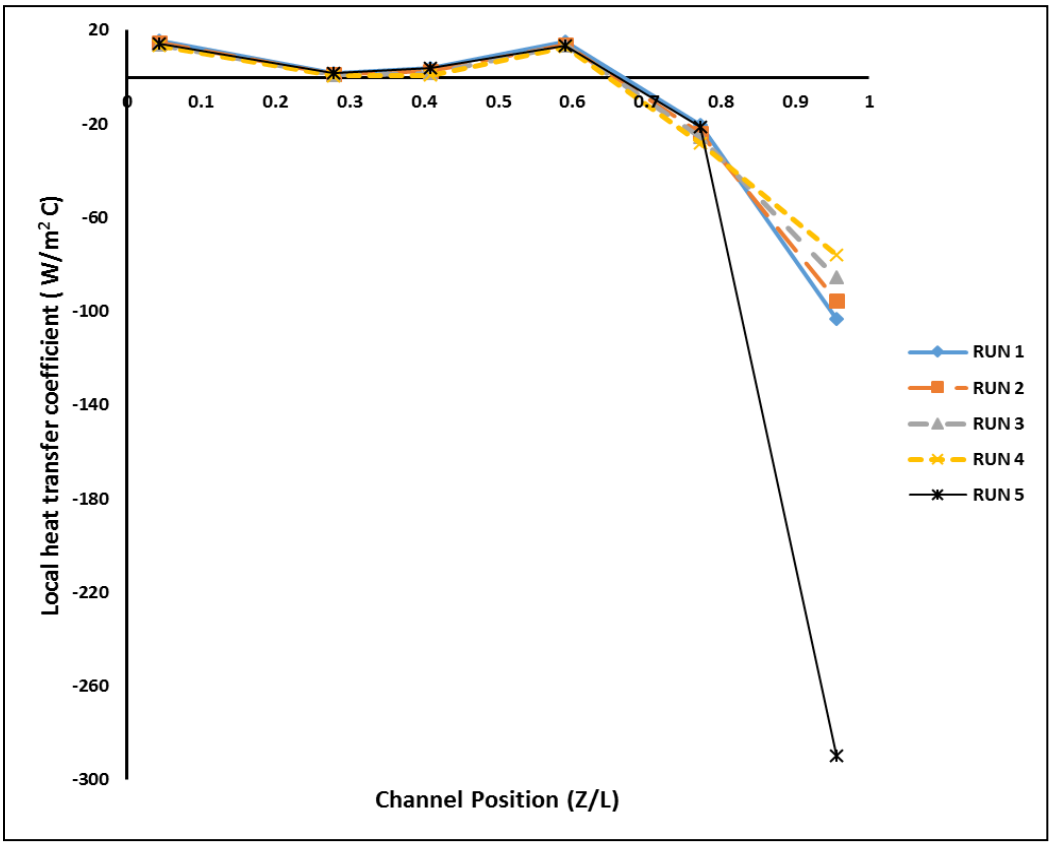

Figure 3.10. Stepwise-increasing heating heat transfer coefficient

(b)

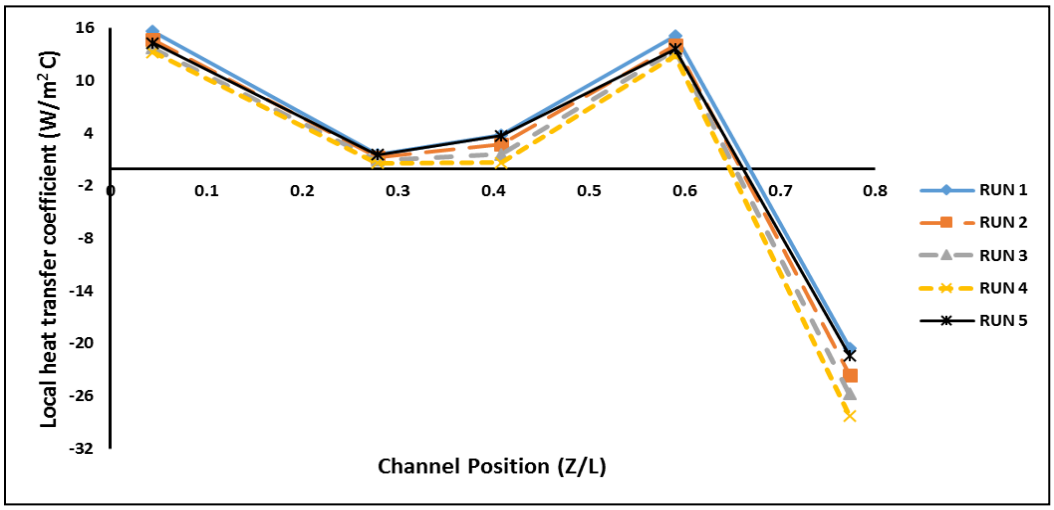

(c)

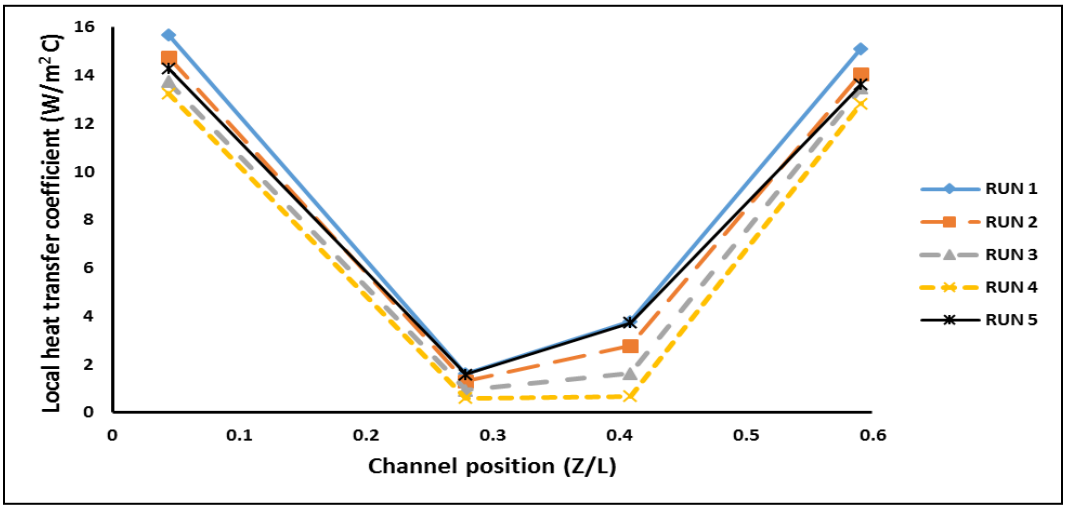

Figure 3.10. Stepwise-increasing heating heat transfer coefficient (Cont.)

3.4.4. The Average Values of the Heat Transfer Coefficient($\bar{h}_L$) and the Average Nusselt Number ($\overline{Nu}_L$). Heat transfer coefficient is a quantitative characteristic of convective heat transfer efficiency between the bulk fluid temperature and inner surface temperature of the riser channel and is used to calculate the dimensionless group

Nusselt number as shown in Eq 7. For stepwise-reducing heating, the average values of the heat transfer coefficient($\bar{h}_L$) and the average Nusselt number ($\overline{Nu}_L$) were decreased with reducing the heating (for runs 1 to 4) by 21% and 5%, respectively, as shown in Figure 3.11 (a). Moreover, Figure 3.11 (b) shows the average values of the heat transfer coefficient ($\bar{h}_L$) and the average Nusselt number ($\overline{Nu}_L$) for the stepwise-increasing heating investigations, which decreased with decreasing the heating (for runs 1 to 4) by 32% and 13%, respectively. The negatives values of heat transfer coefficient at positions Z/L= 0.733 and Z/L=0.956 were excluded in calculating the average heat-transfer coefficient($\bar{h}_L$) and Nusselt number plots ($\overline{Nu}_L$).

(a)

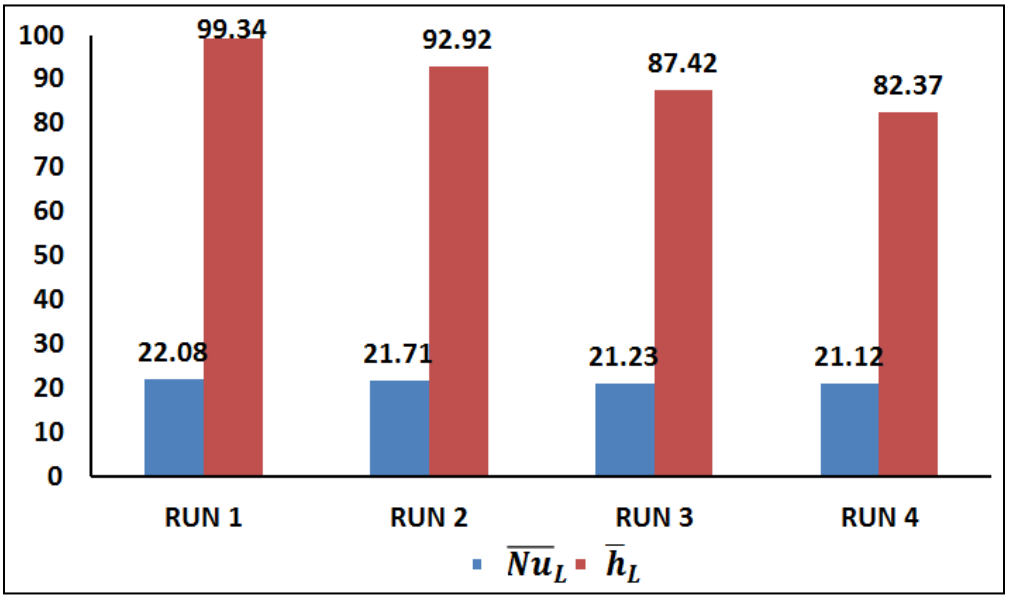

Figure 3.11. The average values of the heat transfer coefficient and the average Nusselt number along the riser channel

(b)

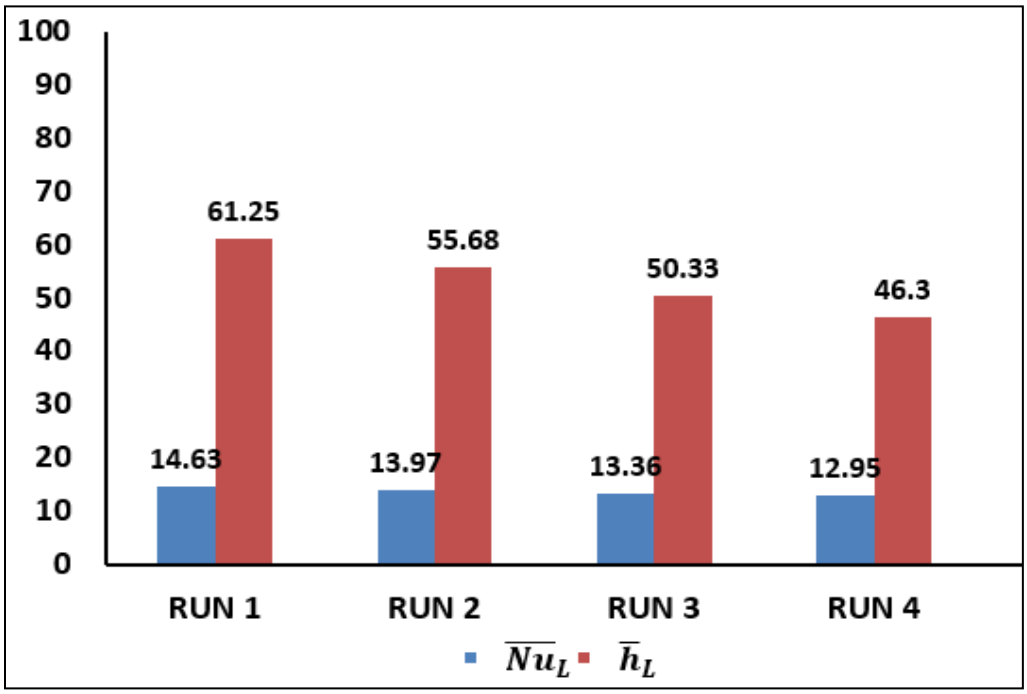

Figure 3.11. The average values of the heat transfer coefficient and the average Nusselt number along the riser channel (Cont.)

3.4.5. Radial Variation of Air Temperatures along the Riser Channel. The radial distribution of air was collected by radial temperature adjuster Figure 3.2 (c). It was similar in all trials for the selected condition (RUN1), as shown in Figures 3.12. ((a) stepwise-reducing, (b) stepwise-increasing, (c) uniform heat flux RUN 5). From the entrance of the riser channel to Z/L=0.591, a developing profile was observed. A flattened profile was observed at Z/L=0.773, and when the air could not remove any more heat, a reversed profile was observed at Z/L=0.956 because heat was being removed through end effects from the upper plenum. The developing profile corresponds with areas where heat is transferred from the wall to the air, the flattened profile corresponds

with the hottest part of the model, and the reversed profile corresponds with the area where heat transferred from the gas to the wall.

(a)

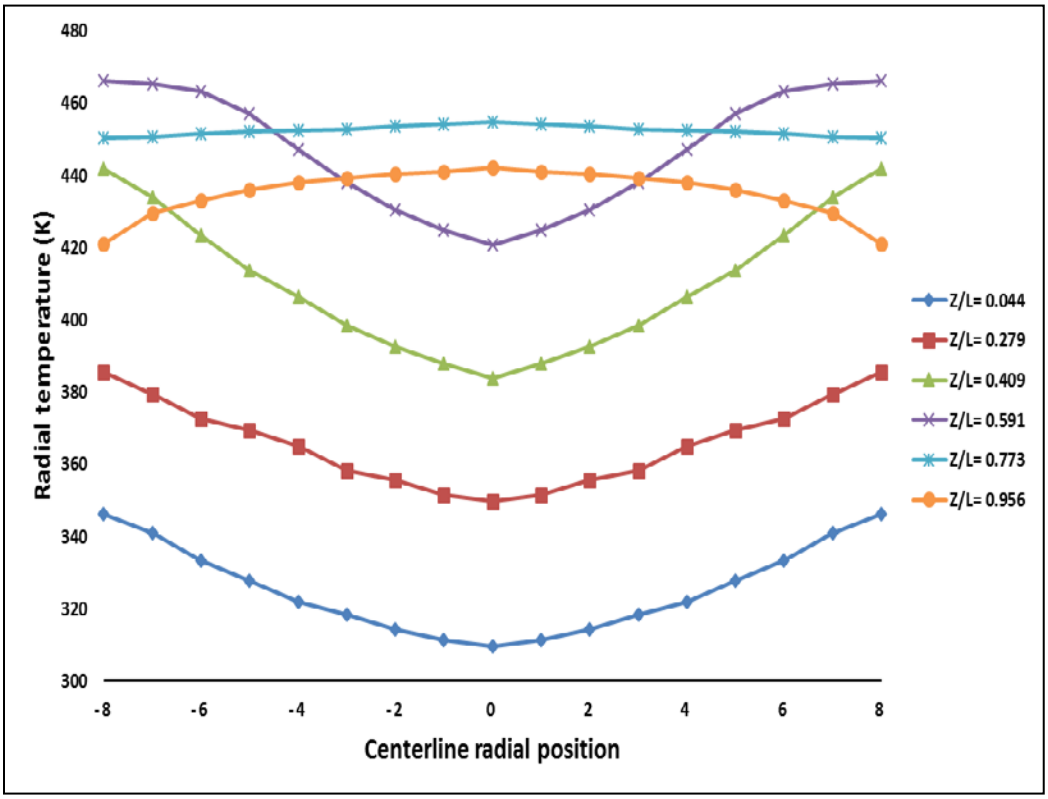

Figure 3.12. Radial temperature distribution for air at RUN 1 along the riser channel

(b)

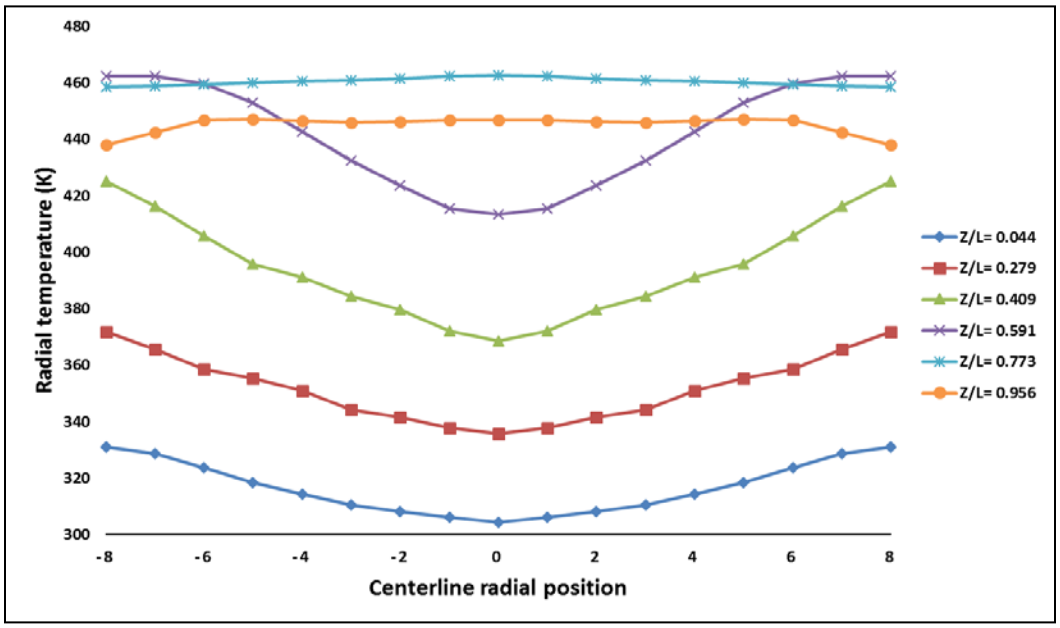

(c)

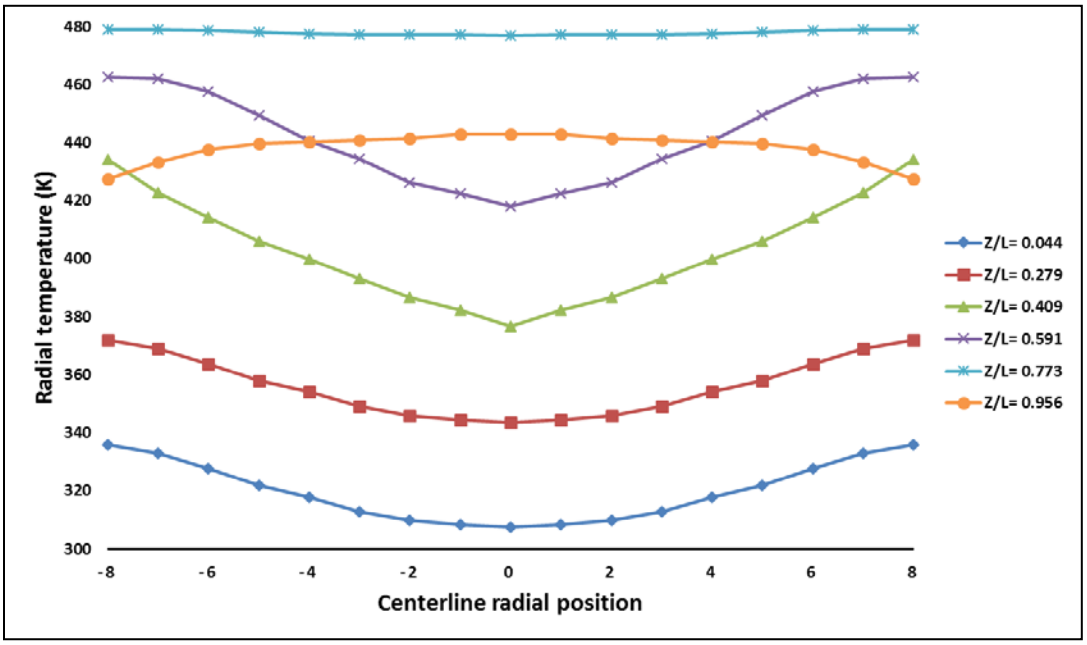

Figure 3.12. Radial temperature distribution for air at RUN 1 along the riser channel (Cont.)

Variations of the physical properties of the coolant, including heat capacity, density, dynamic viscosity, and thermal conductivity have significant influence on the intensity of natural circulation in the PMR. Figures 3.13 to 3.18 show the variations of air density, dynamic viscosity, and thermal conductivity in terms of dimensionless values for selected axial positions along the riser channel. The physical properties are plotted at local radial temperature divided by the bulk value [105, 106]. The bulk values of density, thermal conductivity, and dynamic viscosity are calculated at the operating pressure and characteristic fluid temperature of air ($T_{b,i} = \frac{1}{8}\sum_{j=1}^{j=8} T_{fi,j}$), while the local radial values (eight measurements with a step size of 1mm from the inner surface of riser channel) are measured at same corresponding operating conditions using the radial adjuster for T-thermocouple.

The air properties used in the current study are based on using peace software [140]. Viscosity and thermal conductivity are below the bulk value in the center, above near the edges. This is reversed for density. The normalized viscosity and thermal conductivity curves are very similar, showing that viscosity is the main indicator of conductivity. Figure 3.18 shows instability for physical properties for stepwise-increasing that is not observed in stepwise-reducing, which could be attributed to heat flux which is high close to Z/L=0.956 in stepwise-increasing more than stepwise-reducing (Figure 3.15). Figures 3.15 and 3.18 show the radial distribution of the physical properties close to the end of the riser channel. It is clear the instability in physical properties for stepwise-increasing which is not observed in stepwise-reducing case. This difference can be attributed to end-effect which was starting early in stepwise-reducing condition.

(a)

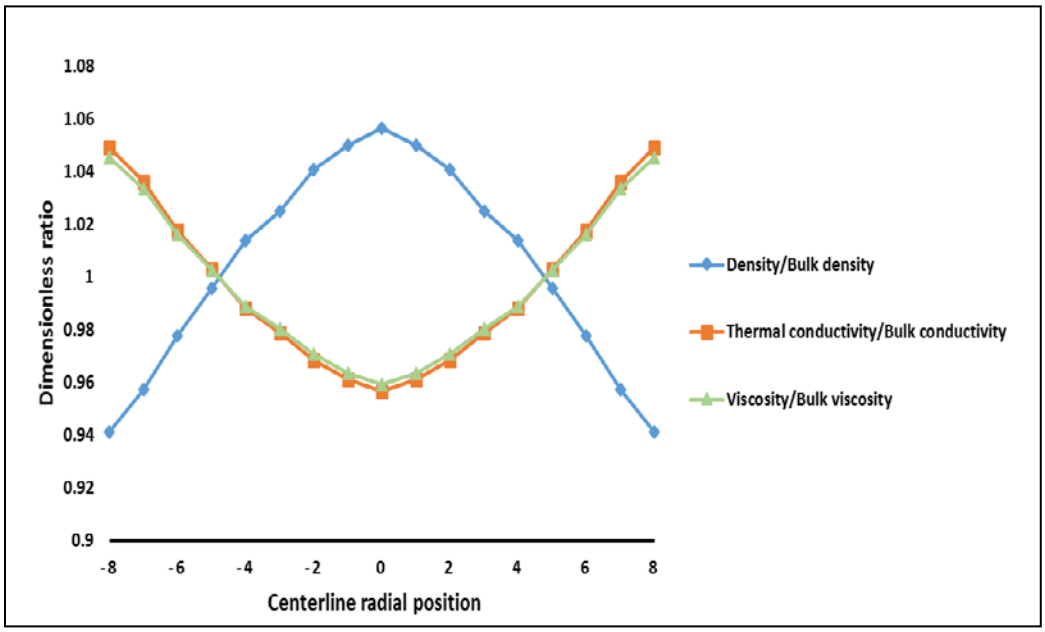

(b)

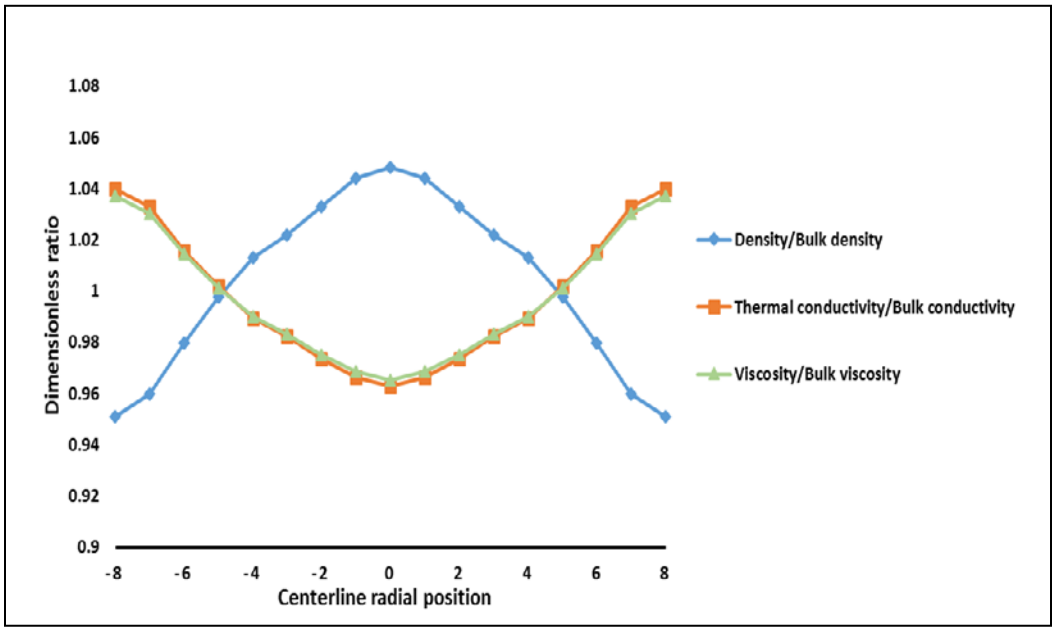

Figure 3.13. Radial distribution of the physical properties at Z/L= 0.044 for stepwise-reducing (a) RUN1, (b) RUN3, (c) RUN5

(c)

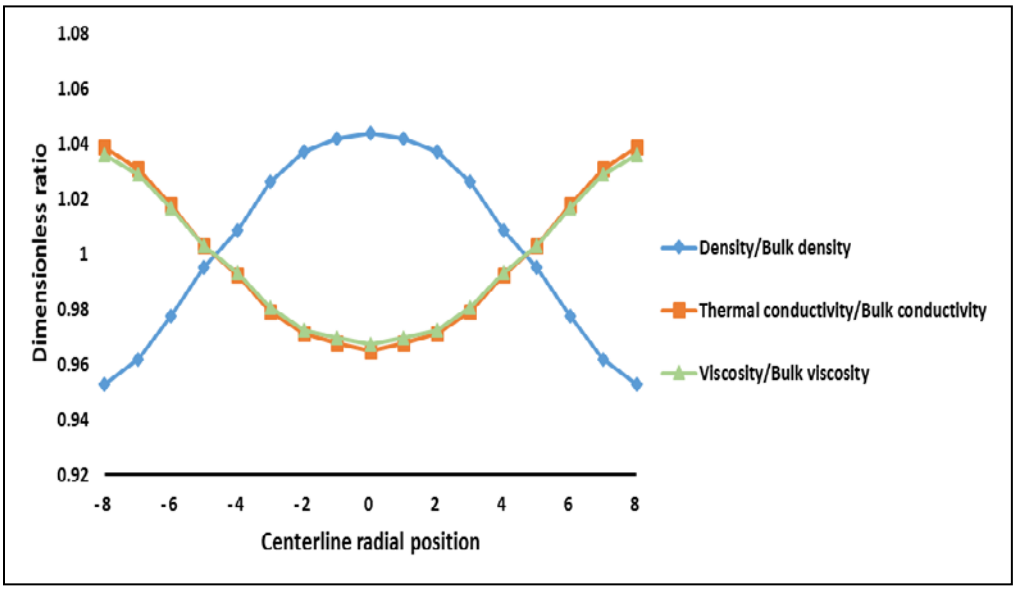

Figure 3.13. Radial distribution of the physical properties at Z/L= 0.044 for stepwise-reducing (a) RUN1, (b) RUN3, (c) RUN5 (Cont.)

(a)

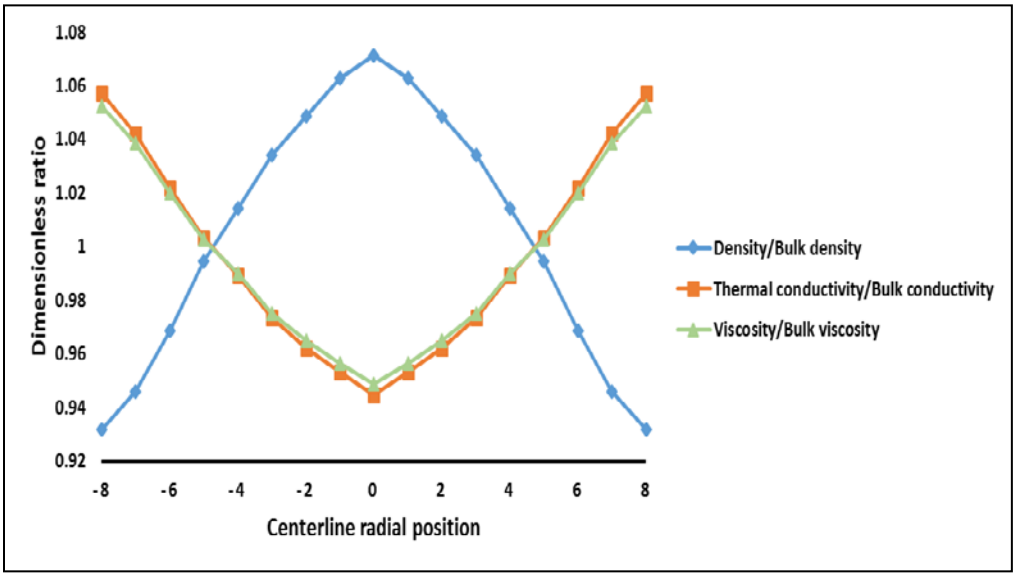

Figure 3.14. Radial distribution of the physical properties at Z/L= 0.409 for stepwise-reducing (a) RUN1, (b) RUN3, (c) RUN5

(b)

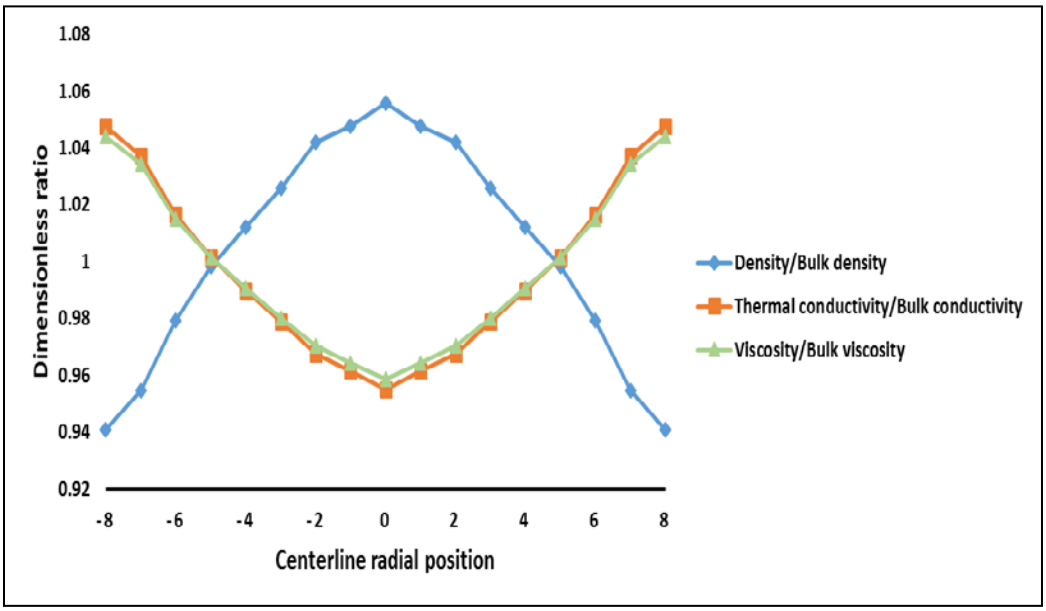

(c)

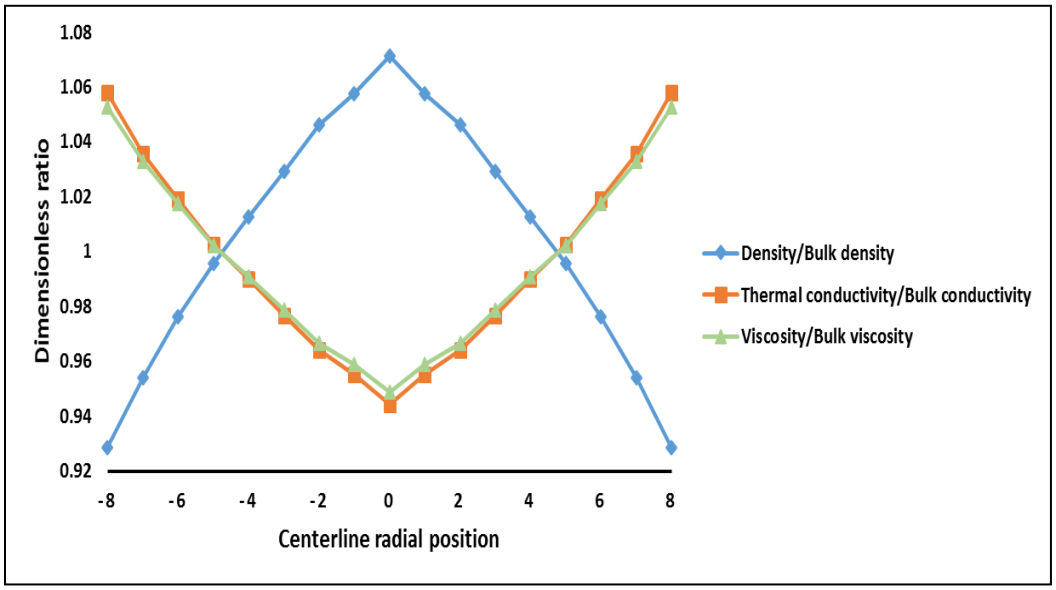

Figure 3.14. Radial distribution of the physical properties at Z/L= 0.409 for stepwise-reducing (a) RUN1, (b) RUN3, (c) RUN5 (Cont.)

(a)

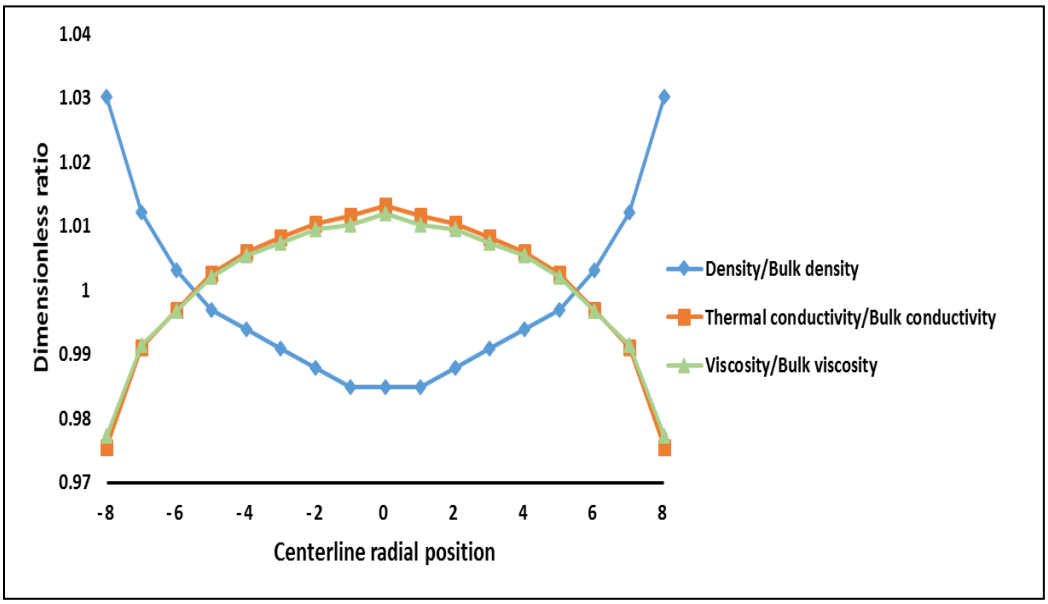

(b)

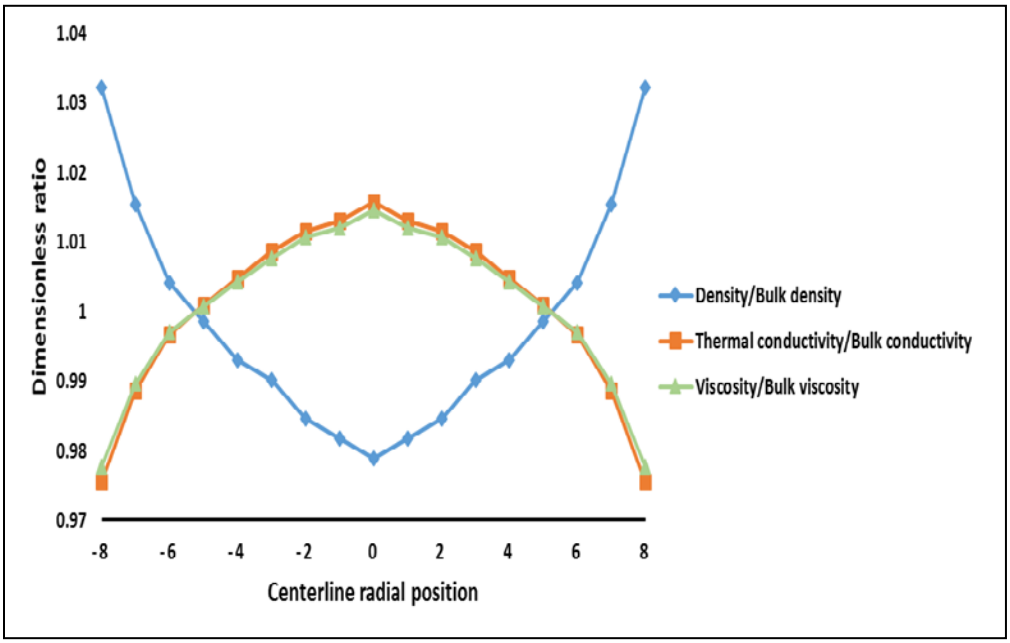

Figure 3.15. Radial distribution of the physical properties at Z/L= 0.956 for stepwise-reducing (a) RUN1, (b) RUN3, (c) RUN5

(c)

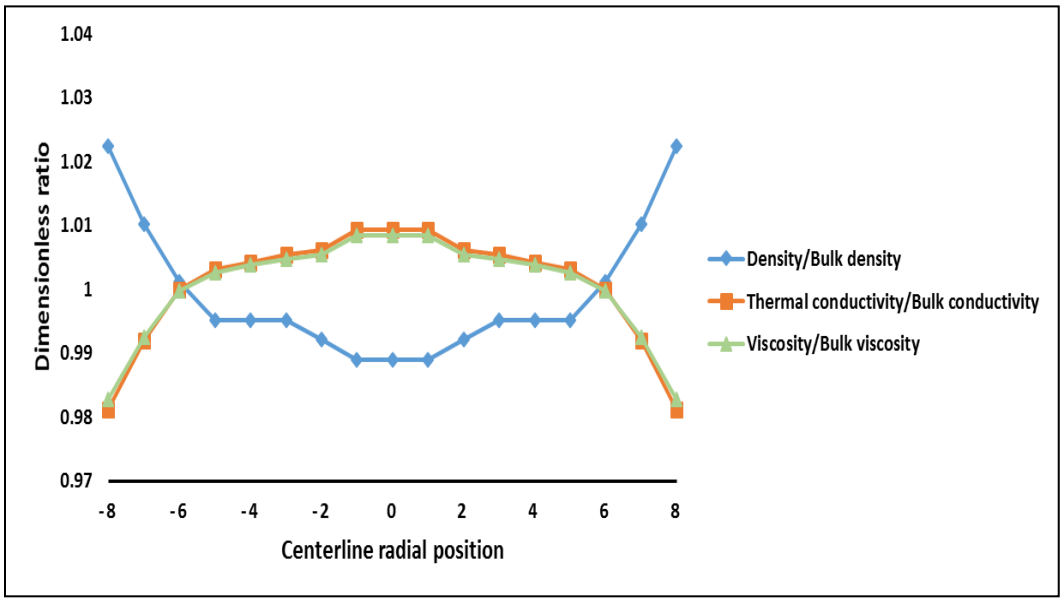

Figure 3.15. Radial distribution of the physical properties at Z/L= 0.956 for stepwise-reducing (a) RUN1, (b) RUN3, (c) RUN5 (Cont.)

(a)

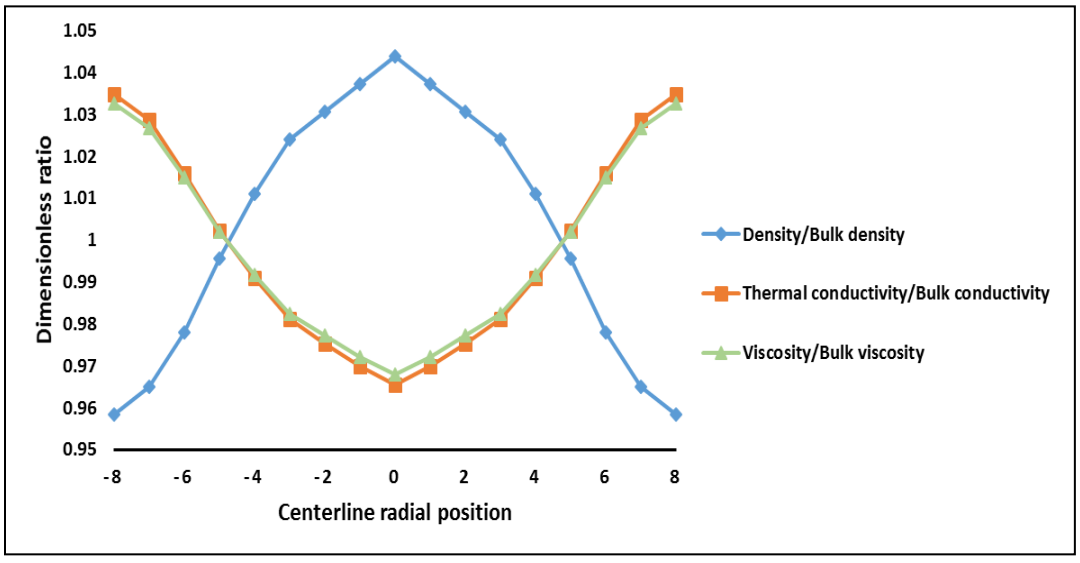

Figure 3.16. Radial distribution of the physical properties at Z/L= 0.044 for stepwise-increasing (a) RUN1, (b) RUN3

(b)

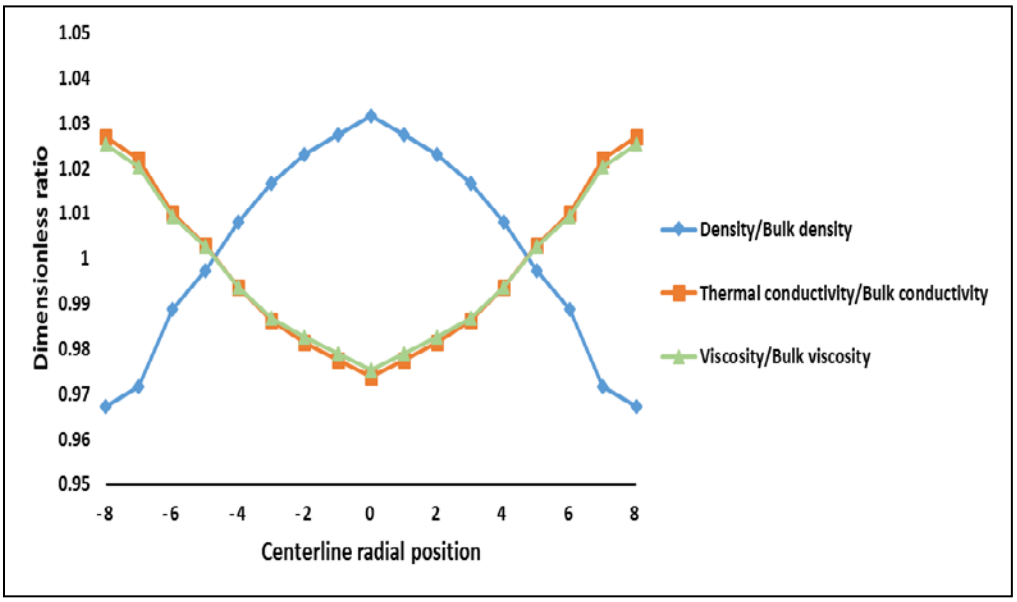

Figure 3.16. Radial distribution of the physical properties at Z/L= 0.044 for stepwise-increasing (a) RUN1, (b) RUN3 (Cont.)

(a)

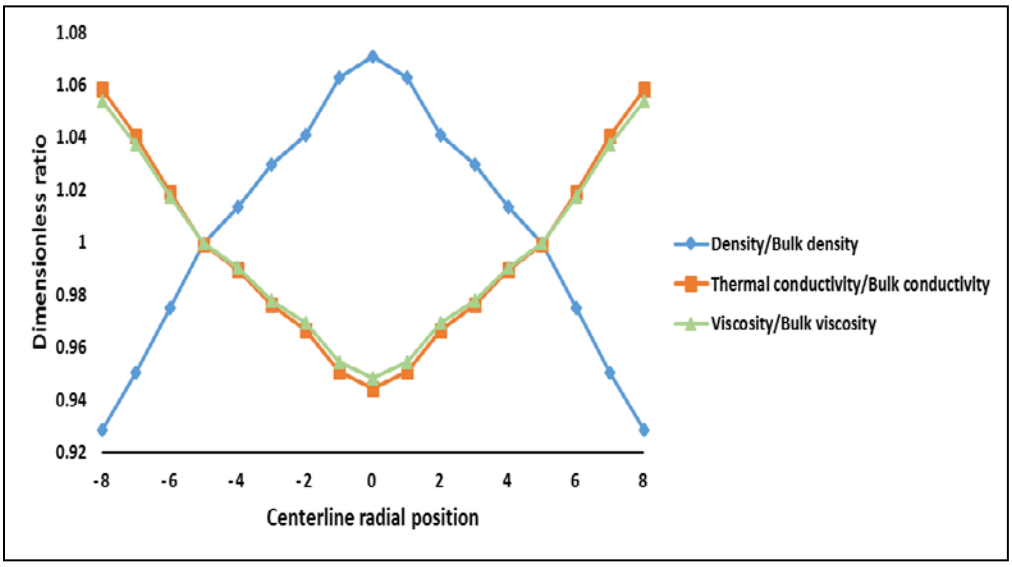

Figure 3.17. Radial distribution of the physical properties at Z/L= 0.409 for stepwise-increasing (a) RUN1, (b) RUN3

(b)

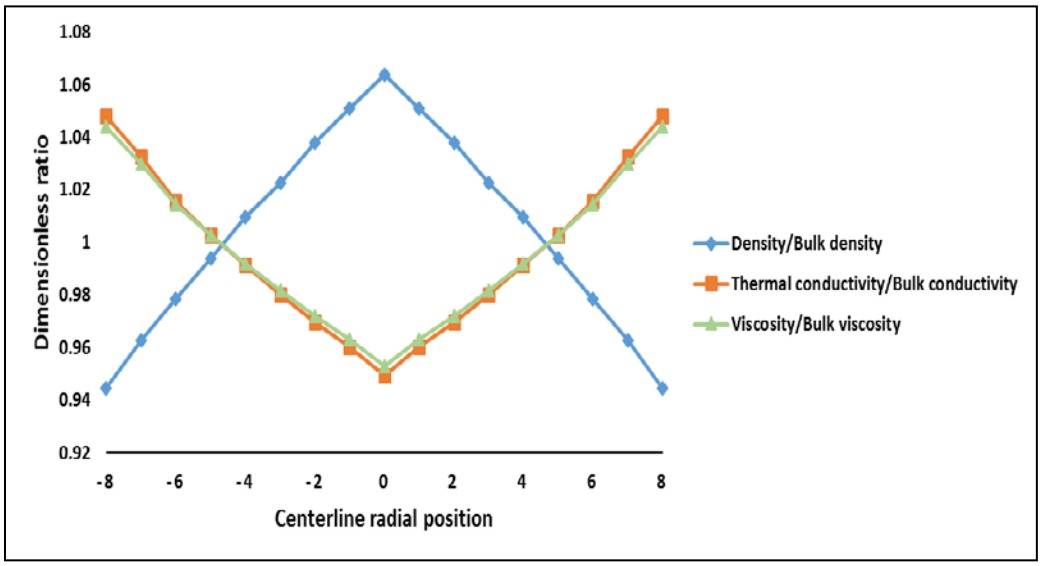

Figure 3.17. Radial distribution of the physical properties at Z/L= 0.409 for stepwise-increasing (a) RUN1, (b) RUN3 (Cont.)

(a)

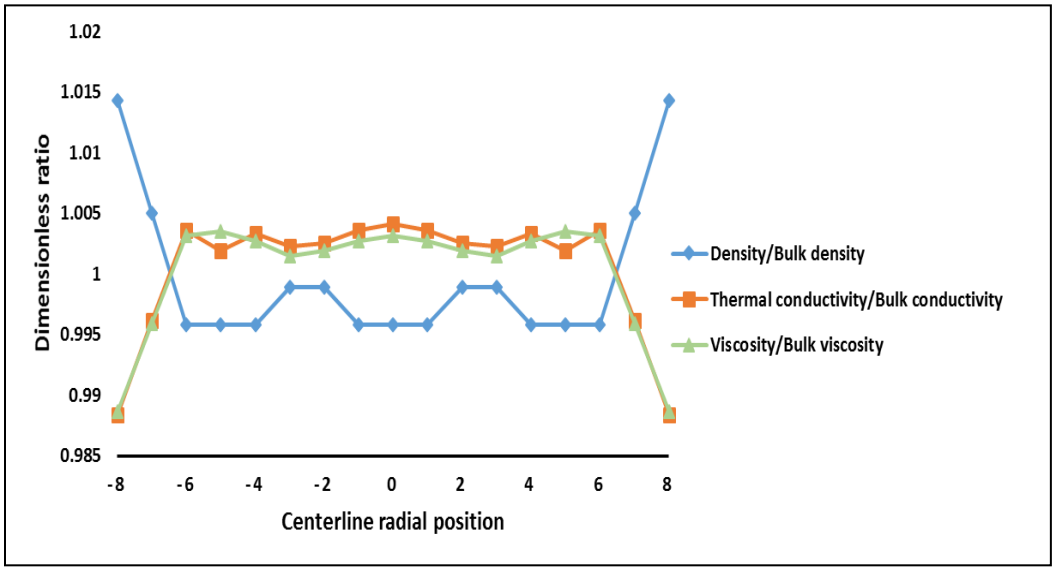

Figure 3.18. Radial distribution of the physical properties at Z/L= 0.956 for stepwise-increasing (a) RUN1, (b) RUN3

(b)

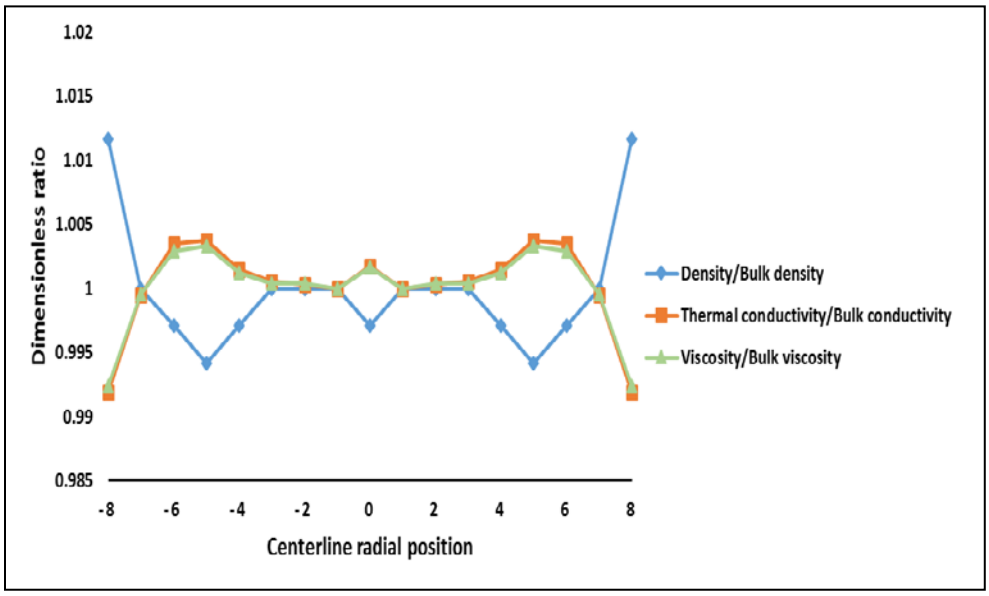

Figure 3.18. Radial distribution of the physical properties at Z/L= 0.956 for stepwise-increasing (a) RUN1, (b) RUN3 (Cont.)

4. INVESTIGATE THE INFLUENCE OF CENTER PEAKING COSINE HEAT FLUX ON HEAT TRANSFER DURING NATURAL CIRCULATION

Among the promising candidates for the next generation nuclear plant (NGNP) is the prismatic modular reactor (PMR). Reactor core of PMR is made up of hexagonal graphite blocks with channels for fuel rods and coolant flow. The removal of the post-shutdown decay heat relies on natural circulation. Under off-normal shutdown and accidental scenarios such as loss of forced cooling accident (LOFA), adequacy of natural convection must be evaluated to ensure passive safety. Pressurized conduction cooldown accidents (PCC) is a loss of flow accident, meaning the forced flow of working fluid to the reactor is suspended. During PCC, high working fluid pressure is maintained. In contrast to depressurized conduction cooldown (DCC) where working fluid pressure drops down immediately. Understanding how reactor properties affect natural convection during PCC is crucial to passive safety. It is important to understand how the coolant circulates to design reactors that safely shut down in the event of a loss of coolant flow accident. When pressurized conduction cooldown (PCC) accident takes place, the heat transfer characterization in the PMR is addressed by numerous computational studies in the open literature [77,92,120,141,142]. Recent experimental studies used some sophisticated measurement techniques to advance the current knowledge of the PMR under natural circulation in a unique dual-channel facility [97,99,105,106,110,143-145]. However, the focus of the initial studies was on uniform heat flux conditions, which is not a typical scenario of the PMR during the LOFA scenarios. Due to the cosine nature power distribution of a typical cylindrical reactor, one would expect the decay heat to follow the same cosine shape. Therefore, additional emphasis is placed on generated heat

transfer data, in terms of field temperatures and heat transfer coefficients, for nonuniform heating center peaking step (approximating cosine shape). There is a real need to extend this investigation to include more realistic conditions of nonuniform axial heat flux distributions. In this study, experimental results and analysis are provided for natural circulation with air (working fluid) using advanced instrumentation detailing heat transfer data in terms of temperature fields (centerline air and inner wall surface temperatures) and heat transfer coefficients under natural circulation. The effect of the intensity of nonuniform heat flux at steady state is investigated for air at 413.685 kPa. The collected data in this study can provide the necessary benchmark to validate thermal-hydraulic codes such as; RELAP5-3D, CFD-STAR-CCM1, CFD-Fluent, and so forth.

4.1. METHODOLOGY

Multiphase Reactors Engineering and Applications Laboratory (mReal) at Missouri S&T developed a dual-channel facility to imitate the coolant flow in PMR [97,99,105,106,143]. The current facility is constructed with reference to OSU-HTTF with a scale ratio of ¼ axially and radially [142]. The development of the constant diameter's (0.016 m) dual channel is for the upward and downward flows of the coolant at the center block and at an outer block, respectively, with the upper and lower plena as shown in Figure 4.1, and Table 4.1 shows the physical dimension of our facility with HTTF. A cooling jacket around the upper plenum and helical coil heat exchanger around the cooled channel were connected to an automatic high capacity chiller (Applied Thermal Control Ltd, K4 chiller) to keep the outer surface temperature at the desired value (5 °C). A variable voltage regulator with a span of 0-130 volts and a digital power

reader (0.2% precision) was attached to each of four electrical heaters to regulate and monitor the intensity of the power supplied to the heated channel.

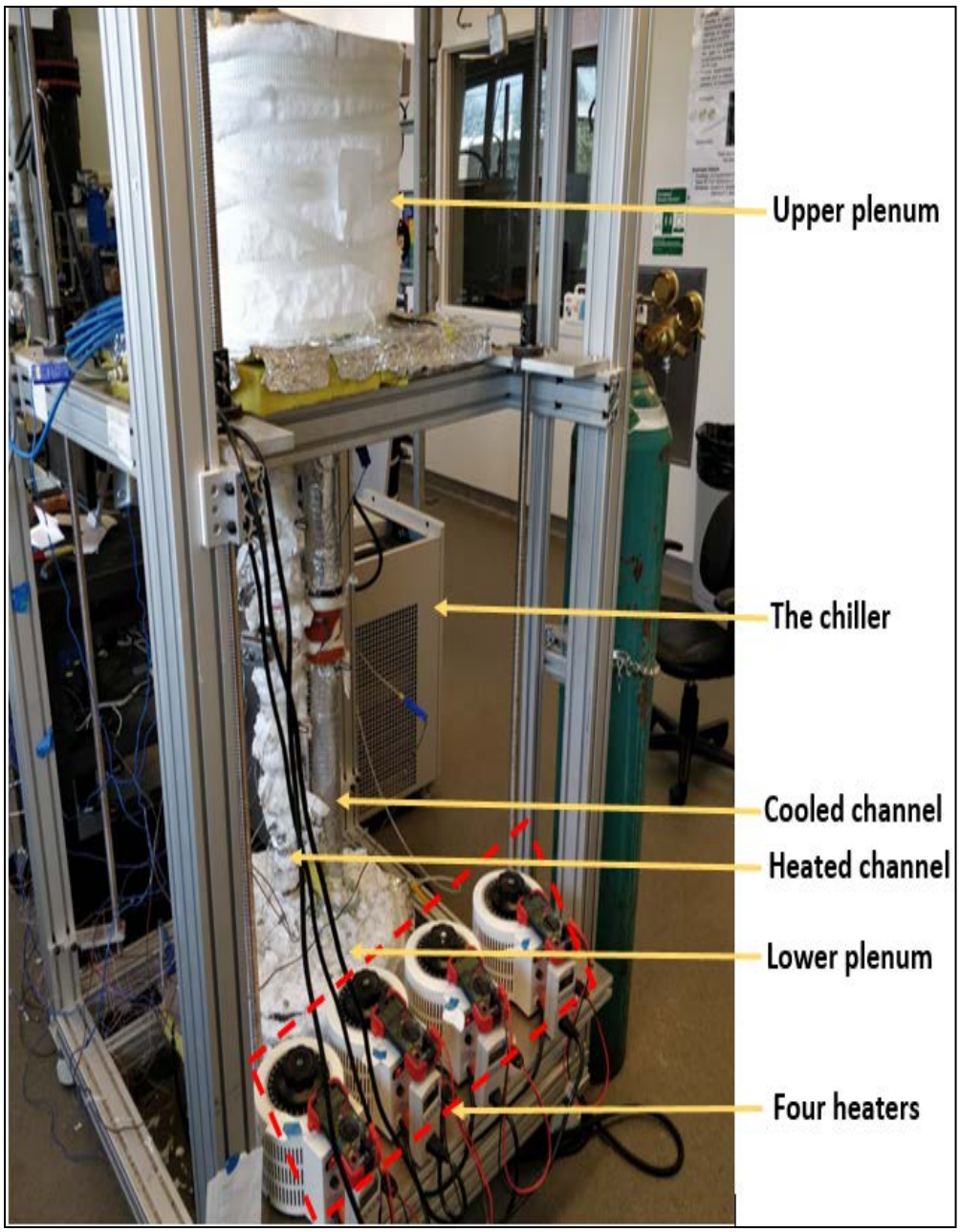

Figure 4.1. The dual-channel facility

Table 4.1. Dimensions of the current facility with reference to OSU-HTTF

Parameter	Current facility	OSU-HTTF
Tube diameter (m)	0.016	0.016
Coolant channel length inside block (m)	1	2
Core diameter (m)	0.3	1.2
Upper plenum height (m)	0.239	0.956
Outer vessel diameter (m)	0.381	1.524
Number of channels	Two channels (one upward flow and other downward flow)	516 coolant channel 210 Heater Rod Six inner gap channel 36 outer gap channel

Each heater covers 25% of the length of the heated channel, and each heater is connected with a separate controller and power reader as shown in Figure 4.1. The heated channel external surface has been carefully insulated using a ceramic fiber blanket of 0.05m in thickness with a low thermal conductivity of 0.07 W/m K in order to reduce heat loss to the environment. The stimulation of the natural circulation takes place within the current setup by heating the heated channel and cooling the upper plenum and cooled channel. In this study, a nonuniform heating center peaking step (approximating cosine shape as shown in Figure 4.2 and Table 4.2) heat flux was applied to investigate the effect of heat flux nonuniformity (sets 1-4) and uniform heat flux equal to 2.865 kW/m^2 for the entire length of the heated channel (set 5). The current experiments have been performed using air as the coolant at 413.7 kPa (60 psi). An advanced heat transfer technique consisting of heat transfer foil sensor (with an uncertainty of 2.5% of the sensor reading) and T-thermocouples (with an uncertainty of 2.2 °C or 0.75% of the reading) is adapted and implemented along the channels. Simultaneous measurements of the inner local heat flux (qi) and the inner surface temperature (Ts,i) were carried out by utilizing the heat

flux foil sensor. The implemented heat flux foil sensor can detect the direction of heat transfer between the surface sensor and the adjacent flowing air based on the sign of heat flux. Negative heat flux signals mean that heat transfers from the air to the surface, while positive heat flux signals imply that heat transfers from the surface of the foil sensor to the air. Centerline air temperature ($T_{b,i}$) in front of the sensor was measured using a T-thermocouple (1.6 mm in diameter). With this technique, instantaneous heat transfer by coefficient (h_i) and local time-averaged heat transfer coefficient (h_{avg}) can be calculated equations (1, 2) [112,113]. Where N is the total data points; N= 2000 was selected to attain stable values. Data was measured for six non-dimensional axial positions along the heated channel (Z/L = 0.044, 0.279, 0.409, 0.591, 0.773, and 0.956) and three non-dimensional axial positions along the cooled channel (Z/L = 0.044, 0.5, and 0.956). The present study calls for the measurement of the heat transfer coefficients along the heated channel for various flux distributions. The current study focused only on measuring the heat transfer coefficients along the heated channel due to the small temperature gradient along the cooled channel [99]. The steady-state condition was achieved when temperature readings did not vary by more than 0.5 K and the local heat transfer coefficient was within ±0.8 W/m2 K for a 30-minute observation. Each experiment is repeated three times with ±1.5% reproducibility.

4.2. RESULTS AND DISCUSSION

The reversal of heat direction and reduction in temperature fields was earlier observed within the heated channel close to the exit (end effect) [97,105,106].

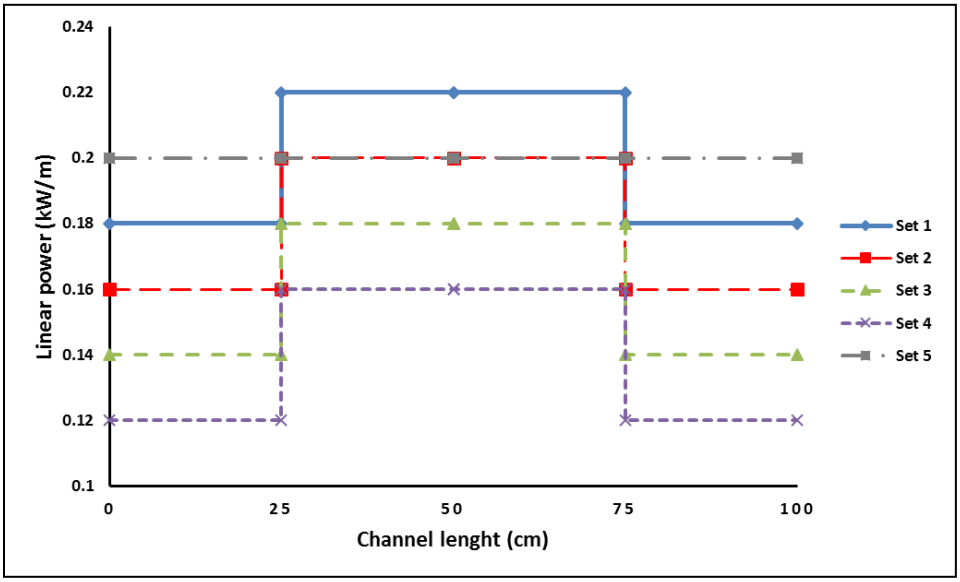

Figure 4.2. Power distribution (nonuniform heating center peaking step (approximating cosine shape)) around the heated channel

Table 4.2. Heat flux distribution around the heat channel

	Axial division			
	0 - 0.25 (m)	0.25 - 0.50 (m)	0.50 - 0.75 (m)	0.75 - 1 (m)
Set 1	2.579 kW/m^2	3.152 kW/m^2	3.152 kW/m^2	2.579 kW/m^2
Set 2	2.292 kW/m^2	2.865 kW/m^2	2.865 kW/m^2	2.292 kW/m^2
Set 3	2.006 kW/m^2	2.579 kW/m^2	2.579 kW/m^2	2.006 kW/m^2
Set 4	1.719 kW/m^2	2.292 kW/m^2	2.292 kW/m^2	1.719 kW/m^2
Set 5	2.865 kW/m^2	2.865 kW/m^2	2.865 kW/m^2	2.865 kW/m^2

Similar thermal behavior was observed in the current study. At two different axial positions along the heated channel (Z/L = 0.773 and 0.956), negative heat fluxes were observed for uniform (Set 5, 50 W) as well as for all cases of nonuniform heating center peaking step (approximating cosine shape). This behavior could be attributed to nonuniform heating in terms of secondary flow [128], and the heat conduction between

the two channels through the upper flange, which results in temperature variation along the heated channel. These negative heat flux signals confirm that there is a reversal in the direction of heat transfer from the flowing air to the inner surface of the heated channel. The heat flow reversal can be caused by axial cooling conduction through the solid wall of the heated channel (conjugate heat transfer) and the presence of the upper plenum as an adiabatic extension with large expansion ratio at the outlet. Figures 4.3 and 4.4 show the reversal in the heat direction (negative signals of heat fluxes) from the adjacent air to the inner wall for Z/L = 0.773 and 0.956. The negative signals of heat fluxes in Figures 4.3 and 4.4 showed that the heat was transferred from air to the inner wall of the heated channel, while positive heat fluxes are observed for the remaining axial locations. Figure 4.5 shows all positive heat fluxes for Z/L =0.591. Negative heat fluxes are observed along the cooled channel for all operating conditions. This confirms the downward flow and establishment of natural circulation between upper and lower plena. It is interesting to see the order of the negative heat flux. For the highest heating case, the negative heat flux is also highest.

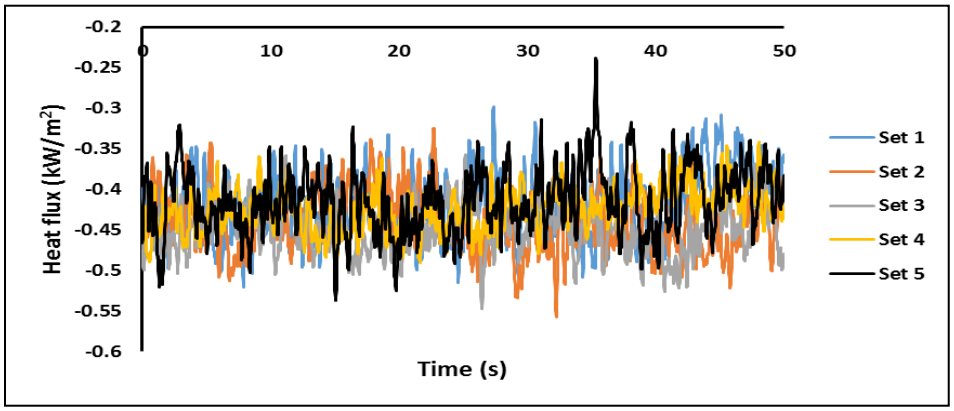

Figure 4.3. End effect at heated channel position Z/L = 0.773

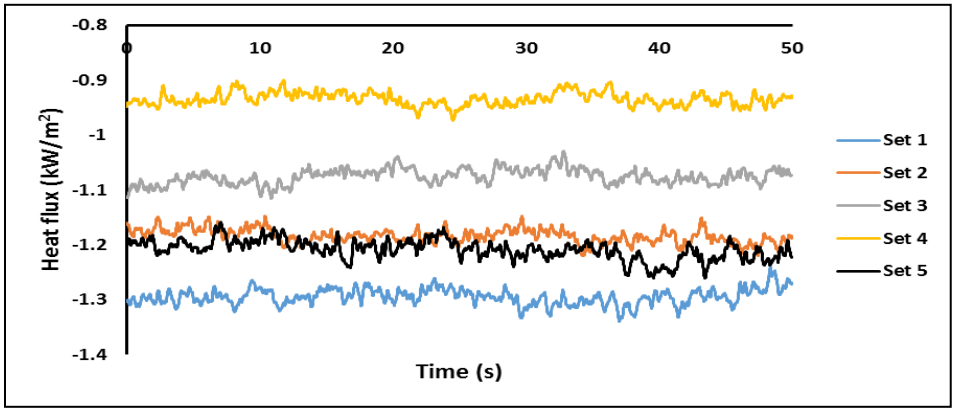

Figure 4.4. End effect at heated channel position Z/L = 0.956

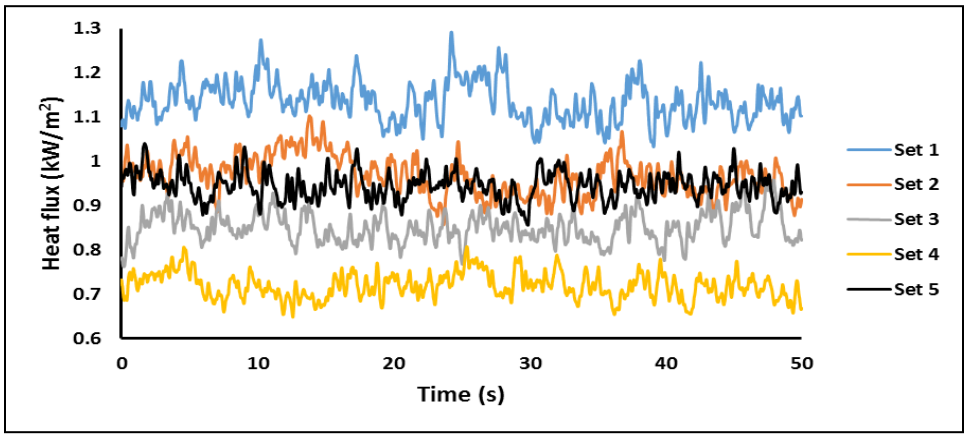

Figure 4.5. End effect at heated channel position Z/L = 0.591

Figures 4.6 and 4.7 show the axial temperature profiles for the inner wall surface and air centerline temperatures along the heated channel. The maximum surface temperature is observed for uniform heat flux (set 5) at Z/L =0.773 and at Z/L =0.591 for all nonuniform heating center peaking step sets. A sharp reduction is observed for uniform heat flux (set 5) after Z/L = 0.773, but for nonuniform heating center peaking step cases from Z/L = 0.591 to Z/L = 0.773, there is a plateau for sets 1, 2, 3, and 4. This plateau is not seen for set 5 (uniform heating), where the temperature is still increasing

after position Z/L = 0.591. For air centerline temperature, the temperature profile is slightly different from inner wall surface temperature profile: 1) The maximum temperature is observed at Z/L = 0.773 for all sets; 2) The plateau that exists in the inner wall surface temperature is not observed in the air centerline temperature profile. This thermal performance in terms of field temperatures could be attributed to an increase in the air thermal conductivity, which leads to lower resistance and an increase in the viscosity, causing the radial flow of the hotter layers of air to move nearer to the surface toward the tube center. Figure 4.8 shows the heat transfer coefficient along the heated channel, and the heat transfers from the adjacent air layer to the inner wall started after Z/L = 0.591. This heat transfer reversal could be attributed to the downward axial cooling conduction inside the solid wall of the heated channel from the upper plenum and co-circulation at the top section of the heated channel, as reported in the literature [99,105,106,138,139]. The heat transfer coefficients decrease from the inlet Z/L = 0.044 to Z/L = 0.279. This could be attributed to the developing of hydrodynamic and thermal boundary layers. Again in the values of the heat transfer coefficients is observed after Z/L = 0.279 to Z/L = 0.591 due to the laminarization effects [115,119,136]. At Z/L = 0.409, the heat transfer coefficient increases by 35% for nonuniform heating center peaking step (sets 1and 2) with respect to the uniform heating (set 5), and it decreases by 56% for nonuniform heating center peaking step (sets 3 and 4) with respect to the uniform heating (set 5). It is very clear in Figure 4.8; there is reorder in the distributions of the local heat transfer coefficients in descending order after the inflection point (after Z/L = 0.773).

This could be attributed to the end effect [97,105,106]. The influence of the end effect on values of the local heat transfer coefficients is very clear after Z/L = 0.591 in terms of a decreasing trend.

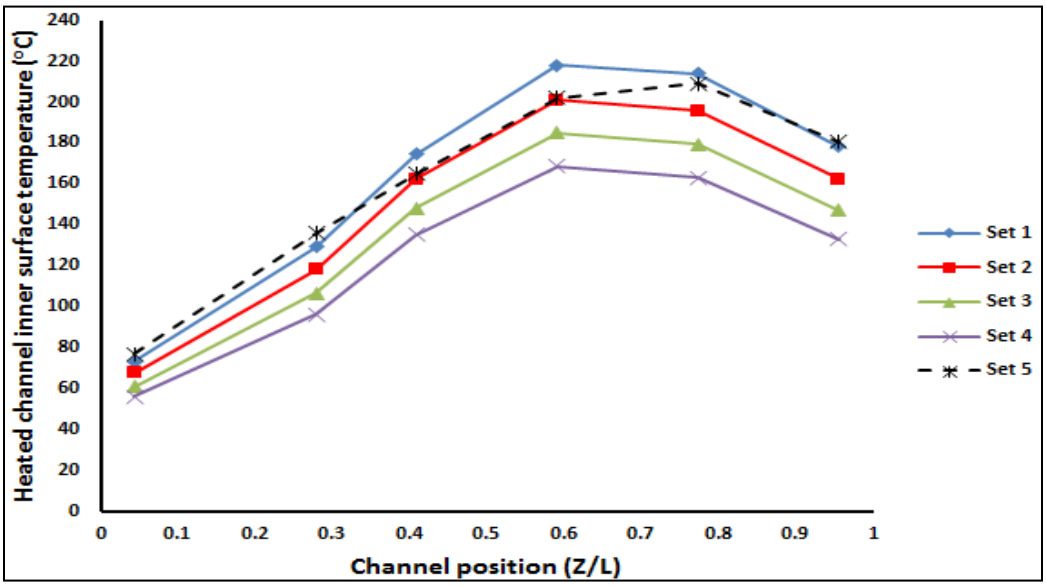

Figure 4.6. Heated channel inner surface temperature

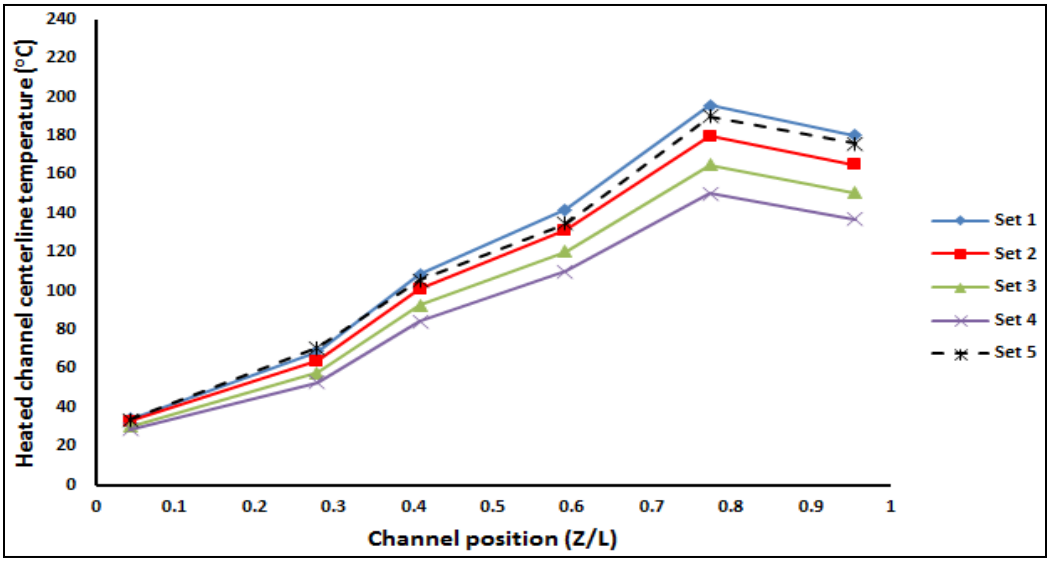

Figure 4.7. Heated channel centerline temperature

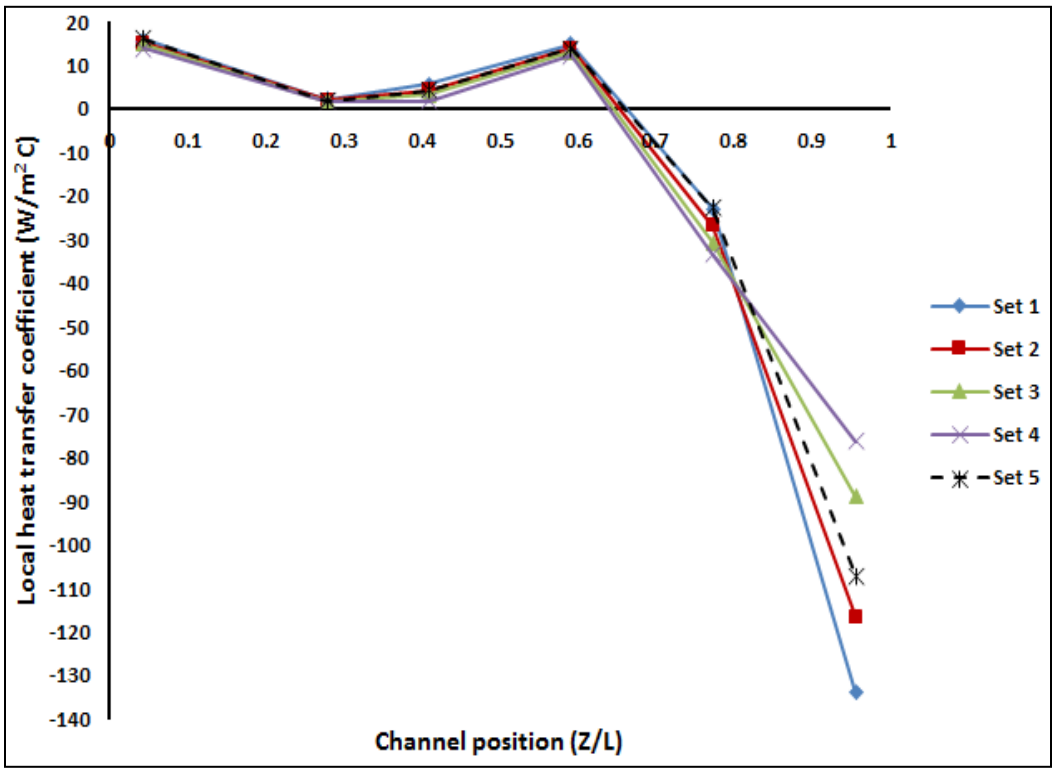

Figure 4.8. Local heat transfer coefficient along the heated channel

Figures 4.9 and 4.10 show the temperature variations along the inner wall surface and air centerline of the cooled channel. A decreasing trend in the field temperatures from Z/L = 0.956 (inlet) to Z/L = 0.044 (outlet) is observed, which confirms the establishment of natural circulation and downward flow.

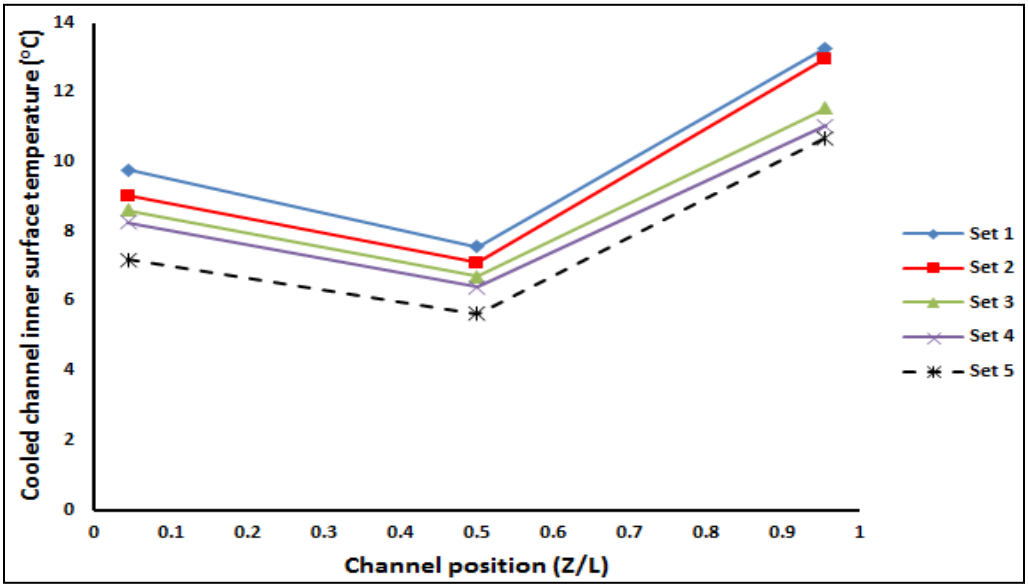

Figure 4.9. Temperature along the inner wall surface of the cooled channel

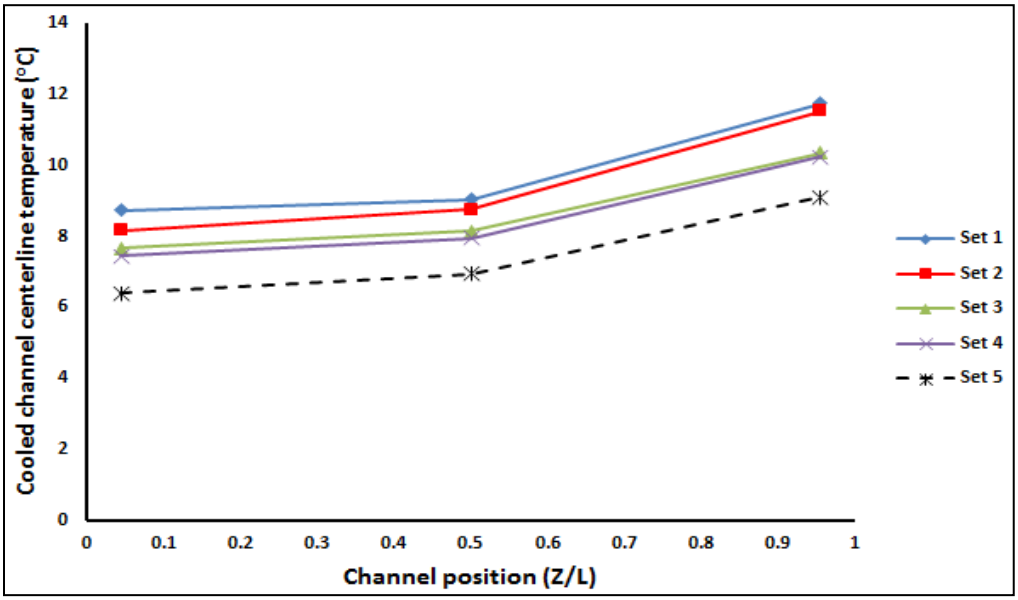

Figure 4.10. Temperature along air centerline of the cooled channel

5. HEAT TRANSFER THERMAL RESPONSE FOR DIFFERENT COOLANTS UNDER NATURAL CIRCULATION

The prismatic modular reactor (PMR) is considered a generation IV nuclear reactor with higher safety, low operation and maintenance costs, and high thermal efficiency. PMR is a gas-cooled and graphite -moderated reactor designed to accomplish future energy needs. The core of the reactor consists of stacks of hexagonal graphite blocks where the coolant channels and fuel rods are arranged. Natural circulation is considered as one of the passive safety features of the prismatic modular reactor to remove core decay heat during the Loss of Forced Cooling Accident (LOFA), especially the pressurized conduction cooldown (PCC) accident scenario. PCC means the loss of coolant flow has occurred, but the primary system remains at full pressure, the hotter coolant channels will have coolant flowing upwards and will be returning from the cooler channels. The second possible accident scenario under LOFA could be that of depressurized conduction cooling down (DCC), where rupture of primary pipe etc. results in rapid pressure drop in the system. In this case, coolant is expected to enter the reactor pressure vessel from the breach. Several computational studies in the open literature address the heat transfer characterization in the prismatic modular reactor during accident scenario of pressurized conduction cooldown (PCC) [77,92,122,141,142]. Some experimental results have been reported, but these studies lack the use of sophisticated measurement techniques for natural circulation phenomena. The current study is particularly significant because of the lack of the published information on the behavior of various possible coolant gases such as nitrogen, carbon dioxide, helium, and argon to investigate the intensity of natural circulation using different gases with different physical

and thermal properties. Moteover, to invesigate the thermal response of the natural circulation in terms of temperature and flow fields under high pressure. This comparative study will enable well-informed selection of the best coolant for VHTR application as well as provide data for CFD simulation validation. In this research, experimental results and analysis are provided for natural circulation with different coolants at 413.7 kPa for center peaking heat flux profile (mimicking cosine shape) along the riser channel. The use of advanced instrumentation, detailed heat transfer data in terms of temperature fields (centerline coolant and inner wall surface temperatures), and heat transfer coefficients under natural circulation are presented here.

5.1. METHODOLOGY

A dual-channel facility of high temperature and pressure has been designed and developed at Multiphase Reactors Engineering and Applications Laboratory (mReal) at Missouri University of Science and Technology (S&T) to mimic the coolant flow in the core of a prismatic very-high-temperature reactor [97,105-107,110,111,143-146]. The current facility is designed with reference to OSU-HTTF [142] with a scale-down ratio ¼ axially and radially.

The core of the current facility mimics seven hexagonal blocks with 1 m height of flow channels. The dual channel of constant diameter (0.016 m) is developed for coolant flow; one for upward flow in the center block and one for downward at the outer block along with the upper and lower plena. The current facility is made of stainless steel alloy 304 series to withstand high pressure and temperature. Figures 5.1 and 5.2 show physical picture and schematic diagram of the current setup.

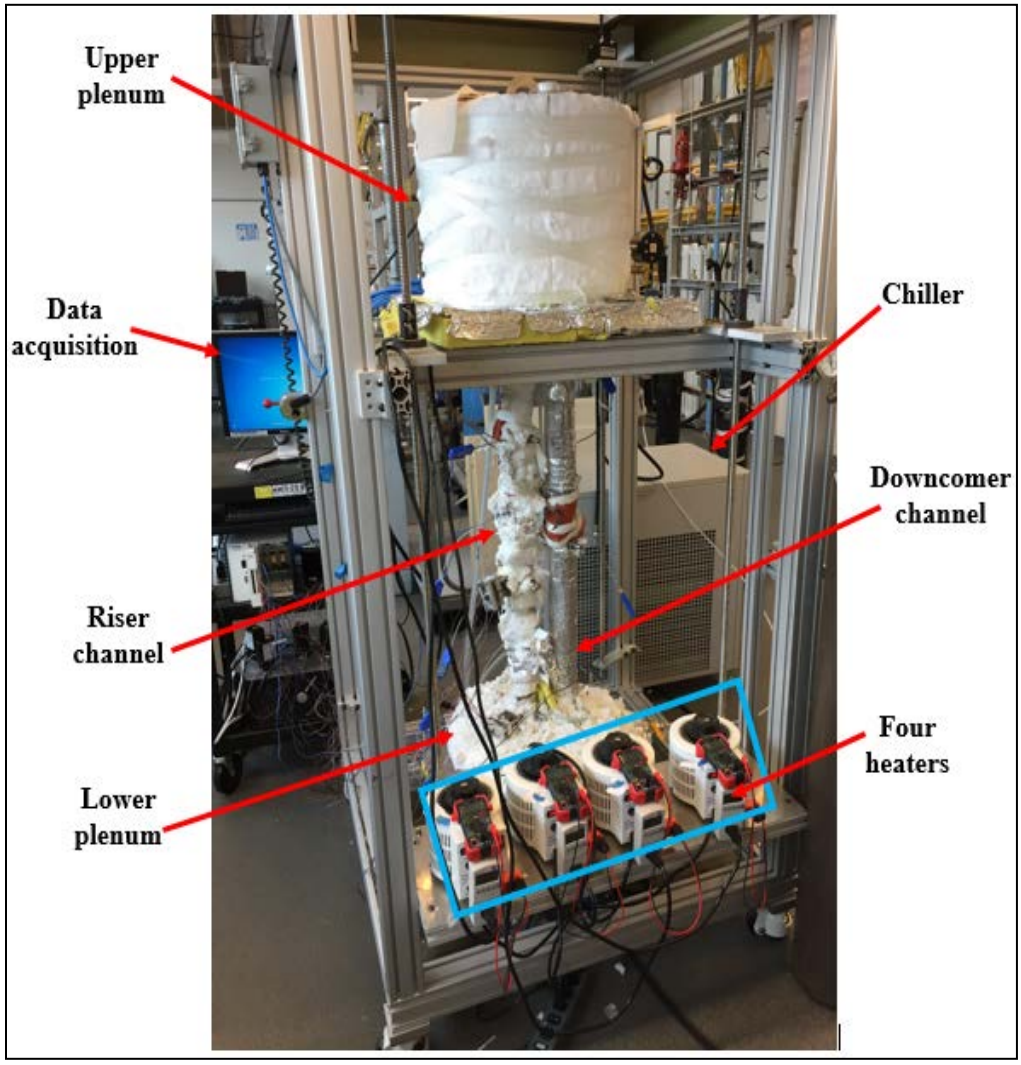

Figure 5.1. The dual channel facility

A cooling jacket is implemented around the upper plenum to control its outside surface temperature of the downcomer channel (downward-flow) using an automatic high-capacity chiller (Applied Thermal Control Ltd, K4 chiller). The natural circulation is stimulated within the current facility by electrically heating the riser channel (near the core center, upward-channel) at a nonuniform heat flux in cosine form as shown in Figure 5.3, and subjecting the other channel and the upper plenum outer surface to cooling by

chilled water. Four gases of coolant are investigated in the current study (nitrogen, carbon dioxide, helium, and argon) to determine the effect of outer surface temperature of the upper plenum and downcomer channel (278.15 K) and nonuniform heat flux on the intensity of natural circulation.

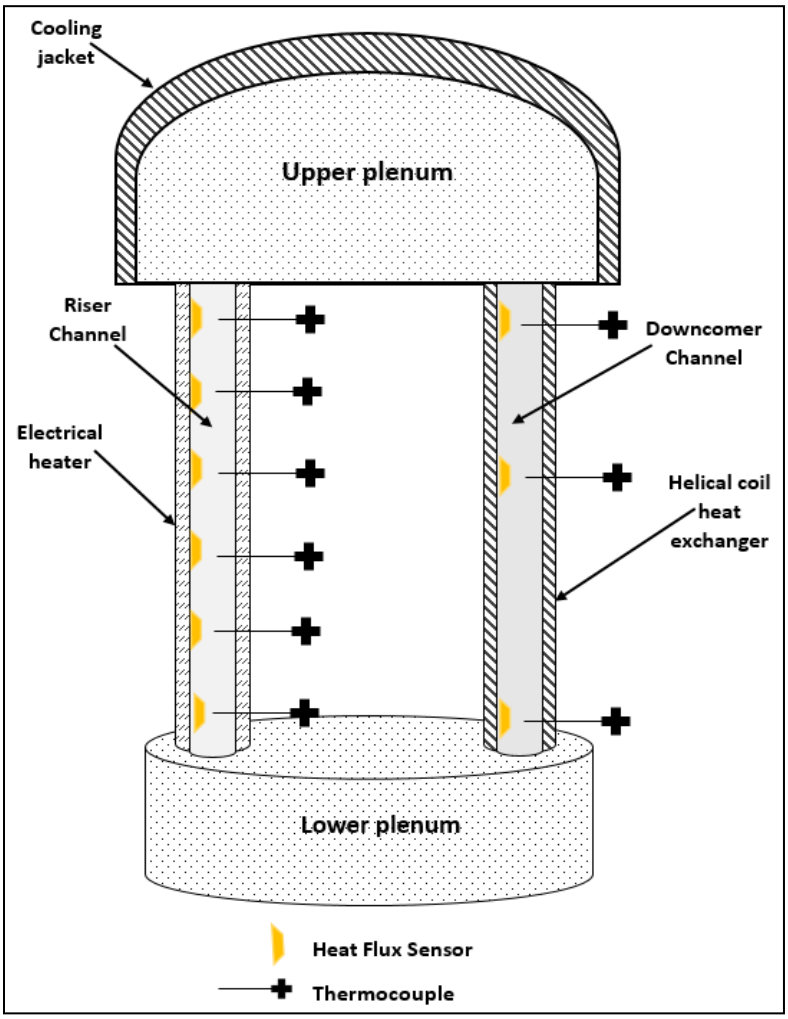

Figure 5.2. Schematic diagram of the dual channel facility

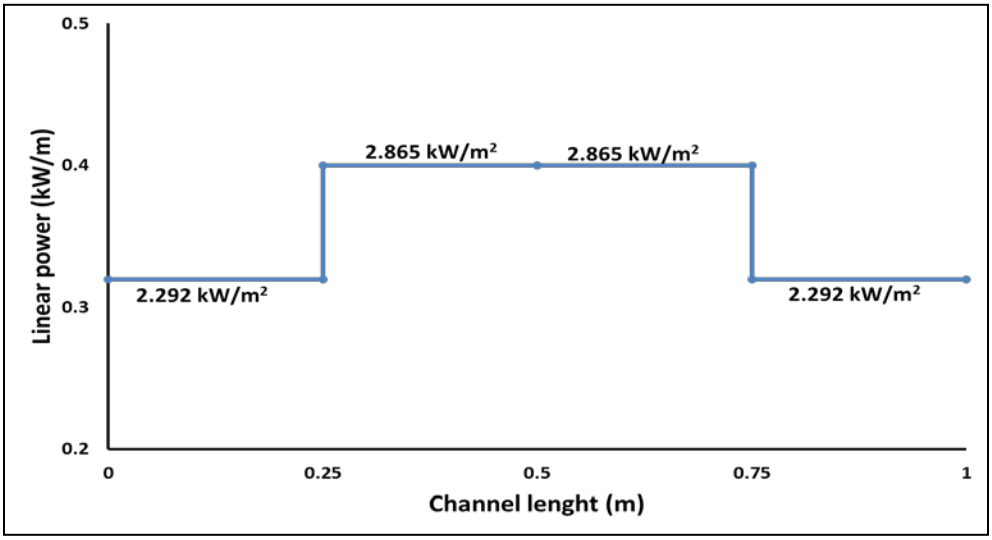

Figure 5.3. Power and heat flux distribution around riser channel

The experiments are carried out at a high operating pressure of 413.7 kPa. An advanced heat transfer technique consisting of a heat transfer foil sensor (with an uncertainty of 2.5% of the sensor reading) and thermocouples (with an uncertainty of 0.75% of the reading) is adapted and implemented along the flow channels in the form of a connection block. The foil sensor is used to measure the inner local heat flux (q_i), simultaneously with the inner surface temperature ($T_{s,i}$). The thermocouple (T-type; 1.6 mm in diameter) were used to measure the centerline adjacent gas temperature ($T_{b,i}$) in front of the sensor. It is important to note that the foil sensor can detect the heat transfer direction. A positive signal indicates that the heat transfers from the inner channel wall to the adjacent fluid, while a negative signal shows that heat transfers from the adjacent fluid to the inner channel wall. By simultaneously measuring the local heat flux (q_i), inner surface temperature ($T_{s,i}$), and gas centerline temperature ($T_{b,i}$), the instantaneous

heat transfer coefficient (h_i) and local time-averaged heat transfer coefficient (h_{avg}) can be calculated by equations (1,2) [97,105,106,112,113]:

The scaled-down dual channel was pressurized by coolant gas from the commercially available cylinders at the desired pressure of 413.7 kPa. The chiller provides chilled water at desired cooling temperatures of 278.15 K. The riser channel was heated nonuniformly. N is the total data points; N= 2000 was selected to attain stable values. Six non-dimensional axial positions along the riser channel (Z/L= 0.044, 0.279, 0.409, 0.591, 0.773, and 0.956) and three non-dimensional axial positions along the downcomer channel (Z/L= 0.044, 0.5, and 0.956) were used to collect and measure the heat transfer data during steady-state conditions. In the current study, we focused only on measuring the heat transfer coefficients along the riser channel due to the small temperature gradient along the downcomer channel [97,105-107,143,146,147]. Steady state was achieved when temperature readings did not vary by more than 0.5 K and the local heat transfer coefficient was within ±0.8 W/m2 K for a 30-minute observation. Each experiment was repeated three times with ±1.5% reproducibility.

5.2. RESULTS AND DISCUSSION

5.2.1. Inner Surface Temperature Profile. The axial distribution of the inner surface temperature profile along the circulation loop is shown in Figure 5.4. The temperature distribution shows that the axial temperature increased from the riser channel inlet (Z/L=0.044) to the axial position of Z/L=0.591 for nitrogen, carbon dioxide, helium, and argon. But the unique feature of helium temperature distribution is the observation that from the riser channel inlet (Z/L=0.044) the temperature keeps rising till the axial

position (Z/L=0.773). Also, higher temperatures are achieved for helium. The temperature rise across the riser channel was observed to be 84, 95, 98 and 150 K for carbon dioxide, nitrogen, argon, and helium respectively. Beyond these positions (Z/L=0.773 for helium and Z/L=0.591 for all other gases), a reduction in the inner surface temperature was observed. The initial temperature increase is attributed to the continuous nonuniform heating applied around the riser channel. The reversal in the direction of the heat transfer (end effect) and reduction in temperature profile were observed within the riser channel close to the exit [97,105,106]. This behavior could be attributed to three factors :1) nonuniform heating in terms of secondary flow [128], 2) the heat conduction between the two channels through the upper flange, which results in temperature variation along the riser channel, and 3) the phenomena of back-mixing (co-circulation) that is also possible for this setup and hence would be a concern for VHTR. Back-mixing is caused by the interaction of the rising plumes from the riser channel and the working fluid in the upper plenum which in turn results in decreasing of the inner surface temperature of heat flow direction reversal [97,105,106,115,116]. The distribution of the inner surface temperatures along the downcomer channel exhibits similar thermal behavior, as shown in Figure 5.4. A decreasing trend in the surface temperature from Z/L= 0.956 (inlet from the upper plenum) to Z/L= 0.044 (outlet) was observed in the downcomer channel which confirms the establishment of natural circulation.

5.2.2. Gas Centerline Temperature Profile. The distribution of the coolant centerline temperature profile along the circulation loop is shown in Figure 5.5.

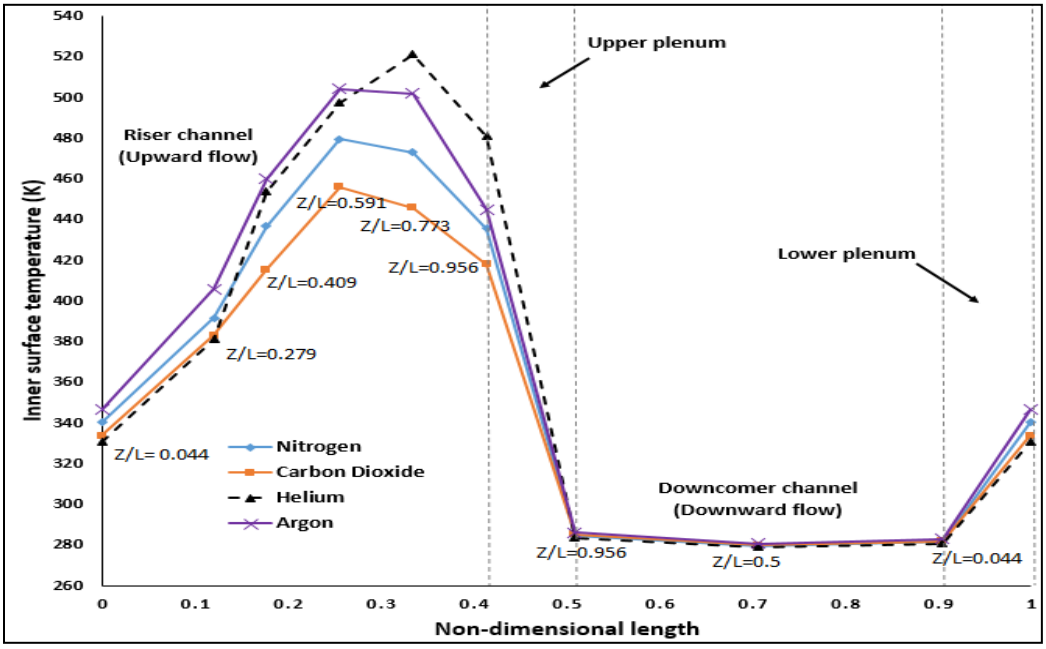

Figure 5.4. Steady -state temperature profile for inner surface temperature along the circulation loop

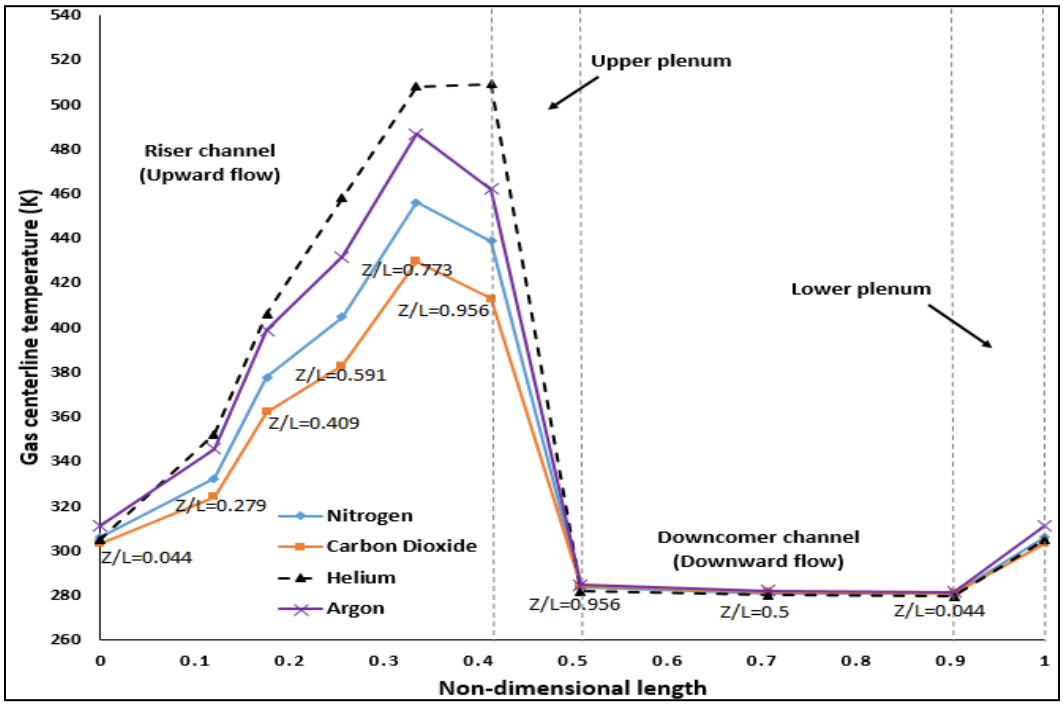

Figure 5.5. Steady -state temperature profile for gas centerline temperature along the circulation loop

One can notice that the axial distribution of the gases' centerline temperature is slightly different from the inner wall surface temperature. Notably; 1) The maximum centerline temperature is observed at Z/L=0.773 for all gases; 2) A small plateau is observed for helium centerline temperature between Z/L = 0. 773 and Z/L=0.956, while a sharp reduction is observed for nitrogen, carbon dioxide, and argon centerline temperatures as shown in Figure 5.5 due to the influence of end effect. The presence of plateau suggests that the centerline temperature peaking is higher than Z/L=0.773 but lower than Z/L=0.956. The appearance of a plateau instead of a sharp reduction for helium close to the exit of the riser channel in terms of centerline helium temperature could be attributed to the five-time higher specific heat of helium as compared to the other gases [117]. A significant average increase of centerline temperature along the riser channel was recorded as 110, 133, 151 and 204 K for carbon dioxide, nitrogen, argon, and helium, respectively. The distribution of the centerline temperatures along the downcomer channel exhibits similar thermal behavior, as shown in Figure 5.5. A decreasing trend in the temperature from Z/L= 0.956 (inlet) to Z/L= 0.044 (outlet) was observed in the downcomer channel which confirms the establishment of natural circulation and downward flow.

5.2.3. Heat Transfer Coefficient. Heat transfer coefficient is a quantitative characteristic of convective heat transfer efficiency between the flowing coolant and the heated channel surface. The magnitude of the local heat transfer coefficient along the riser channel for all different gases decreases between (Z/L= 0.044) to Z/L = 0.279 where the value is at its minimum. This could be attributed to the development of hydrodynamic and thermal boundary layers. After this point, the local heat transfer

coefficient starts to increase again, as shown in Figure 5.6, to a position of Z/L = 0.591. An increase in the values of the heat transfer coefficients is observed after Z/L = 0.279 to Z/L = 0.591 due to the laminarization effects (buoyancy-induced acceleration) [147]. The highest heat transfer coefficient is observed at Z/L=0.591 for all gases. The highest value is for helium followed by carbon dioxide, nitrogen, and argon, respectively. The decrease between helium and argon was found to be 84%. The influence of end effect is very clear on values of the local heat transfer coefficients after Z/L=0.591 in terms of a decreasing trend. Negative heat transfer coefficients are observed for nitrogen, carbon dioxide, and argon at Z/L = 0.773 and beyond, but for helium, only negative heat transfer is observed at only Z/L=0.956. For the lower plenum and downcomer channel temperature, the intensity of natural convection would be higher, giving rise to enhanced convection.

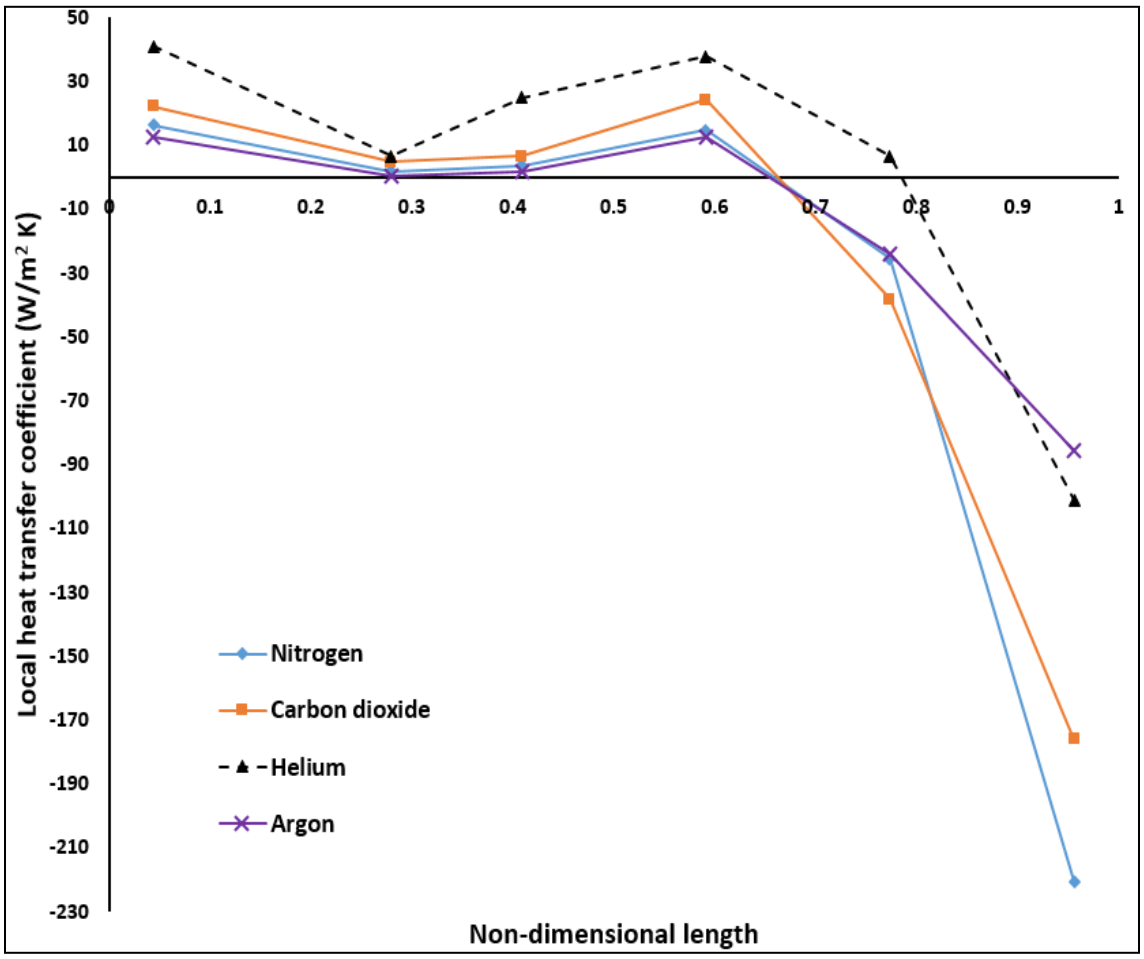

Figure 5.6. Axial distribution of heat transfer coefficient along the riser channel

6. CONCLUSIONS

The GCR design characteristics are very different from existing reactors. For the optimum design and safety analysis of GCR system, new developments are required for technology analysis. In this chapter, a fundamental research articles were introduced to establish the GCR safety analysis technology statues. As part of an effort to understand the current status of GCR safety analysis technology, this chapter introduced the GCR phenomena identification and event categorization and acceptance criteria developed at home and abroad. This chapter presents the review outcome of current status and prospect of the safety analysis technology of GCR. While these studies based on assumptions which needs to be validated using benchmark data, and existing data are carried out in simple geometries with limited measurement techniques and cannot be extended to complex reactors, there is a real need to acquire local experimental data on the natural circulation using sophisticated measurement techniques in a representative geometry which is covered in my dissertation.

A scaled-down dual channel facility has been designed and developed at Missouri S&T to investigate the heat transfer characterization of natural circulation experimentally inside the core of a prismatic block reactor under pressurized conduction cooled-down (PCC) accident scenario. In the current study, an advanced fast-response heat transfer technique of flush-mounted foil sensors in conjunction with series of thermocouples was used to measure the local heat transfer coefficients, inner surface temperatures, and coolants centerline temperatures along the flow channels simultaneously.

A uniformly heated dual channel circulation loop has been designed and developed to investigate the natural circulation heat transfer within the prismatic block nuclear reactor under the accident flow scenarios. Four values of the outer surface temperatures of the upper plenum and downcomer channel (278.15, 288.15, 298.15, and 308.15 K) have been used to investigate the natural circulation heat transfer along the riser channel. Helium is used as a working fluid at 413.685 kPa. A downward flow is achieved along the downcomer channel in terms of negative A downward flow is achieved along the downcomer channel in terms of negative heat fluxes and a decreasing trend of temperature fields, confirming the presence of natural circulation. Similar to air, negative heat transfer coefficients are observed for 288.15, 298.15, and 308.15 K at Z/L = 0.0.773, with the exception that for air this phenomenon was only observed for the very last observation point. A reversal in the direction of heat transfer is observed close to the exit due to interaction between rising lighter helium from the riser channel and denser helium within the upper plenum. This phenomenon was also observed for air. A sharp reduction in the inner wall surface temperature is observed close to the exit of the riser channel, which is similar to the air behavior. However, the centerline gas temperature for helium showed a plateau in contrast to a sharp reduction of air centerline temperature. The temperature difference across the riser channel for the centerline helium temperature is much greater than the inner wall surface temperature, and this could be attributed to the higher specific heat of the helium. Results showed that the thermal performance of helium is quite different than air in terms of temperature field's distribution and end effects and perhaps better suited as a coolant for natural circulation.

The most significant study variable is the nonuniform heating distribution that comes in the form of stepwise- reducing and stepwise-increasing cases (1.432 kW/m^2 to 3.152 kW/m^2) along the riser channel in dual-channel circulation. The impact of flux shape was pronounced in air as a working fluid at 413.7 kPa and outer surface temperature of 5°C for downcomer and upper plenum. Similar to the case of uniform heating, heat transfer reversal was observed for all experimental conditions with different values of stepwise-reducing and stepwise-increasing close to the exit (Z/L = 0.773 and 0.956). The maximum temperature in the inner wall surface was observed at Z/L=0.591 and the air centerline at Z/L=0.773 for all cases of stepwise-reducing flux. For stepwise-increasing cases, the maximum temperature in the inner wall surface and the air centerline were both observed at Z/L=0.773. A significant reduction of the field temperatures along the riser channel was observed (24.5% and 22.4%) for inner surface and air centerline temperatures, respectively. For stepwise-increasing cases, a significant reduction of riser channel temperature is observed with decreasing stepwise-increasing heating by 25.6 % and 23.1% for the inner surface and air centerline temperatures, respectively. The average values of the heat transfer coefficient($\bar{h}_L$) and the average Nusselt number ($\overline{Nu}_L$) were decreased with reducing the heating by 38% and 19% for stepwise-reducing heating, respectively, and by 32% and 13% for the stepwise-increasing heating, respectively. Negative heat transfer coefficients were observed for all experimental conditions from Z/L = 0.773 to Z/L= 0.956, and these values were excluded for calculations of the average heat transfer coefficient and Nusselt number along the riser channel.

Nonuniform heating center peaking step (approximating cosine shape) within the dual-channel circulation loop of upper and lower plena have been designed and developed to investigate the natural circulation heat transfer within the prismatic block nuclear reactor (PMR) under the PCC accident scenario at a higher operating pressure of 413.7 kPa (60 psi). In figure 4.7, one can notice that case 1 (center peaking case) and case 5 with uniform heat flux with the same total heat input produce different results. The exit temperature of the center peaking case is higher than the uniform heating case. Therefore, the heat flux profile is expected to play a significant role in the overall heating of the coolant. Moreover, a reversal of heat direction and reduction in temperature fields is observed at two different axial positions along the heated channel (Z/L = 0.773 and 0.956). The maximum surface temperature is observed for uniform heat flux (set 5) at Z/L = 0.773 and at Z/L = 0.591 for all nonuniform heating center peaking step sets. Negative heat transfer coefficients were observed for all experimental conditions from Z/L = 0.773 to Z/L = 0.956, and there is reorder in the curves in the descending order after the inflection point (after Z/L = 0.773).

A scaled-down dual channel facility has been to investigate the effect of the upper plenum and downcomer channel outer surface temperature of 278.15 K on the heat transfer characterization of natural circulation was investigated by using four different working fluids (nitrogen, carbon dioxide, helium, and argon) at a higher operating pressure of 413.7 kPa (60 psi). The heat transfer reversal was observed close to the exit (Z/L = 0.773 and 0.956) for all experiments with different values of flux peaking. The maximum temperature in the inner wall surface was observed at Z/L=0.591 for all gases except helium for which the maximum was observed at Z/L=0.773. The measured data

clearly shows the advantage of using helium as compared to other gases. Due to its higher heat transfer coefficient and temperature fields for all operating conditions. Hence, helium is capable of absorbing and transferring significantly more heat in the riser channel enhancing the overall thermal efficiency of the system. Furthermore, the temperature peaking was observed at a higher location along the riser channel.

BIBLIOGRAPHY

1. Doug Chapin, S.K., and Jim Nestell, The very hight temperature reactor: A technical summary. 2004, MPr Associates, Inc.

2. Thomas, S., The pebble bed modular reactor: An obituary. Energy Policy, 2011. 36: p. 2431-2440.

3. J. Kelly, T.D.a.H.P., GIF's rule in developing the nuclear technologies of the future. 2013, NEA news.

4. Forum, G.I.I., Generation IV Roadmap: Description of Candidate Gas-cooled Reactor systems Report. "Appendix C: Very-High Temperature Reactor (VHTR) Systems Summary Report. 2002.

5. Cameron, P.J., The background and status of the gas cooled reactor in the United Kingdom. Annals of Nuclear Energy, 1978. 5(8–10): p. 489-505.

6. Price, M.S.T., The dragon project origins, achievements and legacies. Nuclear Engineering and Design, 2012. 251: p. 60-68.

7. Schulten, R., The AVR Nuclear Power Plant —A Milestone in High-Temperature Reactor Development. Nuclear Science and Engineering, 1985. 90: p. 388-357.

8. Ziermann, E., Review of 21 years of power operation at the AVR experimental nuclear power station in Jülich. Nuclear Engineering and Design, 1990. 121(2): p. 135-142.

9. Gottaut, H. and K. Krüger, Results of experiments at the AVR reactor. Nuclear Engineering and Design, 1990. 121(2): p. 143-153.

10. Bäumer, R., et al., Construction and operating experience with the 300-MW THTR nuclear power plant. Nuclear Engineering and Design, 1990. 121(2): p. 155-166.

11. Walker, R.F., Experience with the Fort St. Vrain reactor. Annals of Nuclear Energy, 1978. 5(8–10): p. 337-356.

12. Brey, H.L. and H.G. Olson, The Fort St. Vrain high temperature gas-cooled reactor: XIII. Radiological and shielding performance of Fort St. Vrain. Nuclear Engineering and Design, 1982. 72(2): p. 147-152.

13. Olson, H.G., H.L. Brey, and F.E. Swart, The Fort St. Vrain high temperature gas-cooled reactor: VII. Prestressed concrete reactor vessel (PCRV) performance. Nuclear Engineering and Design, 1982. 72(2): p. 111-123.

14. Olson, H.G., et al., The Fort St. Vrain high temperature gas-cooled reactor: XII. The dew point moisture monitor testing program. Nuclear Engineering and Design, 1982. 72(2): p. 139-145.

15. Olson, H.G., H.L. Brey, and D.W. Warembourg, The Fort St. Vrain high temperature gas-cooled reactor: X. Core temperature fluctuations. Nuclear Engineering and Design, 1982. 72(2): p. 125-137.

16. Shiozawa, S., et al., Overview of HTTR design features. Nuclear Engineering and Design, 2004. 233(1–3): p. 11-21.

17. Kunitomi, K., et al., Japan's future HTR—the GTHTR300. Nuclear Engineering and Design, 2004. 233(1–3): p. 309-327.

18. Yan, X., et al., GTHTR300 design and development. Nuclear Engineering and Design, 2003. 222(2–3): p. 247-262.

19. Takeda, T., Research and development on prevention of air ingress during the primary-pipe rupture accident in the HTTR. Nuclear Engineering and Design, 2004. 233(1–3): p. 197-209.

20. Ueta, S., et al., Development of high temperature gas-cooled reactor (HTGR) fuel in Japan. Progress in Nuclear Energy, 2011. 53(7): p. 788-793.

21. X. Yang, W. Hu, and S. Jiang, Experimental Investigation on feasibility of two-regiondesigned pebble-bed high-temperature gas-cooled reactor. Nuclear Science and Technology, 2009. 46(4): p. 374-381.

22. Khane, V.b., Experimental and computational investigation of flow of pebbles in a pebble bed nuclear reactor, in Chemical & Biochemical Engineering. 2014, Missouri University S&T: Rolla, MO.

23. Koster, A., H.D. Matzner, and D.R. Nicholsi, PBMR design for the future. Nuclear Engineering and Design, 2003. 222(2–3): p. 231-245.

24. LaBar, M.P., et al., Introducing the GT-MHR. Nuclear Engineering International, 2004. 49(596): p. 18-23.

25. LaBar, M.P., et al., The Gas Turbine-Modular Helium Reactor. Nuclear News, 2003. 46(11): p. 28-37.

26. McDonald, C.F., et al. GT-MHR helium gas turbine power conversion system design and development. in Proceedings of the American Power Conference. 1994.

27. La Bar, M.P. and W.A. Simon, Modular Helium Reactor - a design for the 21st century. Nuclear Engineer, 2000. 41(1).

28. Galushkin, V., GT-MHR - An advanced reactor. Nuclear Plant Journal, 2001. 19(1).

29. IAEA, Considerations in the Development of Safety Requirements for Innovative Reactors: Application to Modular High Temperature Gas Cooled Reactors, 2003, INTERNATIONAL ATOMIC ENERGY AGENCY,.

30. ANS, nuclear safety design process for modular helium-cooled reactor plants. 2011, American Nuclear Society: Illinois 60526 USA.

31. IAEA, ACCIDENT ANALYSIS FOR NUCLEAR POWER PLANTS. 2002, International Atomic Energy Agency: Vienna.

32. IAEA, ACCIDENT ANALYSIS FOR NUCLEAR POWER PLANTS WITH MODULAR HIGH TEMPERATURE GAS COOLED REACTORS. 2008, INTERNATIONAL ATOMIC ENERGY AGENCY: VIENNA.

33. M.King, B., Natural Circulation Scaling of a Pressurized Conduction Cooldown Event in the Upper Plenum of the Modular High Temperature Gas Reactor, in Department of Nuclear Engineering and RHP. 2012 Oregon State University, Corvallis OR.

34. B.G.King, Scaling Analysis for the Very High Temperature Reactor Test Facility at Oregon State University., in Report OSU-HTTF-XXX. Oregon State University: Oregon State University.

35. Seyun Kim , N.-I.T., Hong-Sik Lim , Sang-Jun Ha Sensitivity study on depressurized LOFC accidents with failure of RCCS in a modular gas-cooled reactor. Annals of Nuclear Energy, 2010. 37: p. 664–671.

36. Woods, B.G., Scaling Study of the Depressurized Conduction Cooldown Event in the High Temperature Test Facility Using RELAP5-3D/ATHENA, in Nuclear Engineering and Radiation Health Physics. 2013, Oregon State University.

37. Ugur Emre SIKIK, P., SIMULATIONS OF AIR AND WATER INGRESS TRANSIENTS FOR THE PEBBLE BED MODULAR REACTOR (PBMR) BY MEANS OF THE TINTE CODE, in Proceedings of the 4th International Topical Meeting on High Temperature Reactor Technology. 2008: Washington, DC USA.

38. Zhai, T., LOCA and Air Ingress Accident Analysis of a Pebble Bed Reactor, in Department of Nuclear Engineering. 2003, MASSACHUSETTS INSTITUTE OF TECHNOLOGY.

39. Wei-Hao Huanga, S.-C.T., I-Che Chiu, Chien-Hung Chen, Ji-Jung Kai, The oxidation effects of nuclear graphite during air-ingressaccidents in HTGR. Nuclear Engineering and Design, 2014. 271: p. 270–274.

40. Mohamed S. El-Genk, J.-M.T.a.B.T., Graphite Oxidation Simulation in HTR Accident Conditions – 3rd Year and Final Technical Report. 2012, Institute for Space and Nuclear Power Studies.

41. Eung Soo Kim , H.C.N., Experimental study on the oxidation of nuclear graphite and development of an oxidation model. Journal of Nuclear Materials, 2006. 349 p. 182–194.

42. Andrew C. Kadak, T.Z., Air ingress benchmarking with computational fluid dynamics analysis. Nuclear Engineering and Design, 2006. 263: p. 587–602.

43. J.N. Reyes Jr , J.T.G., B.G.Woods, B. Jackson, T.D. Marshall, Scaling analysis for the high temperature Gas Reactor Test Section (GRTS). Nuclear Engineering and Design, 2010. 240: p. 397–404.

44. Groehn, H.G., Disturbance of the cooling gas distribution in HTGR fuel blocks due to bypass flow. In: Proceedings of ANS/ASME/NRC International Topical Meeting on Nuclear Reactor Thermal-Hydraulics,. 1980: NY, USA,.

45. Masaaki NAKANO, N.T., and TAZAWA, Conceptual Reactor Design Study of Very High Temperature Reactor (VHTR) with Prismatic-Type Core. Journal of Power and energy system, 2008. 2(2): p. 768-774.

46. Hiroyuki Sato, R.J.a.R.S., preliminary studiesof coolant by-pass flows in a prismatic very high temperature reactor using computational fluid dynamics, in the 13 thinternational topical meeting on nnuclear reactor thermal hydraulics (NURETH-13). 2009: kanazawa city, Ishikawa Prefecture,Japan.

47. E.takada, core thermal-hydraulic design’. nuclear engineering and design, 2004. 233.

48. Boyce W. Travis , M.S.E. El-Genk , Thermal–hydraulics analyses for 1/6 prismatic VHTR core and fuel element with and without bypass flow. Energy Conversion and Management, 2013. 67: p. 325–341.

49. Pointer WD, T.J., Steady-state, whole-core prismatic VHTR simulation including core bypass. In: Proceedings ICAPP ’10, American nuclear society, in American nuclear society. 2010: San Diego, CA.

50. Sato H, J.R., Schultz R, Computational fluid dynamic analysis of core bypass flow phenomena in a prismatic VHTR. Ann Nucl Energy, 2010.

51. Tak NI, K.M., Lim HS, A practical method for thermal analysis and design of prismatic fuel blocks. In: Proceedings ICAPP ’10, in American nuclear society. 2010: San Diego, CA.

52. Tak, N.-i., Kim, M.-H., Lee, W.J. Numerical investigation of a heat transfer within the prismatic fuel assembly of a very high temperature reactor (2008) Annals of Nuclear Energy, 35 (10), pp. 1892-1899.

53. Travis BW, E.-G.M., Numerical simulation and turbulent convection heat transfer correlation for coolant channels in a very-high temperature reactor. J Heat Transfer Eng 2013. 34.

54. Richard W. Johnson, H.S., Bypass flow computations using a one-twelfth symmetric sector for normal operation in a 350 MWth prismatic VHTR. Nuclear Engineering and Design, 2012. 251: p. 84– 91.

55. Huhu Wanga, E.D.-O., Yassin A. Hassan, Computational fluid dynamics analysis of core bypass flow and crossflow in a prismatic very high temperature gas-cooled nuclear reactor based on a two-layer block model. Nuclear Engineering and Design, 2014. 268: p. 64– 76.

56. J.J. Janse van Rensburg, M.K., Investigating leakage and bypass flows in an HTR using a CFD methodology. Nuclear Engineering and Design, 2011. 241: p. 4960–4971.

57. Su-Jong Yoon, J.-H.L., Min-Hwan Kim, Goon-Cherl Park, The effects of crossflow gap and axial bypass gap distribution on the flow characteristics in prismatic VHTR core. Nuclear Engineering and Design, 2012. 250: p. 465– 479.

58. Bassi, A., Bertrand, F., Barbier, D., Aujollet, P., Anzieu, P., MassiveH2 production with nuclear heating, safety approach for coupling a VHTR with an iodine sulfur process cycle.. In: , in 1st International Conference on Hydrogen Safety (ICHS). 2005: Pisa, Italy.

59. X. Vitart , A.L.D., P. Carles, Hydrogen production using the sulfur–iodine cycle coupled to a VHTR: An overview. Energy Conversion and Management, 2006. 47: p. 2740–2747.

60. F. Bertranda, T.G., F. Bentivoglio, F. Bonnet, Q. Moyart, P. Aujollet, Safety study of the coupling of a VHTR with a hydrogen production plant. Nuclear Engineering and Design, 2011. 241: p. 2580–2596.

61. Shripad T. Revankar , A.A., K. M, Transient analysis of coupled high temperature nuclear reactor to a thermochemical hydrogen plant. i n t e rna t i onal j o u r n a l o f hydrogen energy, 2013. 38: p. 6 1 7 4-6 1 8 1.

62. R.B. Vilim, E.E.F., W.D. Pointer, T.Y.C. Wei, Generation IV Nuclear Energy System Initiative Initial VHTR Accident Scenario Classification: Models and Data. 2005, Argonne National Laboratory: U.S. Department of Energy.

63. Richard R. Schultz, A.M.O., David W. Nigg, Hans D. Gougar, Richard W. Johnson, William K. Terry, Chang H. Oh, Donald M. McEligot, Gary W. Johnsen, Glenn E. McCreery, Woo Y. Yoon, James W. Sterbentz, and J. Steve Herring, Next Generation Nuclear Plant Methods Technical Program Plan. 2007, Idaho National Laboratory.

64. ZUOYI ZHANG and YUJIE DONG, W.S., ASSESSMENTS OF WATER INGRESS ACCIDENTS IN A MODULAR HIGH-TEMPERATURE GAS-COOLED REACTOR. NUCLEAR TECHNOLOGY, 2005. 149.

65. LOHNERT, H.H.a.G., Das Sicherheitskonzept des HTR-Modul, Veranschaulicht am Beispiel des Wassereinbruchs in Primärkreislauf, in KTG-Fachtagung Sicherheit von Hochtemperaturreaktoren. 1985: Jülich,Germany.

66. LOHNERT, G.H., The Consequences of Water Ingress into the Primary Circuit of an HTR-Module—From Design Basis Accident to Hypothetical Postulates. Nucl. Eng. Des., 1992.

67. MARC ROSSELET, R.C., TONY WILLIAMS, INVESTIGATION OF THE k.~-VARIATION UPON WATER INGRESS IN A PEBBLE-BED LEU-HTR. Annals of Nuclear Energy, 1999. 26: p. 75-82.

68. Stempniewicz, M.M., Correlation for steam–graphite reaction. Nuclear Engineering and Design, 2014. 280: p. 285–293.

69. Zheng Yanhua, S.L., Wang Yan, Water-ingress analysis for the 200MWe pebble-bed modular high temperature gas-cooled reactor. Nuclear Engineering and Design, 2010. 240: p. 3095–3107.

70. Yan Wang, Y.Z., Fu Li, Lei Shi, Analysis on blow-down transient in water ingress accident of hightemperature gas-cooled reactor. Nuclear Engineering and Design, 2014. 271: p. 404–410.

71. Valentin, Francisco & Artoun, Narbeh & Kawaji, M & M Mceligot, Donald. (2015). Experimental study of forced convection heat transfer during upward and downward flow of helium at high pressure and high temperature. 10.1615/TFESC1.fnd.012797.

72. Valentin, Francisco & Artoun, Narbeh & Kawaji, M & M Mceligot, Donald. (2015). Investigation of helium flow laminarization at high temperature and high pressure in a graphite flow channel. 10.1615/TFESC1.fnd.012872.

73. Haque, H., Feltes, W., Brinkmann, G.Thermal response of a modular high temperature reactor during passive cooldown under pressurized and depressurized conditions (2006) Nuclear Engineering and Design, 236 (5-6), pp. 475-484.

74. Aldridge, R. J. Scaling study of the depressurized conduction cooldown event in the high temperature test facility using RELAP5-3D/ATHENA,Oregon State University: Department of Nuclear Engineering and Radiation Health Physic, Oregon State University, 2013.

75. Lommers, L.J., Mays, B.E., Shahrokhi, F. Passive heat removal impact on AREVA HTR design (2014) Nuclear Engineering and Design, 271, pp. 569-577.

76. Sambuu, O., Obara, T. Comparative study on HTGR designs for passive decay heat removal (2015) Progress in Nuclear Energy, 82, pp. 37-45.

77. Tung, Y.-H., Ferng, Y.-M., Johnson, R.W., Chieng, C.-C. Study of natural circulation in a VHTR after a LOFA using different turbulence models (2013) Nuclear Engineering and Design, 263, pp. 206-217.

78. Valentín, F.I., Bindra, H., Kawaji, M. Natural circulation in HTGR type system with coolant channels in simplified graphite-fuel matrix (2013) Transactions of the American Nuclear Society, 109 (PART 2), pp. 1652-1655.

79. Valentin, F.I., Anderson, R., Kawaji, M. Study of two particular cases of abnormal heat transfer phenomena occurring in a VHTR reactor core (2013) Transactions of the American Nuclear Society, 109 (PART 2), pp. 1656-1659.

80. Wibisono, A.F., Ahn, Y., Williams, W.C., Addad, Y., Lee, J.I. Studies of various single phase natural circulation systems for small and medium sized reactor design (2013) Nuclear Engineering and Design, 262, pp. 390-403.

81. Sambuu, O., Obara, T. Conceptual design for a small modular district heating reactor for Mongolia (2012) Annals of Nuclear Energy, 47, pp. 210-215.

82. Valentin, F.I., Pulido, J., Anderson, R., Kawaji, M.Investigation of abnormal heat transfer and flow in a VHTR reactor core (2014) Transactions of the American Nuclear Society, 110, pp. 653-656.

83. Castaneda JA. Scaling Analysis of the OSU High Temperature Test Facility during a Pressurized Conduction Cooldown Event using RELAP5-3D. Corvallis, OR: Nuclear Engineering, Oregon State University, 2014.

84. Valentin, F.I., Kawaji, M. Role of radiation heat transfer in cooling of a scaled model of a prismatic graphite core in a VHTR (2015) International Topical Meeting on Nuclear Reactor Thermal Hydraulics 2015, NURETH 2015, 10, pp. 8519-8532.

85. Valentín, F.I., Artoun, N., Anderson, R., Kawaji, M. Study Of abnormal heat transfer during forced and natural convection scenarios in a prismatic core of a VHTR: Numerical and experimental results (2015) International Topical Meeting on Nuclear Reactor Thermal Hydraulics 2015, NURETH 2015, 9, pp. 7913-7926.

86. Kim, S., Tak, N.-I., Lim, H.-S., Ha, S.-J. Sensitivity study on depressurized LOFC accidents with failure of RCCS in a modular gas-cooled reactor (2010) Annals of Nuclear Energy, 37 (5), pp. 664-671.

87. Yu-Hsin Tung, Yuh-Ming Ferng, Richard W. Johnson, Ching-Chang Chieng, Transient LOFA computations for a VHTR using one-twelfth core flow models, Nuclear Engineering and Design,301,2016,https://doi.org/10.1016/j.nucengdes.2016.03.002.

88. Very-High-Temperature Reactor (VHTR). Retrieved from https://www.gen-4.org/gif/jcms/c_42153/very-high-temperature-reactor-vhtr.

89. Yoon, S. J., Jin, C. Y., Lee, J. H., Kim, M. H., & Park, G. C. (2011). Study on the flow distribution in prismatic VHTR core with a multi-block experiment and CFD analysis. Nuclear Engineering and Design, 241(12), 5174-5182.

90. Nakano, M., et al. (2014). "Core design and safety analyses of 600 MWt, 950 °c high temperature gas-cooled reactor." Nuclear Engineering and Design 271: 560-563.

91. Petti, D., & Bell, G. (2005). The DOE Advanced Gas Reactor (AGR) fuel development and qualification program. Paper presented at the Proceedings of the American Nuclear Society - International Congress on Advances in Nuclear Power Plants 2005, ICAPP'05.

92. Haque, H., Feltes, W., & Brinkmann, G. (2006). Thermal response of a modular high temperature reactor during passive cooldown under pressurized and depressurized conditions. Nuclear Engineering and Design, 236(5-6), 475-484.

93. INL, 2007, high temperature gas cooled test reactor point design: summary report, INL/EXT-16-37661, Idaho National Laboratory, January 2007.

94. Kao, M. T., Jain, P., Usman, S., Said, I. A., Taha, M. M., Al-Dahhan, M. H., & Rizwan, U. (2015). Investigation of plenum-to-plenum heat transfer and gas dynamics under natural circulation in a scaled-down dual channel module mimicking prismatic VHTR core using CFD. Paper presented at the International Topical Meeting on Nuclear Reactor Thermal Hydraulics 2015, NURETH 2015.

95. Tung, Y. H., & Johnson, R. W. (2011). CFD calculations of natural circulation in a high temperature gas reactor following pressurized circulator shutdown. Paper presented at the ASME 2011 International Mechanical Engineering Congress and Exposition, IMECE 2011.

96. Takeda, T., Hatori, H., & Funatani, S. (2016). Experiments and numerical analysis of a control method for natural circulation through helium gas injection. Nuclear Engineering and Design, 306, 108-116.

97. Said, I. A., Taha, M. M., Usman, S., Woods, B. G., & Al-Dahhan, M. H. (2017). Investigation of natural convection heat transfer in a unique scaled-down dual-channel facility. AIChE Journal, 63(1), 387-396.

98. Juhn, P.E., Kupitz, J., Cleveland, J., Cho, B., Lyon, R.B. (2000). IAEA activities on passive safety systems and overview of international development, Nuclear Engineering and Design 201, 41 – 59.

99. Aksan, N et al., (2009). Passive Safety Systems and Natural Circulation in Water Cooled Nuclear Power Plants, IAEA-TECDOC-1624.

100. Basu, D. N., Bhattacharyya S., Das P. K., (2014). A review of modern advances in analyses and applications of single-phase natural circulation loop in nuclear thermal hydraulics. Nuclear Engineering and Design 280, 326-348.

101. Beeny, B., Vierow, K., (2015). Gas-cooled reactor thermal hydraulic analyses with MELCOR, Progress in Nuclear Energy, 85, 404-414.

102. Vijayan, P.K., (2002), Experimental observations on the general trends of the steady state and stability behaviour of single-phase natural circulation loops, Nuclear Engineering and Design, 215, 139-152.

103. Habib, M. A., S. A. M. Said, S. A. Ahmed and A. Asghar (2002). Velocity characteristics of turbulent natural convection in symmetrically and asymmetrically heated vertical channels. Experimental Thermal and Fluid Science, 26(1), 77-87.

104. Budihardjo, I., Morrison, G. L., Behnia, M., (2007). Natural circulation flow through water-in-glass evacuated tube solar collectors. Solar Energy, 81(12), 1460-1472.

105. Said, I. A., Taha, M. M., Usman, S., & Al-Dahhan, M. H. (2018). Effect of helium pressure on natural convection heat transfer in a prismatic dual-channel circulation loop. International Journal of Thermal Sciences, 124, 162-173.

106. Said, I. A., Taha, M. M., Usman, S., & Al-Dahhan, M. H. (2018). Experimental investigation of the helium natural circulation heat transfer in two channels facility using varying riser channel heat fluxes. Experimental Thermal and Fluid Science, 93, 195-209.

107. Taha, M. M., Said, I. A., Usman, S., & Al-Dahhan, M. H. (2018). Buoyancy-driven air flow within plenum-to-plenum facility down-comer channel. Experimental Thermal and Fluid Science, 94, 205-214.

108. Castaneda JA. Scaling Analysis of the OSU High Temperature Test Facility during a Pressurized Conduction Cooldown Event using RELAP5-3D. Corvallis, OR: Nuclear Engineering, Oregon State University, 2014.

109. King BM. Natural Circulation Scaling of a Pressurized Conduction Cooldown Event in the Upper Plenum of the Modular High Temperature Gas Reactor. Corvallis, OR: Nuclear Engineering, Oregon State University, 2012.

110. S.M. Alshehri, I.A. Said, M.H. Al-Dahhan, S. Usman, Plenum-to-plenum natural convection heat transfer within a scaled-down prismatic modular reactor facility, Thermal Science and Engineering Progress (2018).

111. Taha, M. M., Said, I. A., Usman, S., & Al-Dahhan, M. H. Natural convection inside heated channel of a facility representing prismatic modular reactor core, AIChE Journal.

112. Abdulmohsin, R. S., & Al-Dahhan, M. H. (2015). Characteristics of convective heat transport in a packed pebble-bed reactor. Nuclear Engineering and Design, 284, 143-152.

113. Pisters, K., & Prakash, A. (2011). Investigations of axial and radial variations of heat transfer coefficient in bubbling fluidized bed with fast response probe. Powder Technology, 207(1-3), 224-231.

114. Holman, J. P. (2001). Experimental methods for engineers. Boston: McGraw-Hill.

115. Davis, L. P., & Perona, J. J. (1971). Development of free convection flow of a gas in a heated vertical open tube. International Journal of Heat and Mass Transfer, 14(7), 889-903.

116. Bergman TL, Incropera FP, DeWitt DP, Lavine AS. Fundamentals of Heat and Mass Transfer. 7th edition. New York, USA: John Wiley & Sons Inc., 2011.

117. Barnes, J. F. (1960). An experimental Investigation of Heat Transfer From The Inside Surface of a Hot Smooth Tube to Air, Helium, and Carbon Dioxide (NGTE-R-241 AD-237862 England DTIE English).

118. Petersen, H. (1970). The Properties of Helium: Density, Specific Heats, Viscosity, and Thermal Conductivity at Pressures from 1 to 100 Bar and from Room Temperature to about 1800 K: Jul. Gjellerup.

119. Dyer, J. R. (1975). The development of laminar natural-convective flow in a vertical uniform heat flux duct. International Journal of Heat and Mass Transfer, 18(12), 1455-1465.

120. Castañeda, J. A. (2014). Scaling Analysis of the OSU High Temperature Test Facility During a Pressurized Conduction Cooldown Event Using RELAP5-3D: Oregon State University.

121. Simoneau, J.-P., Champigny, J., Mays, B., & Lommers, L. (2007). Three-dimensional simulation of the coupled convective, conductive, and radiative heat transfer during decay heat removal in an HTR. Nuclear Engineering and Design, 237(15), 1923-1937.

122. Tung, Y. H., Johnson, R. W., Chieng, C. C., & Ferng, Y. M. (2012). Modeling strategies to compute natural circulation using CFD in a VHTR after a LOFA. Paper presented at the ASME International Mechanical Engineering Congress and Exposition, Proceedings (IMECE).

123. Qian, L., Qiu, S., Zhang, D., Su, G., & Tian, W. (2010). Numerical research on natural convection in molten salt reactor with non-uniformly distributed volumetric heat generation. Nuclear Engineering and Design, 240(4), 796-806.

124. Okafor, I. F., Dirker, J., & Meyer, J. P. (2017). Influence of non-uniform heat flux distributions on the secondary flow, convective heat transfer and friction factors for a parabolic trough solar collector type absorber tube. Renewable Energy, 108(Supplement C), 287-302.

125. Osiadacz, A. J., & Chaczykowski, M. (2001). Comparison of isothermal and non-isothermal pipeline gas flow models. Chemical Engineering Journal, 81(1), 41-51.

126. Wang, Q., Gao, P., Chen, X., Wang, Z., & Huang, Y. (2017). Investigation on heat transfer characteristics in the test section with non-uniform heat flux distribution under natural circulation. Paper presented at the International Conference on Nuclear Engineering, Proceedings, ICONE.

127. Alves, T. A., & Altemani, C. A. C. (2008). Convective cooling of three discrete heat sources in channel flow. Journal of the Brazilian Society of Mechanical Sciences and Engineering, 30(3), 245-252.

128. Mohammed, H. A., & Salman, Y. K. (2007). Heat transfer by natural convection from a uniformly heated vertical circular pipe with different entry restriction configurations. Energy Conversion and Management, 48(7), 2244-2253.

129. Salman, Y. K., & Mohammed, H. A. (2007). Free convective heat transfer with different sections lengths placed at the exit of a vertical circular tube subjected to a constant heat flux. Al- Khwarizmi Eng J, 3(3), 31-52.

130. Mohammed, H. A., & Salman, Y. K. (2007). Laminar air flow free convective heat transfer inside a vertical circular pipe with different inlet configurations. Thermal Science, 11(1), 43-63.

131. Misale, M., Garibaldi, P., Passos, J. C., & de Bitencourt, G. G. (2007). Experiments in a single-phase natural circulation mini-loop. Experimental Thermal and Fluid Science, 31(8), 1111-1120.

132. Vijayan, P. K., Sharma, M., & Saha, D. (2007). Steady state and stability characteristics of single-phase natural circulation in a rectangular loop with different heater and cooler orientations. Experimental Thermal and Fluid Science, 31(8), 925-945.

133. Mustafa, Z., & Ghani, Y. K. S. (2014). Natural convection heat transfer in inclined open annulus passage heated from two sides. Int J Mech Eng Technol, 5(11), 76-91.

134. Welander, P. (1967). On the oscillatory instability of a differentially heated fluid loop. Journal of Fluid Mechanics, 29(1), 17-30.

135. Al-Arabi, M., Khamis, M., & Abd-Ul-Aziz, M. (1991). Heat transfer by natural convection from the inside surface of a uniformly heated tube at different angles of inclination. International Journal of Heat and Mass Transfer, 34(4), 1019-1025.

136. Ede AJ. Natural Convection on Free Vertical Surfaces, East Kilbride, Glasgow: Mechanical Engineering Research Laboratory Report Heat 141, Department of Science and Industrial Research, 1956.

137. Kageyama M, Izumi R. Natural heat convection in a vertical circular tube. Bull JSME. 1970;13:382–394.

138. Kihm, K. D., Kim, J. H., & Fletcher, L. S. (1995). Onset of flow reversal and penetration length of natural convective flow between isothermal vertical walls. Journal of Heat Transfer, 117(3), 776-779.

139. Sanvicente, E., Giroux-Julien, S., Ménézo, C., & Bouia, H. (2013). Transitional natural convection flow and heat transfer in an open channel. International Journal of Thermal Sciences, 63, 87-104.

140. http://www.peacesoftware.de/einigewerte/einigewerte_e.html.

141. Travis, B.W. and M.S. El-Genk, Thermal-hydraulics analyses for 1/6 prismatic VHTR core and fuel element with and without bypass flow. Energy Conversion and Management, 67: p. 325-341 (2013).

142. Schultz, R.R., et al., Studies Related to the Oregon State University High Temperature Test Facility: Scaling, the Validation Matrix, and Similarities to the Modular High Temperature Gas-Cooled Reactor, Idaho National Lab (2010).

143. Kao, M. T., Jain, P., Usman, S., Said, I. A., Taha, M. M., Al-Dahhan, M. H., & Rizwan-Uddin (2015). Investigation of plenum-to-plenum heat transfer and gas dynamics under natural circulation in a scaled-down dual channel module mimicking prismatic VHTR core using CFD. In International Topical Meeting on Nuclear Reactor Thermal Hydraulics 2015, NURETH 2015 (Vol. 2, pp. 979-995). American Nuclear Society.

144. Salman Alshehri, I.A. Said, Muthanna Al-Dahhan, Shoaib Usman (2018), “Experimental Investigation of Plenum-to-Plenum Natural Circulation Heat Transfer in a Prismatic Very High-Temperature Reactor”, American Nuclear Society Annual Meeting 2018, USA, Phildelphia.

145. Salman Alshehri, I.A. Said, Muthanna Al-Dahhan, Shoaib Usman (2018), “Experimental Investigation on Heat Transfer Characteristics with Non-Uniform Heat Flux Distribution under Natural Circulation”, American Nuclear Society Annual Meeting 2018, USA, Phildelphia.

146. Kao, M. T., Jain, P., Usman, S., Said, I. A., Taha, M. M., Al-Dahhan, M. H., & Rizwan-Uddin. “Investigation of plenum-to-plenum heat transfer and gas dynamics under natural circulation in a scaled-down dual channel module mimicking prismatic VHTR core using CFD”. In International Topical Meeting on Nuclear Reactor Thermal Hydraulics 2015, NURETH 2015 (Vol. 2, pp. 979-995). American Nuclear Society. (2015).

147. M.T. Kao, P.J., S. Usman, I.A. Said, M.M. Taha, M.H. Al-Dahhan, and Rizwan-Uddin, “Investigation of Plenum-to-Plenum Heat Transfer and Gas Dynamics under Natural Circulation in a Scaled-Down Dual Channel Module Mimicking Prismatic VHTR core using CFD”, in ANS-NURTH-16. 2015: Chicago, USA.(2015).

VITA

Salman Mohammed Alshehri was born in Saudi Arabia. He received his B.S. degree in Electrical Engineering from Umm Al-Qura University, Saudi Arabia in 2009. He joined to King Abdulaziz City for Science and Technology, in Riyadh, Saudi Arabia, as a researcher assistant in the National Center for Nuclear Technology in 2009. In 2010, he elected to train at INVAP Company in Bariloche, Argentina. He received his M.S. degree in Nuclear Engineering from Missouri University of Science and Technology in December 2014. Salman joined the Ph.D. program in Missouri University of Science and Technology in Rolla, MO, USA in Spring 2015 to pursue his Ph.D. degree in Nuclear Engineering and he received doctoral degree in Nuclear Engineering in May 2019. Salman worked on investigation of the natural convection heat transfer and gaseous dynamics of the prismatic very high temperature reactor under accident scenarios using advanced sophisticated measurement techniques under guidance of Dr. Shoaib Usman. During his Ph.D. program he published three peer reviewed full papers and two conference papers were presented by him in American Nuclear Society in 2018. Salman received a travel award provided by Council of Graduate Students (CGS) at Missouri University of Science and Technology to attend American Nuclear Society Annual Meeting to present his research outcomes.